UNIVERSITY OF CALIFORNIA
RIVERSIDE

Media Fabrication and Characterization Systems for Three Dimensional - Multilevel Magnetic Recording

A Dissertation submitted in partial satisfaction
of the requirements for the degree of

Doctor of Philosophy

in

Electrical Engineering

by

Nissim Amos

December 2008

Dissertation Committee:
Dr. Sakhrat Khizroev, Chairperson
Dr. Robert Haddon
Dr. Ilya Dumer

The Dissertation of Nissim Amos is approved

_____

_____

_____

Committee Chairperson

University of California. Riverside

ב"ה

ACKNOWLEDGMENTS

First and foremost, I thank G-d for all His blessings.

Professors: Sakhrat Khizroev, Robert Haddon, Ilya Dumer, and Alexander Balandin. UCR College Chancellor's Fellowship, National Science Foundation (NSF), Department of Defense (DoD), Defense MicroElectronics Activity (DMEA), all my colleagues at the Center for 3D Electronics at UCR (listed in the order of their first name): Alexander (Sasha) Krichevsky, Andrey Lavrenov, Beomseop Lee, Bing Hu, Chen Zang, Jeongmin Hong, Rabee Ikkawi, Robert Fernandez, Steven Chen, and Yuan Tian. Special thanks to Andrey and Sasha for their help with FIB fabrication and MOKE setup, respectively.

DEDICATION

I dedicate my work to my precious family, Nava and Zohar, for being patient, understanding, and supportive of my educational goals. Thank you for all the personal sacrifices you needed to make for this accomplishment.

ABSTRACT OF THE DISSERTATION

Media Fabrication and Characterization Systems for Multilevel Three-Dimensional Magnetic Recording

by

Nissim Amos

Doctor of Philosophy, Graduate Program in Electrical Engineering
University of California, Riverside, December 2008
Dr. Sakhrat Khizroev, Chairperson

The data storage industry recently substituted its five-decade-old technology (longitudinal magnetic recording), which reached its fundamental limitations due to thermal instabilities in the recording media, with perpendicular magnetic recording. Nonetheless, the lifetime of this newly adopted technology and other next generation alternatives including heat-assisted magnetic recording (HAMR) and bit patterned media (BPM) is comparably short. In order to defer the superparamagnetic limit substantially beyond 1 Tbits/in^2, it may be necessary to stack information in a third (vertical) dimension.

This vertical stacking underlies the concept of multilevel (ML) three-dimensional (3D) magnetic recording and memory. In 3D magnetic devices, information is recorded, not only on one surface (as in all modern 2D applications), but in the entire 3D bulk of the recording media. As a result, substantially larger amount of data could be recorded on the same surface area (as compared to any 2D alternative). This study addresses design configuration, media fabrication, and characterization techniques for a particular ML 3D

magnetic recording device. A newly developed ML 3D magnetic recording media enables selective reading and writing of up to 4 distinct signal levels, in comparison to only two signals in conventional 2D-based magnetic recording media. It is believed that at least over six layers (or over $2^6 = 64$ signal levels) could be independently accessed in a ML 3D magnetic recording device. Gallium ion implantation as a potential method to alter the magnetic properties of 3D media is also discussed.

Furthermore, with every emerging technology, both fabrication systems and characterization techniques must be developed. One of the most crucial characterization tools, which enable the direct visualization of the smallest bit of magnetic information, is Magnetic Force Microscopy (MFM). MFM is thus an integral part of the development and characterization of ML 3D magnetic recording devices. Nevertheless, the best lateral resolution conventional state-of-the-art probes can produce under ambient conditions is limited to about ~ 25 nm. In this study, newly developed fabrication techniques for MFM probes are presented. Specifically, plateau probes to enhance the overall capabilities of MFM and high lateral resolution (below 10 nm in ambient conditions) multi-domain MFM probe. The enhancement in MFM capabilities has the potential to facilitate the development of HAMR, BPM, and ML 3D magnetic systems.

Table of Contents

Research Motivation

Demand for High-Density Data Storage Devices

Magnetic based information storage with its reliability and continuous development guaranteed hard disk drives (HDDs) an expanding market since the inception of computers in 1956. In fact, the 2006 market for HDDs of about $31 billion is expected to rise to $46 billion in only three years. A growing market for HDDs initiated with emergence of personal computers (PCs) and continued to rise for the past four decades. In recent years, this traditional market shifted into other avenues since the integration of HDDs into other systems such as servers, DVRs, digital camcorders, MP3 players, game boxes, high definition televisions (HDTVs), and GPS for automobiles took place. As an illustration, about 380 million HDDs were sold in the year 2005 out of which an astonishing 45% did not go into PCs or laptops. These HDDs were incorporated into a new and expanding market for HDDs; a market eager for greater capacity and faster HDDs which the current state-of-the-art products are yet to provide.

Nevertheless, while the market for better HDDs is growing exponentially, the data storage industry is living a new decade in which their traditional technology is passing on and new technologies must take over in order to insure the advancement of higher-density data storage devices. A sister technology to the traditional (longitudinal magnetic recording) known as perpendicular magnetic recording is already taking over the HDDs market. However, this technology is a short-term solution to the growing demand for improved HDDs and shell meet the same fate as the conventional technology in a few years. Due to the fundamental limitations of longitudinal and perpendicular magnetic

recording together with the ever-increasing demand for higher capacity information storage, both the industry and research groups around the globe are forced to develop alternate technologies to further advance the current state of conventional technologies.

Conventional Technology Limitations

In 1956, IBM introduced the first magnetic hard disk drive (HDD) in the world. RAMAC (Random Access Method of Accounting and Control) had fifty 24-inch magnetic disks and capable of storing 4.4 Mbytes with an areal density of 2 kbits/in.^{2} With decades of research, the data storage industry was capable of perfecting the HDD technology and increasing its reliability, efficiency, speed, and areal density. The exercised approach for this advancement was the continuous challenge of scaling the complete HDD system down and hence achieving higher areal densities, faster access rates, low power consumption, and the overall miniaturization of the device (Figure 1).

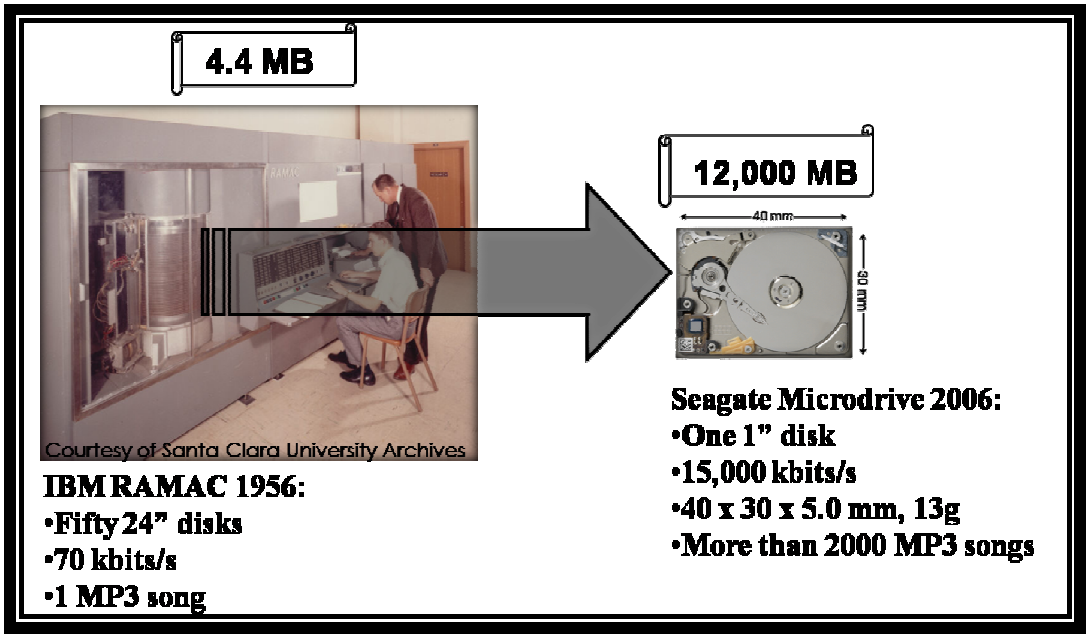

Figure 1: Pictures of the first RAMAC computer (left) and a Seagate mini drive (right) illustrating the progression of HDDs.

In recent years, the conventional (longitudinal) technology remained at a halt without any significant progress. This halt is the result of a fundamental limit known as the superparamagnetic limit [1]. This fundamental limit is caused by thermal instabilities in the recording media when physical bit dimensions are reduced below certain fundamental values. In short, this limit indicates that in longitudinal recording systems, recorded bits of information will not be stable at room temperature if the areal density will surpass about 200 Gbits/in^2 [2]. Consequently, the data storage industry and researchers began investigating alternate technologies that will meet the ever-increasing need for higher areal density data storage devices.

The Superparamagnetic Limit

Magnetic recording media is composed of billions of grains or nanomagnets, which are magnetically isolated from each other with a nonmagnetic matrix. The signal-to-noise-ratio (SNR) of the read]back signal is proportional to the log of the number of grains or nanomagnets encompassing one bit.

SNR $\propto$ log (N), where N is the number of grain (about 40 – 100 grains per bit)

Thus, it is crucial to maintain the same number of grains when attempting to scale down the dimensions of a bit. Assuming that the grains are cubic:

$$a \approx \frac{1}{\sqrt{areal\ density}}\ , a^3 \approx \text{ volume of the grain}$$

Since the number of grains must be preserved, the only way to achieve higher areal densities is by reducing the effective volume of the grains. However, reducing the grain volume for the particular magnetic media used (in-plane oriented: CoCrPt-based) will

result in thermal fluctuations and hence alterations in the magnetic states of the grains, resulting in bit instability and corrupted data storage. The lifetime of the magnetic state in each grain or the thermal activation switching time (τ) for each grain is directly proportional to the volume of the grain and the anisotropy energy density for the particular media being used.

$\tau = \text{Thermal activation swiching time}$

$$\tau \propto e^{\left(\frac{K_U V}{k_B T}\right)}$$

$K_U \text{V} = \Delta E = \text{Barrier energy}$

$K_U = \text{anisotropy energy density}$

$V = \text{grain volume}$

$\text{T} = \text{Absolut temperture}$

$k_B = \textit{Boltzmann's} \text{ constant}$

Theoretical and experimental analysis indicate that the ratio of $\frac{K_U V}{k_B T}$ should be greater than about 40 in order to maintain bit stability for a few years. For example, for

$$\frac{K_U V}{k_B T} = 60,\ \tau = 3.6 \text{x} 10^9 \text{ sec.} \quad \text{whilefor} \quad \frac{K_U V}{k_B T} = 25,\ \tau = 72 \text{sec.}$$

Observing the factors which affect τ, the only parameter left for modification is the anisotropy energy density, K_U. Using high K_U materials will enable the utilization of smaller grain volume, and thus the squeezing of more bits per unit area. Nevertheless, conventional transducers cannot generate the magnetic field required to record information on high anisotropy materials. The write magnetic field, H_{Write}, required to switch the magnetization of a grain/bit is directly proportional to K_U. For example, the

maximum H_{Write} which can be generated by a ring-head transducer is limited to the magnetization, M_S, of the transducer's core, for which high M_S materials have been optimized already. Since neither the grain volume can be reduced nor the anisotropy energy density of the material increased, the superparamagnetic limit has been reached for the conventional longitudinal-based magnetic recording technology [3].

Alternate Technologies

Perpendicular Magnetic Recording

The most convenient and conventional technology related is the so-called perpendicular method of recording information [4,5,6,7,8,9]. With this technology, the major components changing with respect to the conventional HDD are the media and the read/write transducer (Figure 2). In longitudinal recording, the media in composes of grains which are randomly magnetized within the plane of the media. Each bit encompasses about 40 - 100 grains to statistically insure bit stability and readability. On the other hand, in perpendicular recording the media has a well-defined magnetic anisotropy with magnetization pointing in or out of the media plane. In addition, due to the presence of a magnetic soft under layer (SUL), the effective write field almost doubles. While in longitudinal recording the write process is done with the fringing fields with $H_{Write} \sim 2\pi M_S$, in perpendicular recording the write process effectively occurs in the gap with $H_{Write} \sim 4\pi M_S$. These two factors permit the use of higher anisotropy materials with greater volume per grain, and hence lead to greater areal density. Some suggest that perpendicular recording will reach the superparamagnetic limit at about 1 Tbits/in^2 [10,11,12]. However, there are still many unresolved issues that must be addressed such

as noise levels due to the presence of SUL and adequate magnetic torque to switch magnetization at high frequencies. This may suggest that perpendicular recording in its current form might not be proper to maximize its predicted areal density.

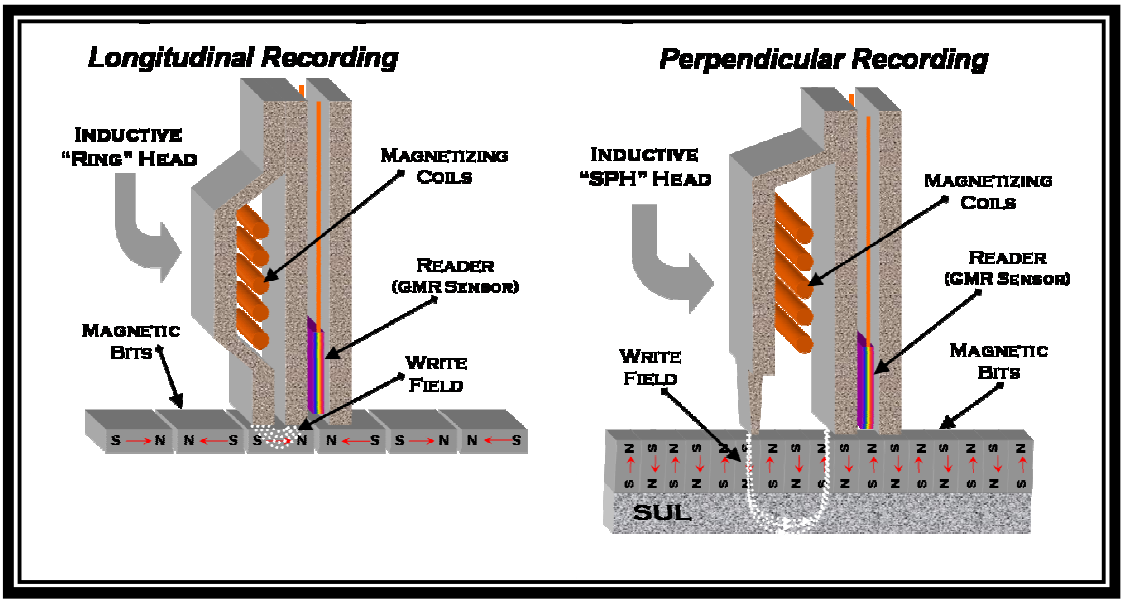

Figure 2: A schematic illustrating the main differences between longitudinal and perpendicular magnetic recording systems. In these two cases, magnetization in the recording media is directed along the plane and perpendicular to the plane of the disk, respectively.

Bit Patterned Media

Another way of deferring the superparamagnetic limit exploits media patterning [13,14,15,16]. With this method the areal density will be predetermined by lithographical or self-assembly limitations. The idea is to separate individual islands/bits in order to break quantum-mechanical interaction and hence effectively eliminate the transition noise between opposite bits and increase bit stability [17]. It is also possible to achieve optimal recording magnetic fields by patterning soft magnetic layers, which may be used for both perpendicular magnetic recording and 3D magnetic recording devices [18].

Various nanofabrication methods can be implemented to pattern magnetic media. Among the methods are: electron-beam lithography [19], UV-optical lithography [20], self-assembled media synthesis [21,22], ion milling [23,24], nanoimprinting [25], and many others. An atomic force microscopy (AFM) image of a patterned media fabricated using a FIB system is shown in Figure 3. Each island in the pattern is approximately 50 nm in diameter. Ideally, magnetic islands with diameter as small as 10 nm can be manufactured with this method.

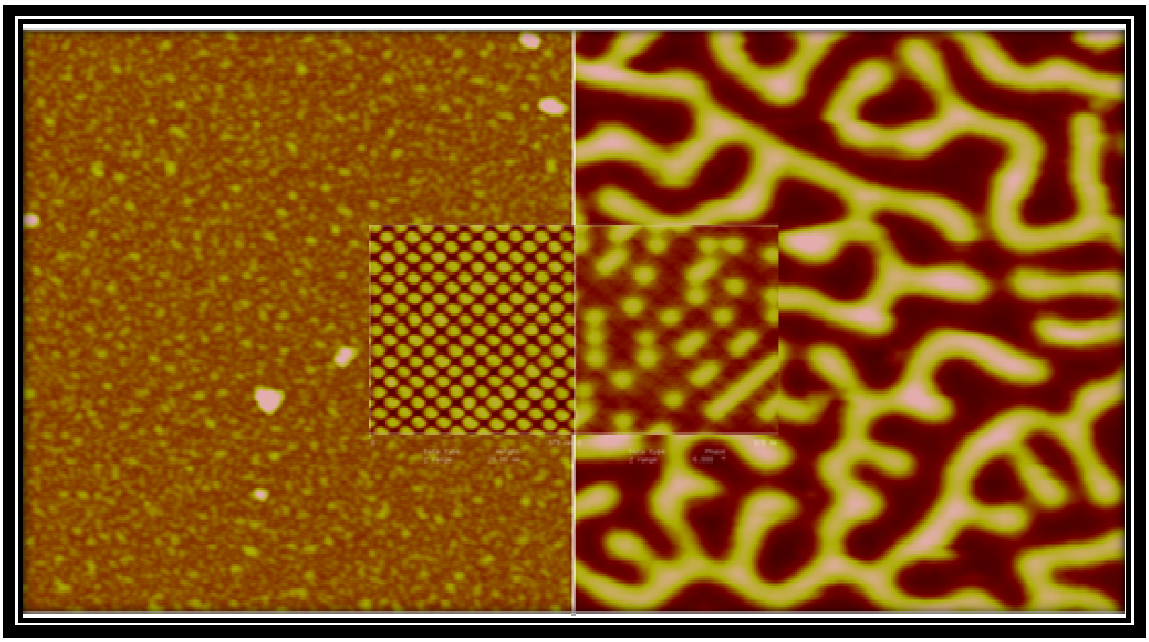

Figure 3: AFM/MFM images of a Co/Pd multilayers perpendicular media (3 μm scan size) and FIB-fabricated patterned media with an island diameter of approximately 50 nm (1 μm scan size).

The major issue with patterned media is its yield cost and throughput. Therefore, for the time being, the data storage industry is not ready for mass production of patterned media disks; though, further investment on cost effective media and greater throughput will become inevitable for the industry as incorporation of media patterning will become a necessity for areal densities beyond 1 Tbits/in^2. Currently, Motorola is working on the

development of patterning whole disks, utilizing the Nano-imprinting method. Figure 4 shows SEM images of a relatively small nanoimprinting template which was fabricated via E-beam lithography using a Nabity module on a dual beam SEM/FIB system from Zeiss. Success in the effective fabrication of patterned media has the potential to defer the superparamagnetic limit and hence increase the areal density of both longitudinal and perpendicular based magnetic storage systems.

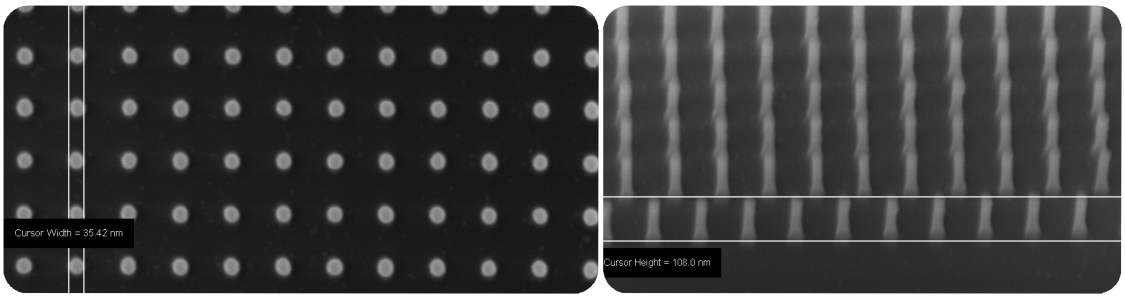

Figure 4: 200 x 200 µm2 temples: (left) SEM image showing ~ 35 nm in diameter islands (right) SEM image showing an island height of ~ 110 nm

Patterned Soft Magnetic Underlayer (SUL)

In perpendicular magnetic recording, a magnetically "soft" under layer (SUL) is deposited below the magnetically "hard" recording layer. Due to the presence of the SUL, an image of the recording head is formed, Figure 5. In such a scenario, the recording magnetic field effectively doubles when compared to the longitudinal method of recording. While in perpendicular recording the magnetic recording field flows in a close magnetic circuit, due the presence of the SUL, in longitudinal recording stray fields emanating from a ring head are used to record the information. By patterning the SUL, the image of the recording head effectively moves closer to the recoding layer, as compared to the real recording head, and thus increases the net recording field and the

field gradient across the thickness of the media. These properties make patterned SUL a great media component for both perpendicular and ML 3D magnetic recording.

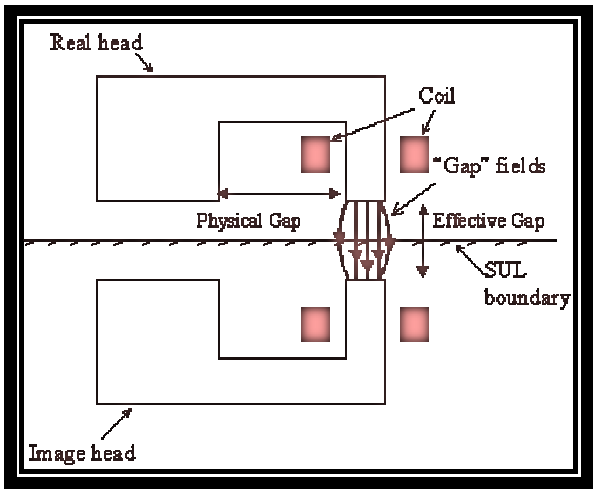

Figure 5: A diagram illustrating the "mirror" image model of the perpendicular recording mode with a soft underlayer.

Numerical models have been developed using commercially available FEM and BEM software suites (ANSYS and Ampere) to demonstrate the key advantages of patterned SUL in perpendicular media [26,27]:

- The read back signal-to-noise ratio (SNR) drastically increased
- The patterning of SUL created field profiles that were more localized in the vicinity of the bits (critical for maximizing areal densities)
- The invention was relatively trivial to integrate into existing technologies

Heat-Assisted Magnetic Recording

Furthermore, the combination of patterned perpendicular media and Heat-Assisted Magnetic Recording (HAMR) can facilitate the use of higher anisotropy materials [28,29]. Currently, recording heads have almost reached perfection in the magnetic write field due to the complexity of producing material with saturation

magnetization greater than about 2.5 Tesla. Because the write field required to switch bit magnetization and the stability of the bit are directly proportional to the media's anisotropy energy density, the recording media is limited to relatively low anisotropy compositions. On the other hand, magnetic coercivity dramatically decreases as temperature increases. Therefore, a hybrid system with both a heating and a magnetic source can be used in order to record on high anisotropy magnetic media. Nonetheless, there are numerous obstacles to overcome before such a technology will be actualized, namely the integration of a near field optical source with sufficient energy throughput [30,31]. Detailed explanation on the design, fabrication, and characterization of near-field energy sources are already in press [32,33,34].

In summary, perpendicular magnetic recording is driving the conventional technology out of the market and is expected to defer the superparamagnetic limit to ~ 1 Tbits/in.^{2} However; perpendicular magnetic recording is considered a temporary technology that will reach its fundamental limitation in a few years. Heat Assisted Magnetic Recording (HAMR) and bit-patterned media (BPM) are alternate technologies, which have the potential to extend the areal densities of magnetic-based data storage devices beyond the 1Tbits/in^2 mark. Nevertheless, these technologies have their own obstacles to overcome and will eventually reach the same fate as any other 2D-based technology. Ultimately, both scientists and the industry will be compelled to investigate the alternative of performing data storage, not just on the surface, but also in the bulk of the material. "There's plenty of room at the bottom."

Multilevel (ML) Three-Dimensional (3D) Magnetic Recording

The concept of three-dimensional (3D) magnetic recording was proposed in the onset of this decade [35,36]. The technology is different from the traditional approach, which deals with one surface (of a magnetic recording media) only. Instead, a third vertical dimension is used to store information not only on the surface but also in the volume of the recording media (Figure 6). In other words, the information is packed also across the thickness. As a result, substantially more information could be recorded per unit area and thus the fundamental data density limit could be extended substantially further. This means that this technology has strong potential to revive the currently relatively slow progress in the multi-billion-dollar data storage industry. In addition, the exploitation of multi-level signal will substantially loosen fabrication requirement. In other words, unlike conventional magnetic and silicon-based technologies, this effort will not be limited by the many problems arising during fabrication of sub-50-nm devices. In this context, "multi-level" implies the ability to record more information per unit surface area.

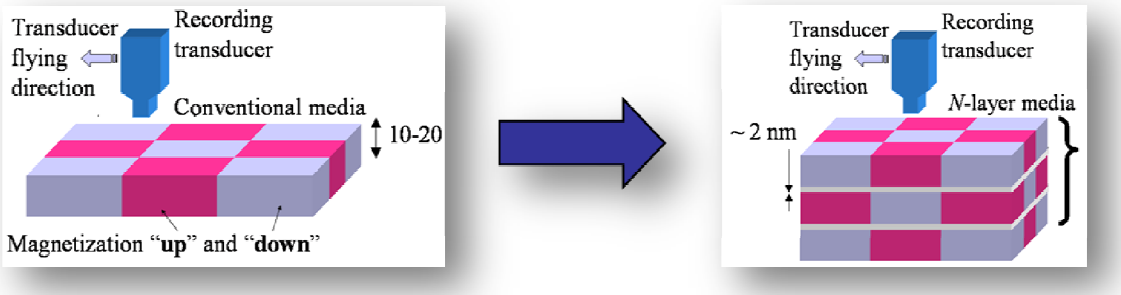

Figure 6: A schematic showing the effective use of the 3D space in a 3D-based magnetic recording system

Another advantage, at least at this early stage of the development, is the relative simplicity of multilevel (ML) 3D recording. This is due to the fact that this technology

has similarities with perpendicular recording. Similar to perpendicular recording, the write/read process will be performed from a magnetic transducer flying above the media surface and the information will be recorded perpendicular to the disk. However, other media configurations shell not be disregarded. For example, longitudinally oriented media or media with the magnetization tilted at some arbitrary angle may have some advantages perpendicular media don't have. As the complexity of ML 3D recording system increases with each next generation, it might become beneficial to eventually switch to one of the non-perpendicular modes.

Finally, because of the two obvious technology merits, 3D magnetics and ML signal configuration, respectively, the technology has long-term potential compared to any other next generation data storage technology. The research effort has already triggered industry-wide interest in the new topic [37]. The current study is aimed at bringing the research to the next level.

Research Focus

The proposed research will shed light on the feasibility of ML 3D magnetic recording systems as a next generation technology. The research is focused on key aspects of the technology, which include methods to fabricate and evaluate ML 3D media. Additionally, development and customization of characterization tools and fabrication methods are also established. In particular, magnetic force microscopy enhanced capabilities. This work will not discuss fundamental theories and basic techniques. Thus, a reader who is not familiar with the fundamentals of magnetism, magnetic recording, thin-film fabrication, and scanning probe microscopy is encouraged to firstly get well-informed [38,39,40,41,42,43,44,45].

Multilevel Three-Dimensional Magnetic Recording

Introduction

Today, people and organizations generate more and more information that is increasingly valuable, but also increasingly hard to locate and use in a meaningful way. The number and complexity of information sources are growing constantly, which results in people storing more data in more places. In disagreement with the traditional skepticism regarding the need for more data capacity, we constantly need devices with ever increasing data densities. Magnetic recording has been the mainstream data storage technology for over four decades [46,47]. After many attempts to extend the life of longitudinal magnetic recording, the data storage industry is finally coming to terms with the reality [48,49]. Researchers, indeed, witness that the recorded data become highly unstable as the areal density increases beyond approximately 200 Gbit/in^2 [50]. A number of technologies have been proposed by research teams all over the world to address the fundamental (superparamagnetic) limit. Perpendicular magnetic recording [51,52] is the closest alternative to the conventional technology and is already being commercialized. Other alternative technologies include discrete-track-media [53,54], patterned media [55,56,57] and heat-assisted magnetic recording (HAMR) [58,59,60,61]. It is expected that these two-dimensional (2D) and single-level technologies can defer the superparamagnetic limit somewhat above 1 Tbits/in^2.

This chapter will review a new realm of opportunities resting from exploiting a third device dimension. Particularly, multilevel three-dimensional (ML 3D) magnetic recording will be discussed as one of the promising next-generation data storage

technologies. Moreover, the feasibility of using more than two signal levels to code recorded information is explored. This is in contrast with conventional recording schemes in which binary coding methods are used, meaning that the signal recorded into or read back from magnetic media has only two states: presence or absence of the magnetization reversal in a bit transition. For example, Figure 7 (a) and (b) illustrate the concept of so called frequency modulation (FM) encoding, probably the most trivial encoding scheme, as it could be used in longitudinal and perpendicular recording, respectively. The only difference between the two recording modes is in the orientation of the magnetization, which is along or perpendicular to the plane of the disk, respectively. In both cases, encoding has a simple one-to-one correspondence between the bit to be encoded and the magnetization reversal pattern.

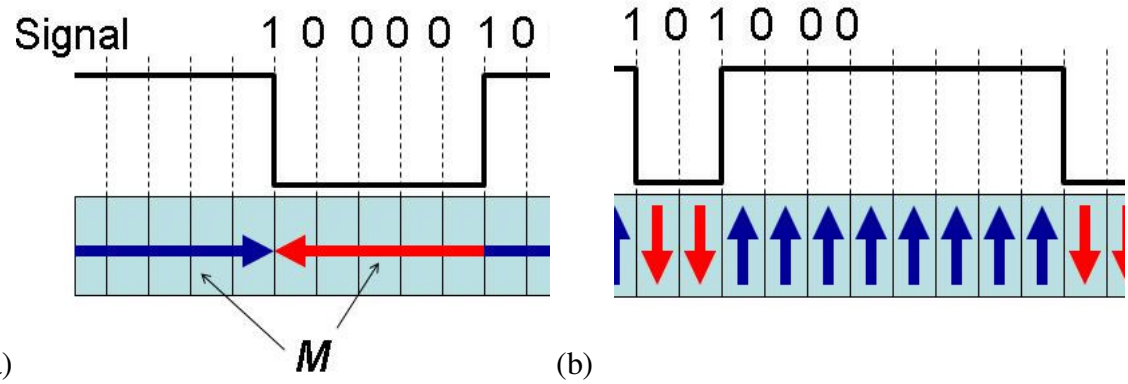

Figure 7: A binary signal representation with a trivial FM encoding in **(a)** longitudinal and **(b)** perpendicular recording modes.

ML 3D magnetic recording refers to the use of multiple signal values to encode data onto a magnetic disk. By using more than two levels, more information could be put in the minimum feature size. Figure 8 illustrates how a multilevel code could be used in a system with a 3D media, which is based on perpendicular orientation of magnetization.

This is a simplified case; in general, the magnetization could be oriented along or at some arbitrary angle to the plane of the disk. As described below in more detail, the main concern would be to engineer a magnetic recording system which could maintain signal to noise ratio (SNR) between any two adjacent levels sufficient for a data encoding channel to maintain a certain data bit error rate. The novel multilevel data coding methods discussed in this chapter is designed to deal with SNR of approximately 5 dB. Therefore, it is clear that with the goal to develop a practical ML 3D recording system with as many levels as possible, it is necessary to engineer a magnetic recording system with as many signal levels as possible, separated by at least 5 dB SNR between any two adjacent levels. It is expected that the magnetic system discussed in this chapter could use at least twenty "distinguishable" signal levels. Finally, it could be mentioned that ideally the ML 3D approach could be applied also to any of the above mentioned alternative technologies to further increase the data capacity.

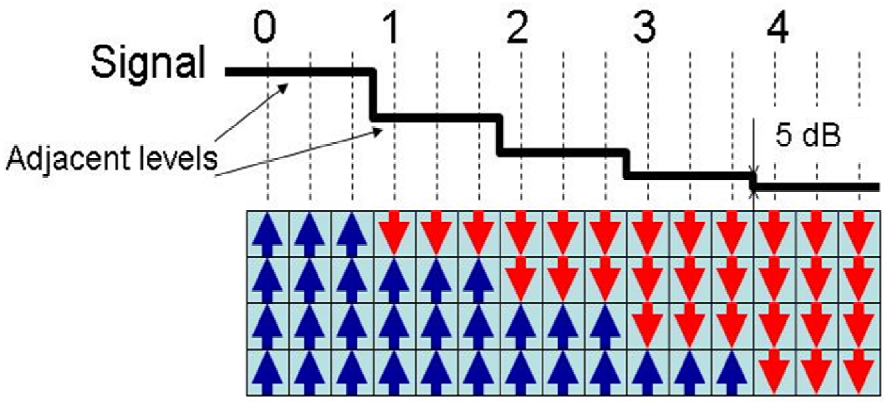

Figure 8: A trivial example of a system with multilevel data encoding.

History of Multilevel Optical Recording

Before exploring the feasibility of ML 3D magnetic recording, it may be helpful to learn from the experience of other industries with regard to ML data coding. For example, in 2004, one of the electronics giants LSI Logic acquired Calimetrics – the first company which focused on the development of a multilevel optical recording system for CD or DVD technologies. In conventional DVDs and CDs a binary based encoding system, known as Eight-to-Fourteen Modulation (EFM), is utilized to store data, Figure 9. Calimetrics invented a system in which eight signal levels, instead of only two, were recorded in a physical area otherwise occupied by only one bit, Figure 10. Though Calimetrics ceased to exist mostly because of the suddenly raised popularity of writable DVD technology, it was successful in introducing a multilevel signal standard in the world of information related technologies, especially overseas. Today, it is becoming normal for new technologies to start to prosper first overseas where it is often easier to launch new standards because of the lack of a well-established traditional technology infrastructure. It could be noticed that though the ML technology by Calimetrics offered only eight signal levels and was not rewritable, it still appeared successful especially in its tremendous impact on modern DVD technologies.

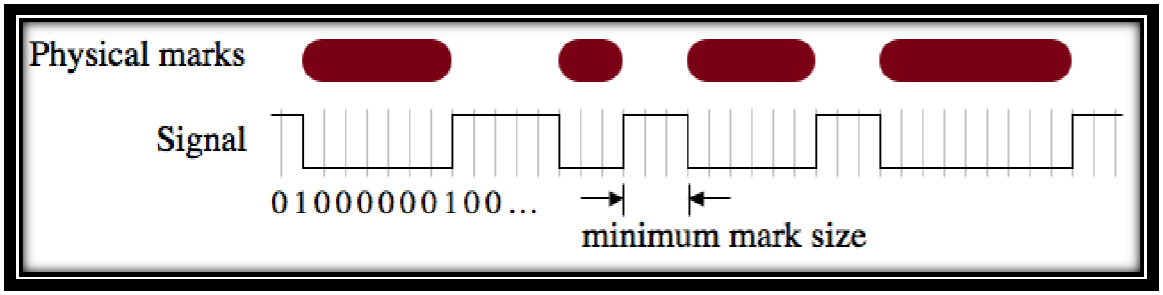

Figure 9: Diagram of the physical marks (upper) and the waveform (lower) of the EFM modulation code used in CDs and DVDs.

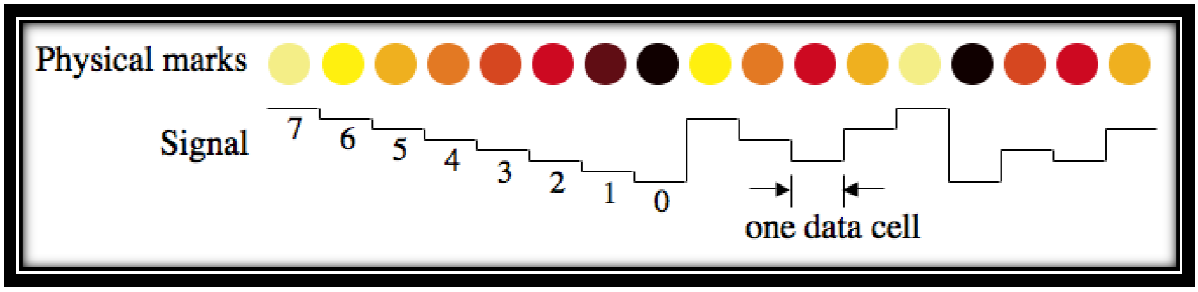

Figure 10: Diagram of the physical marks (upper) and the corresponding waveform (lower) on a multilevel disc.

Below, the most obvious differences between ML 3D magnetic recording and ML optical technology are summarized:

A: The ML technology developed by Calimetrics competed in the market of DVD/CD technologies while the analyzed ML magnetic technology, at least at this early stage, is targeting the market of hard drives.

B: The Calimetrics technology was optics-based while the currently proposed technology is magnetics-based. Consequently, the magnetic technology would be rewritable, which is in contrast with the read-only Calimetrics technology.

C: The optical technology used only eight signal levels while the ML magnetic technology has potential for over forty levels.

Magnetics of Multilevel 3D Recording

This technology is different from the traditional approach, which deals with one surface (of a magnetic recording media) only. Instead, a third vertical dimension is used to store information not only on the surface but also in the volume of the recording media. In other words, the information is packed also across the thickness, Figure 11. As a result, more than one signal level would be exploited to record, store, and retrieve information from the same unit surface area of the recording media. This opens a new window of opportunities not only to develop the most superior near-future data storage device (ML 3D (m3d) drive) but also for the far future to exploit groundbreaking advantages of an entirely new dimension.

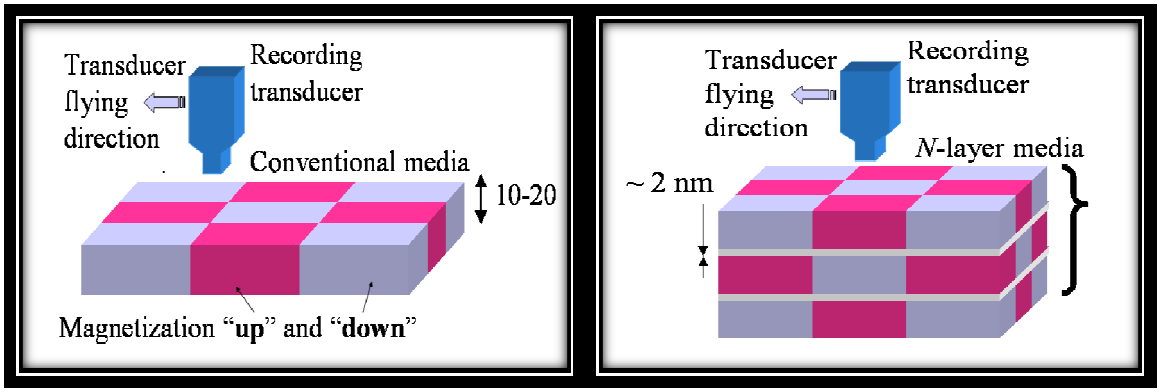

Figure 11: Comparison between a conventional recording system with recording on a surface (left) and a proposed ML 3D system with recording across the thickness of a recording media.

Multilevel 3D versus Absolute 3D

Two different modes of 3D recording with respect to addressing separate magnetic layers will be referred to as ML 3D and absolute 3D modes, respectively. In the ML 3D mode, though a 3D space is utilized for recording, it is not used efficiently. In a trivial case, the signal recorded and read back from a vertical stack is defined by the recording head

above the stack. In this case, the information in all N layers within the stack simultaneously contributes to a particular signal above the surface of the 3D media, Figure 12 (a). The number of signal levels (L) is different from the number of magnetic layers (N) and is determined by the ability to fabricated 3D media for which the magnetization of each layer is sufficient to generate a distinct signal with adequate SNR for L levels to be distinguished from each other. The number of signal levels is also limited by the recording element capabilities of addressing each magnetic layer across the 3D media. In this case, the effective density increases by a factor of Log_2L with respect to the density of the equivalent binary single-layer media. In contrast, in the absolute 3D recording mode, each (n-th) layer in the N-layer recording media would be addressed separately, Figure 12(b), via some physical process (to be explored). In this case, the effective areal density would increase by a factor of N with respect to the areal density of the equivalent single-layer media. For example, if one thousand layers are used, assuming a bit cell cross-section of 160 x 160 nm^2, 25 terabits of data could be stored in one square inch.

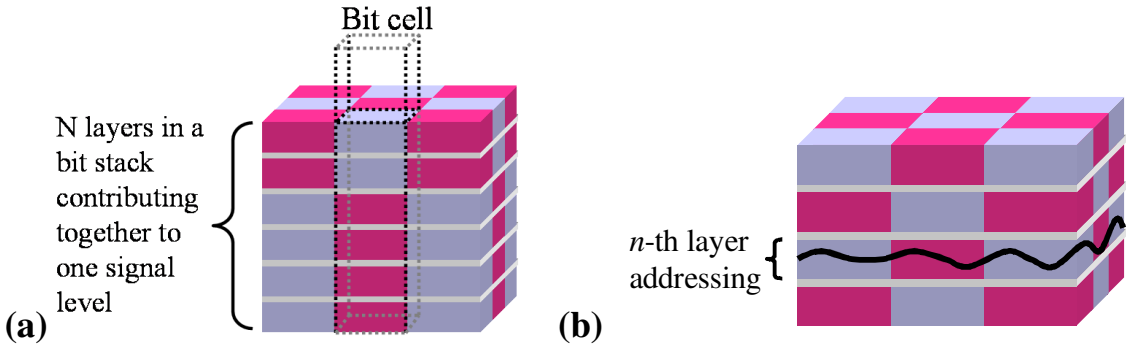

Figure 12: Schematic diagrams illustrating how information is addressed in cases of **(a)** ML 3D and **(b)** absolute 3D recording modes, respectively.

ML 3D Magnetic Writing/Reading

A more detailed review on various 3D based magnetic recording/reading methods can be found in previously published letters [62,63]. These publications identify the ML 3D mode as a likely form of 3D recording which has the potential to impact the near-future world of memory and storage applications. In this mode, a varying recording field could be used to sequentially record across the media thickness, Figure 13 (a).

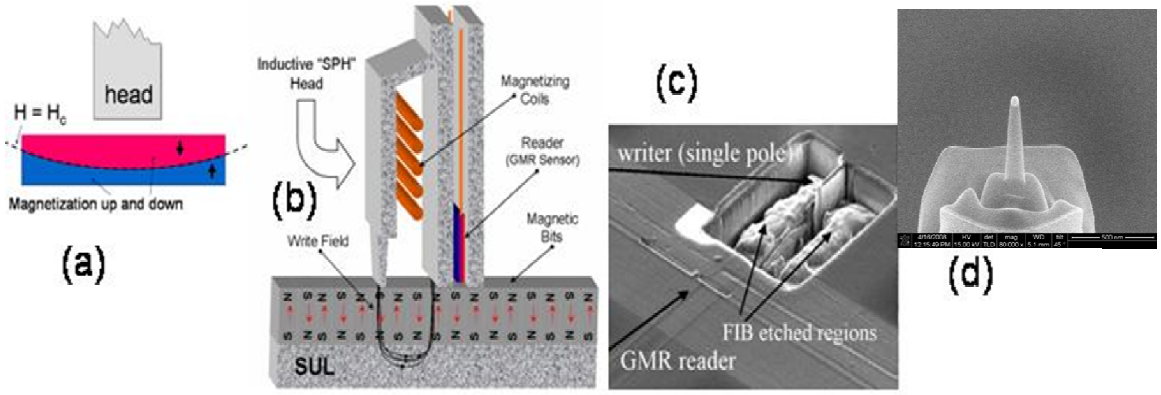

Figure 13: (a) Schematic illustrating recording across the thickness via continuous variation of the recording field. The boundary curve is the field profile when $H = H_c$, where H_c is the coercivity. (b) A diagram of a perpendicular recording system. FIB images of FIB-fabricated (c) single pole writer with a 80-nm track width and (d) a MFM nanoprobe for reading a component of the stray magnetic field.

ML 3D media could be developed in a similar form of, but are not limited to, the popular perpendicular media configuration [64]. To generate adequate perpendicular field, a recording system with a single pole head (SPH) and magnetic recording media with soft underlayer (SUL) should also be used, Figure 13 (b) [65]. SUL should be incorporated into the system in order to force the magnetic flux to flow in the perpendicular direction. Either SPH or FIB-modified longitudinal ring head and a magnetic force microscopy (MFM) nanoprobe could be used to write and read information from ML 3D media, respectively. As an illustration, Figure 13 (c) and Figure 13 (d) are SEM images of FIB-

fabricated SPH with 80-nm track-width and MFM nanoprobe, respectively. The write head should be in the form of a SPH [66], while the MFM nanoprobe should be designed to read the out-of-plane component of the magnetization [67,68].

A schematic illustrating recording into a ML 3D media is shown in Figure 14 (a). For simplicity, only two magnetic layers across the thickness are considered. The layers can be deposited via regular sputtering systems. Continuous and patterned versions of ML 3D media could be used. For illustration purposes and the prototype development, focused ion beam (FIB) was used to further pattern the ML 3D media within the plane of the disk, as illustrated in Figure 14. A straightforward MFM experiment can be performed to demonstrate the presence of more than one signal levels. In this example, a continuous CoCrPt-based 3-layers ML 3D media was sputter-deposited and then patterned via FIB-milling into a square periodic arrays with a linear period of 80 nm. Then, the media was demagnetized using a rapidly alternating and decaying external magnetic field. AFM (left) and MFM images of the surface of the fabricated media are shown in Figure 14 (b). A digitized sectional profile of the signal along the highlighted line going through a track of bits is shown above the AFM and MFM images. Clearly, over three different signal levels could be detected, as shown in Figure 14 (b) (top).

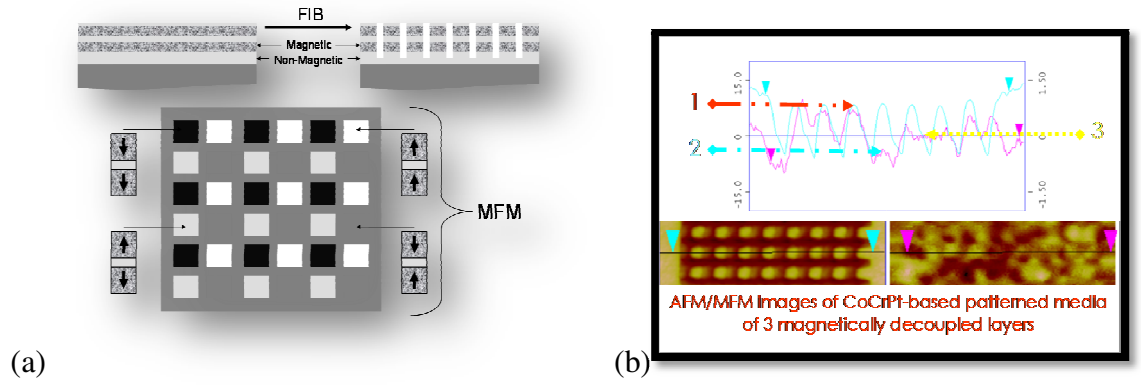

(a) (b)

Figure 14: (a) A schematic illustrating a 2-layer ML 3D media. (b) A MFM image of a patch on the surface of FIB-fabricated continuous CoCrPt-based 3-layer ML 3D media. A digitized sectional profile of the signal along the highlighted line is shown above the AFM/MFM images.

This experiment illustrates that ML 3D media could be partially polarized across the thickness, thus resulting in a multilevel signal configuration. On the contrary, it is known that in conventional recording the magnetization remains in one of the two saturated states and no partial polarization is feasible. The following section entails a discussion of potential ML 3D media compositions and configurations along with a detailed fabrication and characterization experiment on Co/Pd and Co/Pt multilayers-based ML 3D media.

ML 3D Media Fabrication and Characterization

Previously, it was mentioned that one approach to substantially (by a factor of three or so) increase the effective recording and sensitivity field would be through using a patterned soft underlayer (PSUL) or even patterned soft interlayers (PSUI) [69,70]. In the case of ML 3D recording, the number of signal levels the 3D media can generate is directly related to the recording and sensitivity fields. Hence, PSUL may be a crucial component in the optimization stages of ML 3D media.

The key practical advantages due to the use of a PSUL are the following:

- SNR drastically increases as a result of patterning a SUL.

- Patterning of SUL increases both the recording and sensitivity field gradients. The latter is critical for maximizing the areal density during writing and reading, respectively.
- The recording and sensitivity fields remain well localized across the entire thickness to generate a multitude of signal levels.

As was also mentioned in the introductory section, ML 3D magnetic recording has the potential to improve the data capacity of the various proposed alternate technologies. In the case of HAMR, a localized light spot in the order of tens of nanometer is focused in the near-field regime in order to drive down the coercivity of highly anisotropic material, such as FePt-$L1_0$ material [71]. Since the stability of each recorded bit is directly proportional to the effective anisotropy of the material and the effective volume of each grain, it is possible to scale down the grain sizes substantially and thus increase the areal density in a HAMR system. ML 3D recording can further increase the areal density of such system by fabricating media in which isolated magnetic layers exhibit a range of Curie temperatures, resulting in Curie temperature gradient across the thickness of the ML 3D media, Figure 15 . For instance, such media can be fabricated by varying the composition of FePtX, where X can be Cu, Ag, Au, Pd, or Cr. Moreover, the interlayers in this media will act both as exchange decoupling layers and good heat conductors. MgO is a promising composition for both requirements. An optimization in the separation between magnetic signals emanating from each layer and better localization of heat transfer can further be improved by patterning the media, Figure 15. Finally, recording of

each layer within the bulk of the material can be achieved by modulating a particular magnetic field strength with a particular light power.

A more practical way to effectively increase the number of individual layers would be through the formation of coercivity gradient across the thickness of ML 3D media. One proposed mechanism to vary the coercivity in a Co/Pd or Co/Pt multilayers-based ML 3D media is through the variation of processing pressure for each deposited magnetic layer, as schematically shown in Figure 16. Patterning the media will further increase SNR between neighboring bits by significantly reducing the inter-symbol interference (ISI) and thus increasing the number of effective recording levels.

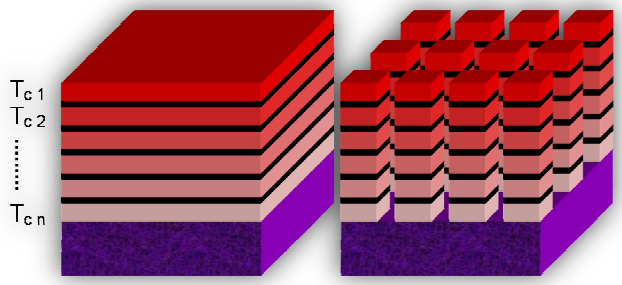

Figure 15: A schematic to illustrate the concept of creating Curie temperature (Tc) gradient across the media in both continuous and patterned ML 3D media, respectively.

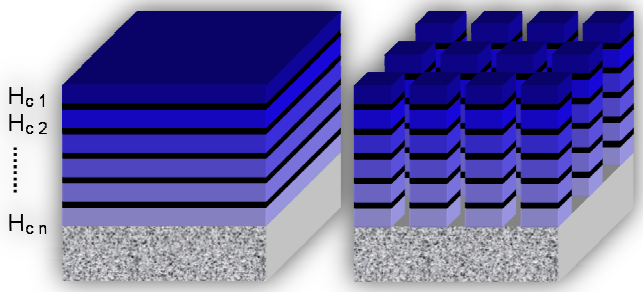

Figure 16: A schematic to illustrate the concept of coercivity (Hc) gradient across the media in both continuous and patterned Ml 3D media, respectively.

Co/Pd Multilayers ML 3D Media

In order to effectively stack decoupled magnetic layers (each exhibiting a unique coercivity value) across the bulk of the media, fabrication conditions and media compositions, which alter the coercivity field of Co/Pd multilayers, have been investigated as a prerequisite for the ML 3D media integration. The coercivity field dependence on the substrate composition and surface conditions, seed and capping layers thickness, processing pressure, and Co and Pd bi-layers thickness have been thoroughly studied. Following the coercivity dependence analysis, dual layer Co/Pd multilayers-based ML 3D media was fabricated and investigated. The out-of-plane and in-plane components of magnetization were measured via polar magneto-optical Kerr microscopy (P-MOKE) and vibrating sample magnetometer (VSM), respectively. The media crystal structure and composition were analyzed with tunneling electron microscope (TEM) and energy dispersive spectrometer (EDS), respectively. The results reveal that the processing pressure could be an effective parameter to alter the coercivity field of the magnetic layers, a palladium interlayer of about 3 nm was sufficient to exchange-decouple the magnetic layers, and that the media is composed of polycrystalline grains with FCC structure, indicative of an CoPd2 alloy.

Roughness (Ra) measurements on both Si and glass substrates were performed with a MikroMasch NSC15 AFM probe in the tapping mode. The glass substrate exhibited lower Ra of 0.318 nm than the Si substrate with Ra of 0.791 nm, Figure 17 (left) and Figure 18 (right), respectively. Both samples were then stationed inside the chamber of an AJA International Orion 5 sputtering system. A two-step substrate RF biasing was

applied to the samples: starting with 25 watts at 30 mtorr argon pressure for about 15 seconds, followed by 12.5 watts at 5 mtorr argon pressure for 2 minutes. Based on the system specifications (as was provided by the sputtering system manufacturer), surface milling of about 2 nm was expected. Therefore, it was presumed that the native SiO_2 on top of the Si substrate had been removed. The roughness analysis of the samples after Ar^+ milling showed improved topographical structure for the glass substrate and substantial roughness improvement (by a factor of about 10) for the Si substrate.

Note that the relatively large particles or bright spots shown in the AFM images were not considered to be a part of the surface properties and had thus been omitted from the roughness measurements. These particles might have landed on the sample due to the environment at which the scanning was performed (not in a cleanroom environment).

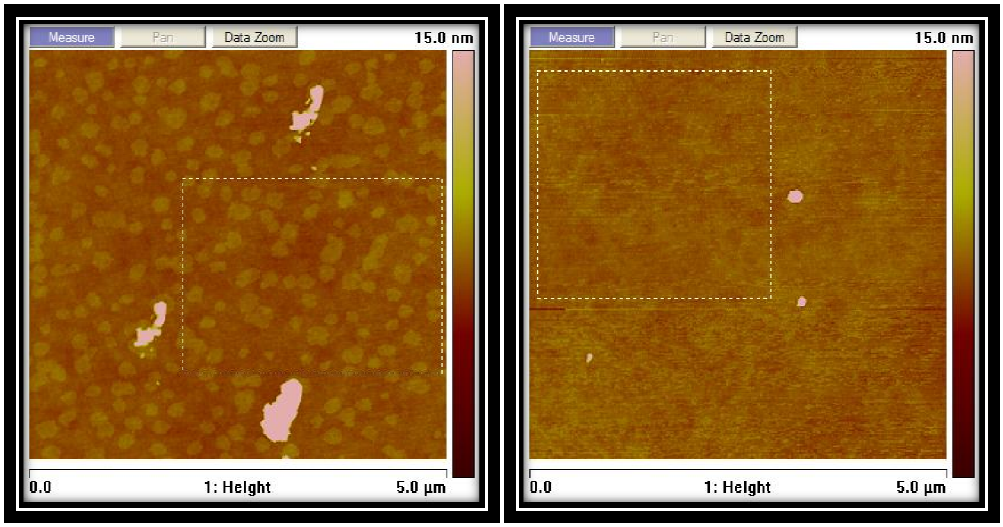

Figure 17: AFM images of roughness measurements: Ra of 0.318 nm before Ar^+ milling (left) and Ra of 0.251 nm after Ar^+ milling (right). The roughness measurements were taken from the highlighted rectangular frames.

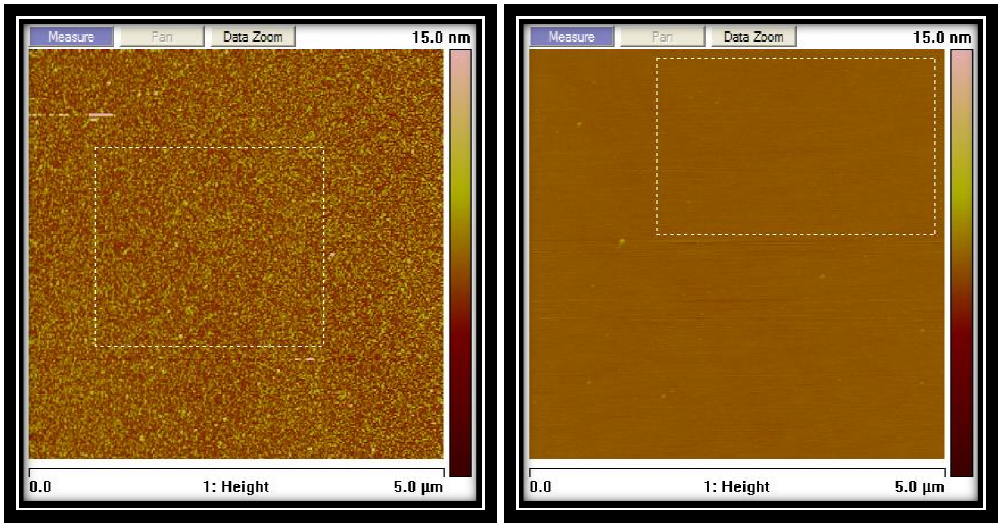

Figure 18: AFM images of roughness measurements: Ra of 0.791 nm before Ar^+ milling (left) and Ra of 0.077 nm after Ar^+ milling (right). The roughness measurements were taken from the highlighted rectangular frames.

A composition of Pd(5nm)/{Co(0.3nm)/Pd(0.55nm)}x7/Pd(5nm) was then sputter-deposited on glass and Si substrates with and without Ar^+ milling in order to determine the surface conditions affect on the magnetic thin film coercivity field. Comparison between glass and Si substrates has also been investigated due the practical application of media fabrication on glass disks for hard disk drives (HDDs). The base and processing pressures were 5 mtorr and 2 x 10^{-7} torrs, respectively. In order to maintain proper uniformity of the thin films, the substrate holder was rotated at 54 RPM. Moreover, the shutters for both the Co and Pd targets where programmed so one shutter opened while the other closed in order to minimize nucleation sites on the thin films. The sputtering rates for both Co and Pd were 0.38Å/s and 0.45Å/s, respectively. Due to the importance of monolayer deposition for both the Co and Pd bilayers, the sputtering rates and thickness uniformity of both thin films were determined via AFM scanning on photo-lithographically defined features exhibiting sharp step-like structures, Figure 19.

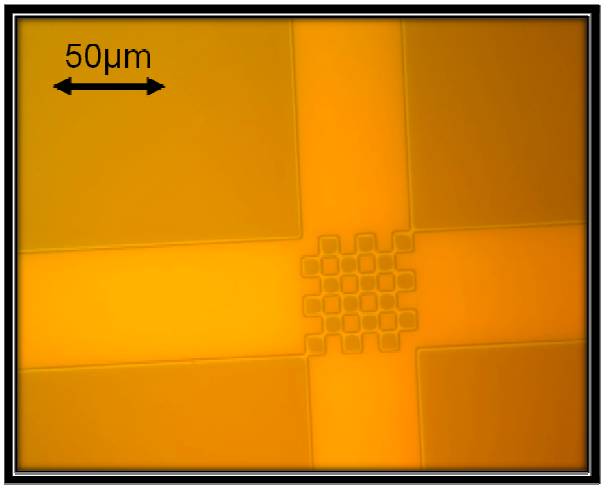

Figure 19: An optical microscope image of a plus-like (+) feature on which thin films were deposited to determine the sputtering rates via AFM scanning. The darker part of the image represents a double layer photoresist.

Figure 20 and Figure 21 show MOKE measurements which reveal that a significant increase in the magnetic media coercivity for both Si and glass could be attained by Ar^+ milling the substrates, respectively. Hence, all the sputter-deposited samples presented from now on had their substrates treated with Ar^+ milling (same milling conditions as listed above).

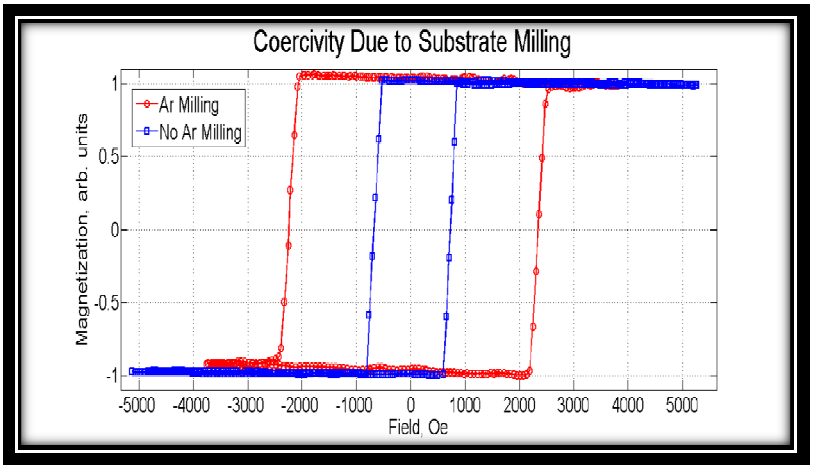

Figure 20: Kerr measurements of Co/Pd multilayers media sputter-deposited on Si substrates with and without Ar^+ milling.

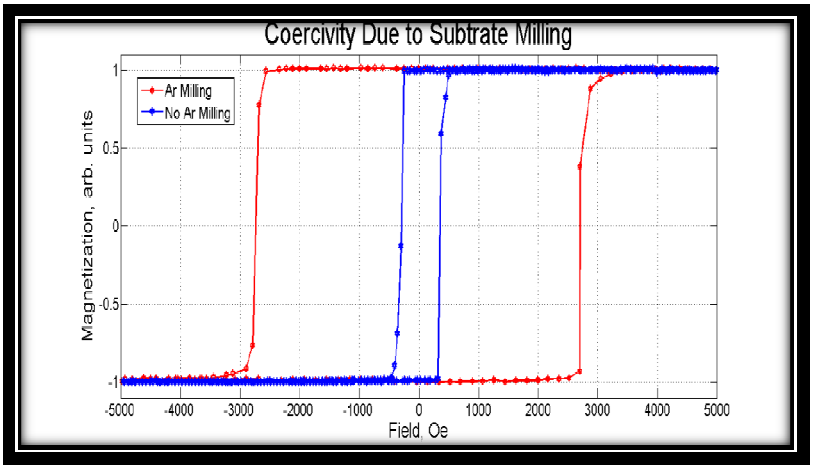

Figure 21: Kerr measurements of Co/Pd multilayers media sputter-deposited on glass substrates with and without Ar^+ milling.

In order to investigate the coercivity dependence on the type of substrate a composition of Pd(5nm)/{Co(0.20nm)/Pd(0.55nm)}x7/Pd(5nm) was sputter-deposited on both Si and glass substrates. All layers were sputtered at 5 mtorr processing pressure. The magnetic media that was deposited on the Si substrates exhibited a higher coercivity value while the media deposited on the glass substrate provided better loop squareness and thus small switching field distribution (SFD), Figure 22.

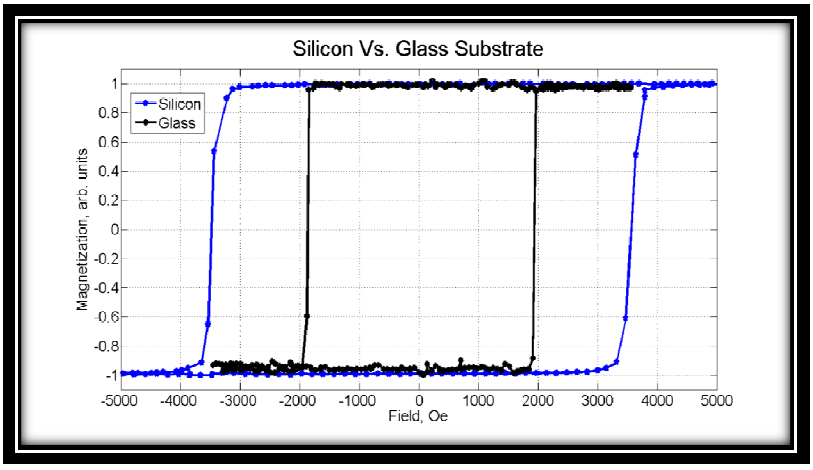

Figure 22: Kerr measurements taken from glass and Si substrates which were sputter-deposited with the same thin film composition.

In order to study the effect of the seed layer on the coercivity field of the magnetic media, the following composition was sputter-deposited on various samples while the Pd seed layer thickness was varied: Pd(x nm)/{Co(0.36nm)/Pd(0.55nm)}x7/Pd(5.3nm), where x was the varying parameter. The processing pressure for the seed and capping layers and for the Co/Pd stack were, 5 and 30 mtorr, respectively. Figure 23 shows the coercivity dependence on the Pd seed layer thickness. The results emphasized a strong coercivity field dependence on the thickness (and thus morphology) of the Pd seed layer, where the highest coercivity field value could be reached with a Pd thickness of about 5 nm.

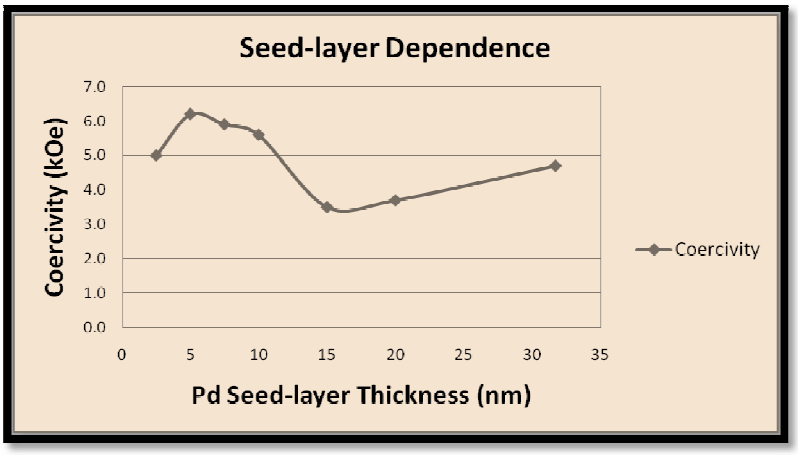

Figure 23: Plot showing the coercivity field dependence of Co/Pd multilayers media on the thickness of a Pd seed layer.

The seed layer was then fixed at a 5 nm Pd thickness with the same bi-layers composition as mentioned above, while the capping layer thickness was varied. The processing pressure for the seed and capping layers and for the Co/Pd stack were, 5 and 30 mtorr, respectively. Figure 24 reveals that the Pd capping layer had a minute affect on the coercivity field of the magnetic media.

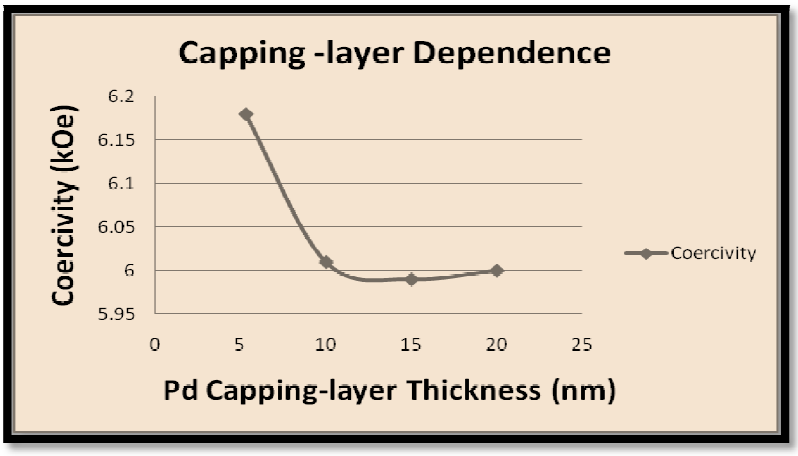

Figure 24: Plot showing the coercivity field dependence of Co/Pd multilayers media on the thickness of a Pd capping layer.

The following composition was then sputter-deposited with the seed and capping layers deposited at 5 mtorr processing pressure, while the Co/Pd bilayers stack was deposited at 5, 15, and 30 mtorr: Pd(5 nm)/{Co(0.36nm)/Pd(0.55nm)}x7/Pd(5.3nm). The results showed an almost linear increase in the coercivity field with increasing processing pressure, Figure 25. Therefore, variation in the processing pressure of decoupled magnetic layers could be utilized to create coercivity field gradient for ML 3D media.

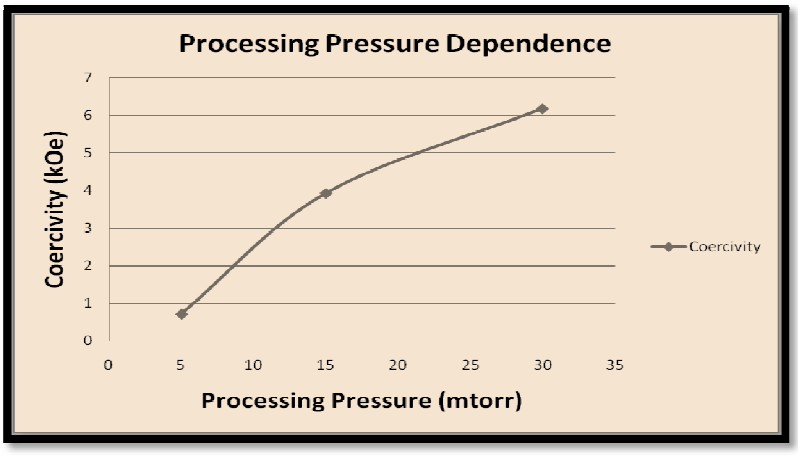

Figure 25: Plot showing the coercivity field dependence on the processing pressure of Co/Pd multilayers media.

Once the coercivity dependence on the substrate milling, capping and seed layers, and processing pressure was determined, an attempt was made to stack two magnetic layers, each exhibiting a different coercivity value. Figure 26 (a) and (b) show hysteresis curves of two 7 bi-layers Co/Pd multilayers magnetic thin films, for which the Co and Pd thicknesses were 0.36 and 0.55 nm, respectively. The same bi-layers composition was sputter-deposited at different processing pressures of 5 and 30 mtorrs, where the higher pressure produced the higher coercivity magnetic layer. Palladium seed and capping layers of about 5 nm were employed in each thin film and were sputter-deposited at 5 mtorr argon processing pressure. The measured coercivity values were approximately 6000 and 750 Oe for the two sets of 30 and 5 mtorr processing pressures, respectively. In general, it is known that the coercivity value for these multilayer structures could be varied from approximately 300 Oe, which is the coercivity of a pure Co, to over 10 kOe, depending on the extent of the "exchange" coupling between two adjacent magnetic grains [72].

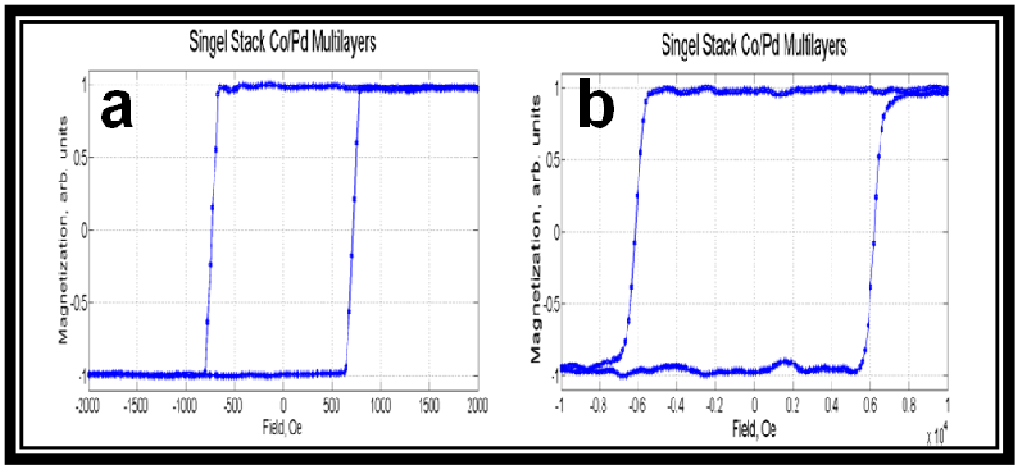

Figure 26: Kerr measurements for two 7 bi-layers Co/Pd multilayers thin films, sputter-deposited with different argon processing pressures (a) 5 mtorr (~750 Oe) (b) 30 mtorr (~6000 Oe)

Co/Pd multilayers-based ML 3D media was then fabricated with two distinct stacks of two different values of coercivity, 750 and 6000 Oe, respectively. Each of the two stacks consisted of 7 Co/Pd pairs and was sputtered at a different processing pressure. The two stacks were deposited on top of each with a separation of approximately 5 nm Pd layer to provide adequate "exchange" decoupling. Each stack had the composition of {Co(0.36nm)/Pd(0.55nm)}x7, where the second layer was sputter deposited at 30 mtorr processing pressure. The resulting product was consequently a dual layer media with the higher coercivity layer being on the top of the stack (close to a writing source). The Kerr measurements, as shown in Figure 27, indicated that indeed the two stacks are not coupled in the quantum-mechanical sense, or, in other words, "exchange" decoupled. Superimposed on the hysteresis graph is the derivative of the magnetization with respect to the applied field. The sharp "spikes" actually represent the switching field distribution of each layer and for the particular case it was shown that the magnetization of each layer could be switched independently.

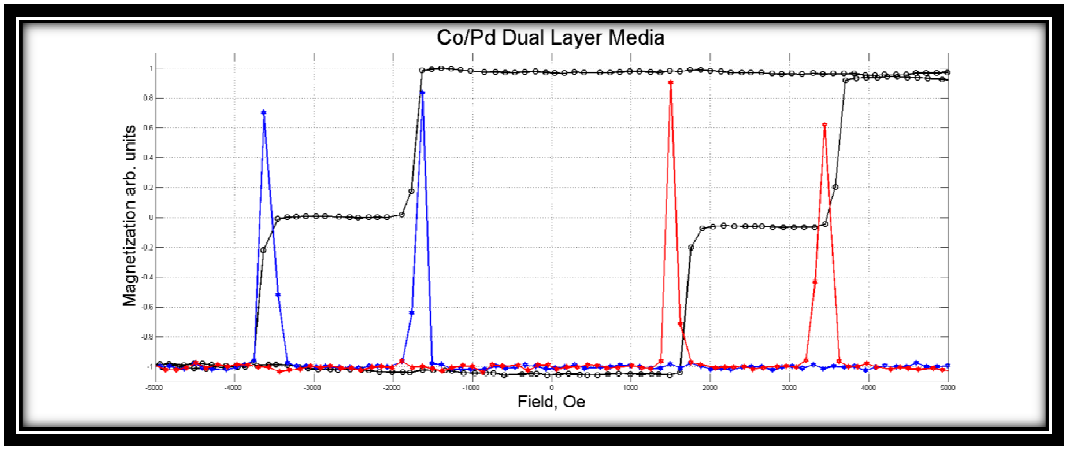

Figure 27: Kerr measurement of a dual layer Co/Pd multilayers-based media showing the independent switching of the two layers. Superimposed, is the magnetization differentiation with respect to the applied magnetic field to illustrate the switching field distribution of each layer.

The dual stack media was then analyzed via P-MOKE. About twenty hysteresis loops were taken, starting from about 1000 Oe and then increasing the maximum applied field by steps of ~ 50 to 100 Oe. For every loop measurement, both layers were firstly saturated in the down direction. Moreover, the Kerr signal was not normalized in order to verify both the relative magnetization and independent switching of the lower coercivity magnetic layer. In other words, if both layers are exchanged decoupled only the lower coercivity layer will switch and the drop in the Kerr rotation signal should be proportional only to the moment of this layer. The results clearly showed that selective switching of the lower coercivity layer magnetization could be achieved with magnetic field ~ 1500 Oe lower than the higher coercivity layer, Figure 28.

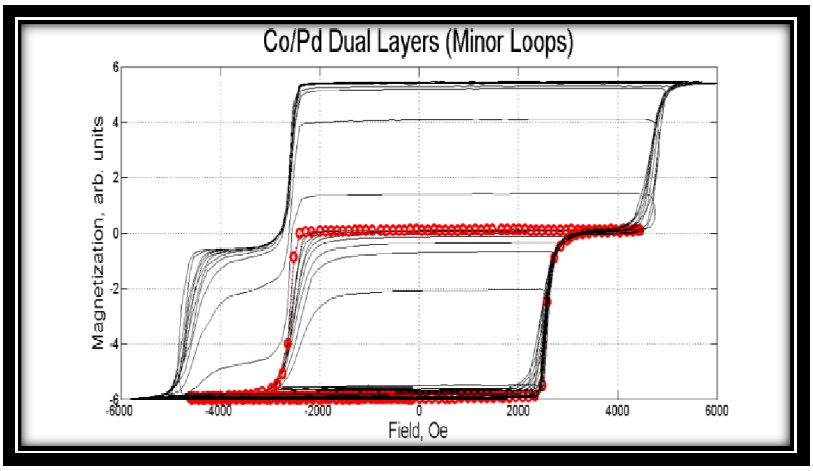

Figure 28**:** Kerr measurements indicating that both magnetic layers within the dual stacks ML 3D media are "exchange" decoupled.

As was expected from the previous analysis of the coercivity dependence on the substrate type, the dual layer magnetic thin film which was sputter-deposited on glass exhibited higher coercivity field values for both layers, Figure 29.

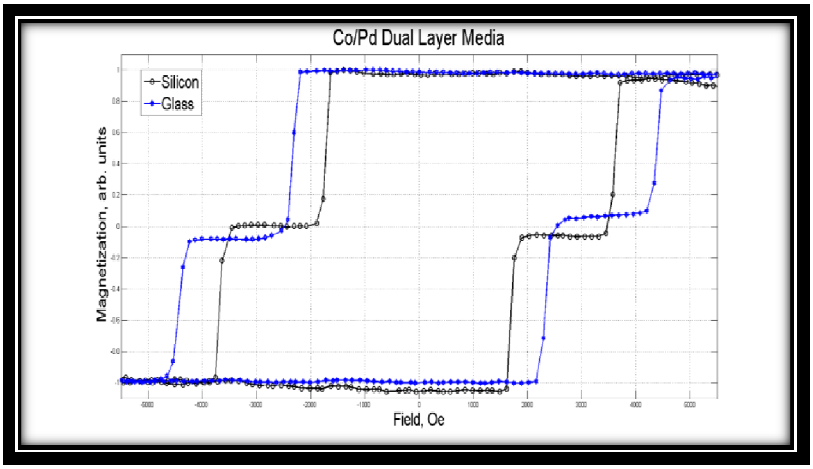

Figure 29: Kerr measurements of a dual stacks media sputter-deposited on silicon and glass substrates.

Ultimately, it would be necessary to stack as many layers across the bulk of the material while making sure that the signals generated from each layer would not cancel the others. Hence, high importance should be given to minimize the thickness of decoupling layers. In order to determine the proper thickness of a Pd decoupling layer, the same dual layer composition was sputter–deposited while the Pd interlayer thickness was varied. For the glass substrate, a 10 nm Pd thickness resulted in lower coercivity fields for both layers with relatively low SFD. A 3 nm thick Pd layer already resulted in higher and overlapping SFD for both layers with a slight decrease in the coercivity field of the top layer. In other words, exchange coupling between the two layers started to occur at a Pd thickness of about 3 nm.

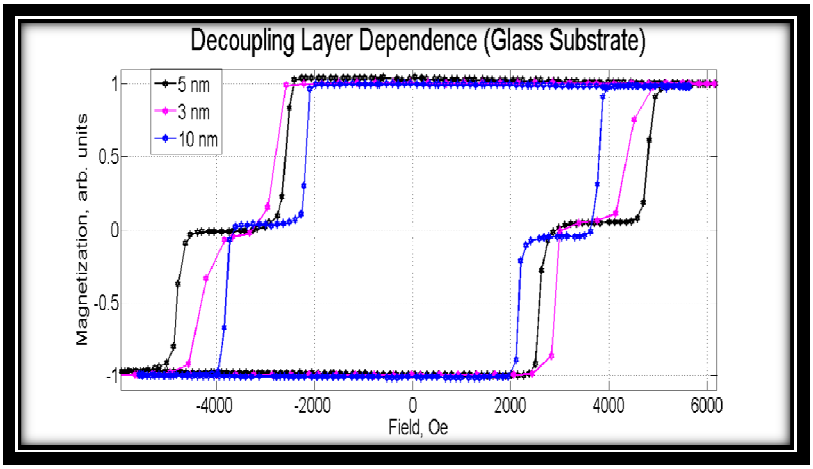

Figure 30: Kerr measurements of dual layer Co/Pd multilayers-based media sputter-deposited on glass substrates with different Pd decoupling layer thickness.

In the case of the Si substrate, an increase in the coercivity of the bottom layer was noted for the 10 nm Pd layer. The 3 nm Pd decoupling layer resulted in an increase in coercivity field for both the bottom and top layers. Both layers also exhibited relatively low SFD. Therefore, substrates with surface conditions similar to the ones found in the Si substrate will be proper candidates in the ultimate goal of stacking the maximum number of layers per unit length across the volume of a ML 3D media.

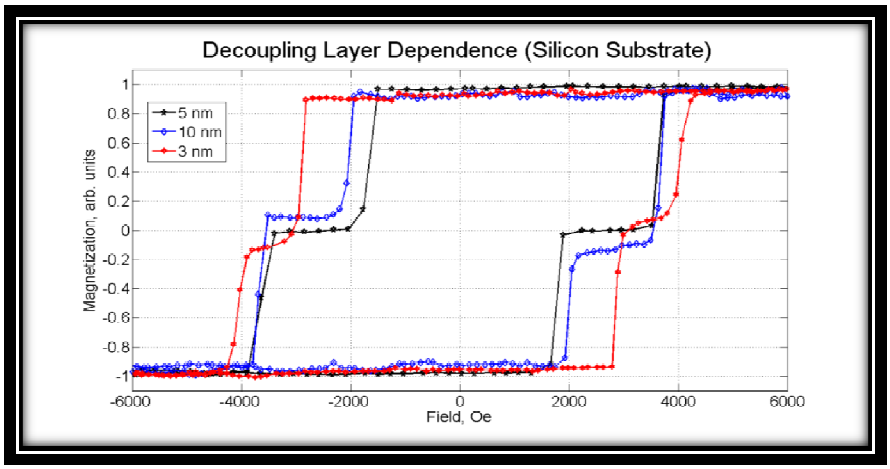

Figure 31: Kerr measurements of dual layer Co/Pd multilayers-based media sputter-deposited on silicon substrates with different Pd decoupling layer thickness.

The anisotropy field of the dual layer media was analyzed with a vibrating sample magnetometer (VSM) as a mode of a Physical Properties Measurements System (PPMS) by quantum design. The Si sample was glued to a glass rode in such a manner that the applied field was along the in-plane direction of the substrate. The analysis was performed with a pressure of ~ 1 mtorr at room temperature. A magnetic field sweep with steps of 50 Oe/sec was used to acquire the loop. The results indicate that the in-plane magnetization switching is mainly due to rotation. Thus, strong perpendicular anisotropy is expected for the dual stack media with anisotropy field (H_K) of about 2 Tesla.

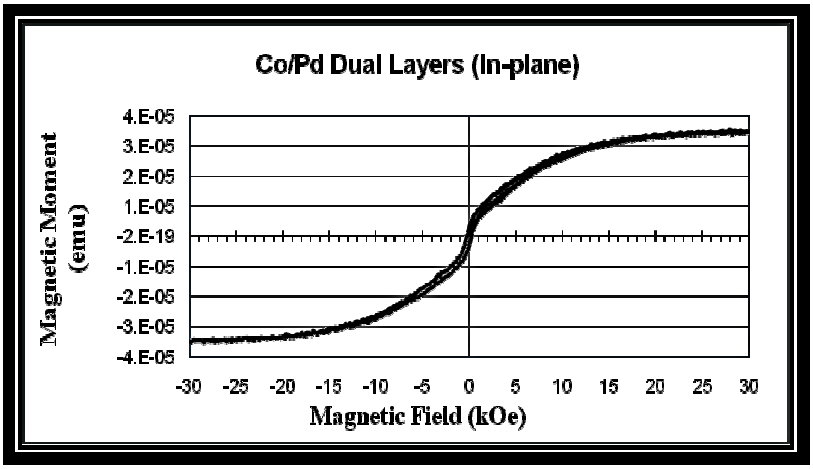

Figure 32: In-plane VSM measurement of a dual Co/Pd multilayers stack.

An FEI Nova 200 dual beam FIB/SEM system was used in order to fabricate a tunneling electron microscope (TEM) cross-sectional sample. TEM analysis was performed with High Resolution TEM FEI Tecnai G2 F20 system. The TEM results do not show signs of individual Co/Pd bi-layers as in the manner the media was sputtered-deposited. Instead, a polycrystalline layer about 30 nm thick is present (in good agreement with the total intended thickness of the whole thin film composition), Figure 33. Selected area diffraction (SAD) pattern of the film and part of the silicon substrate shows diffraction

rings indicative of a polycrystalline material, Figure 34. Indexing those rings, an FCC structure having a lattice parameter around 3.89Å has been found. Depending on the reference, this is consistent with either Pd (lattice parameter 3.8 - 4.0Å) or CoPd2 (3.83Å). A dark field image from these rings indicated crystallite sizes below 20 nm.

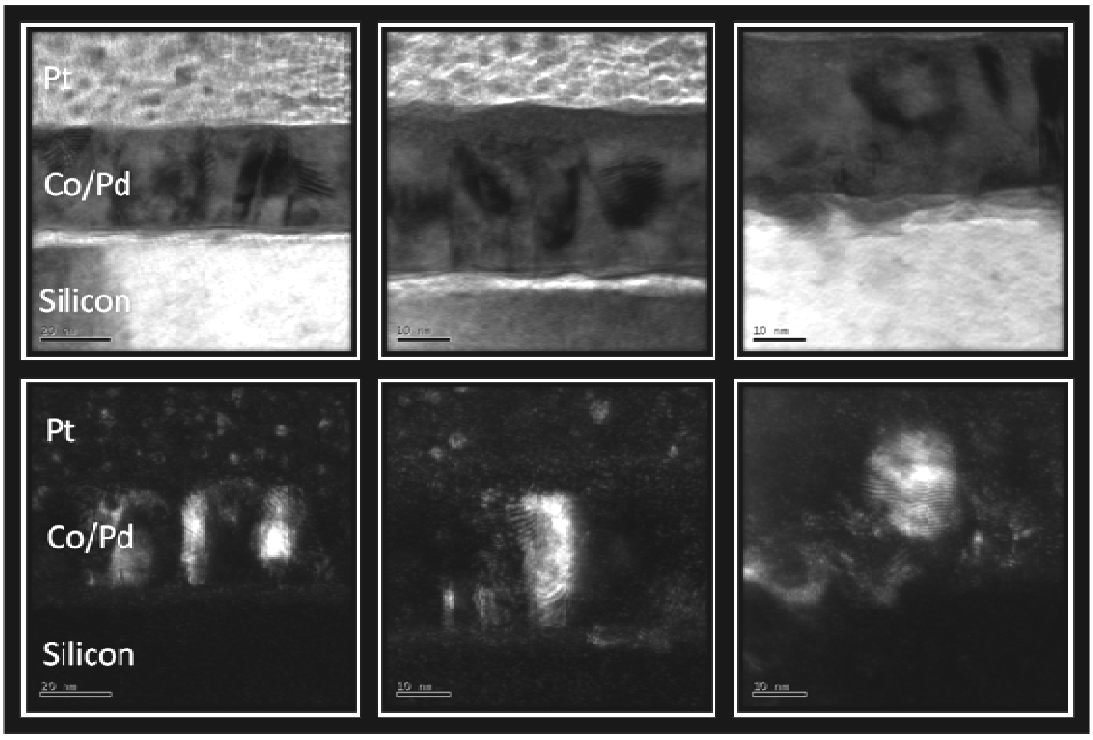

Figure 33: Bright-field (top row) and the corresponding dark-field (bottom row) TEM cross-sectional images of the dual Co/Pd multilayers stack.

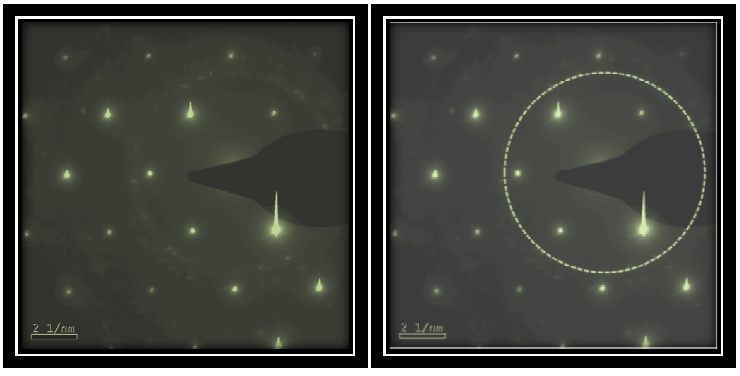

Figure 34: SAD pattern showing single-crystal peaks for the Si substrate and polycrystalline diffraction rings for the dual layer media. Right image highlights the first order diffraction ring.

Energy Dispersive Spectrometry (EDS) was used to verify the presence of both Co and Pd, Figure 35. Since the presence of Co has been verified both with EDS and the Kerr measurements, it seems that the microstructure of the dual layer thin film is polycrystalline CoPd2 alloy. Due to the similarities in lattice spacing between CoPd2 and Pd, it is also difficult to visualize the decoupling Pd layer. The HRTEM images shown in Figure 36 further underscore the polycrystalline nature of the dual layer stack.

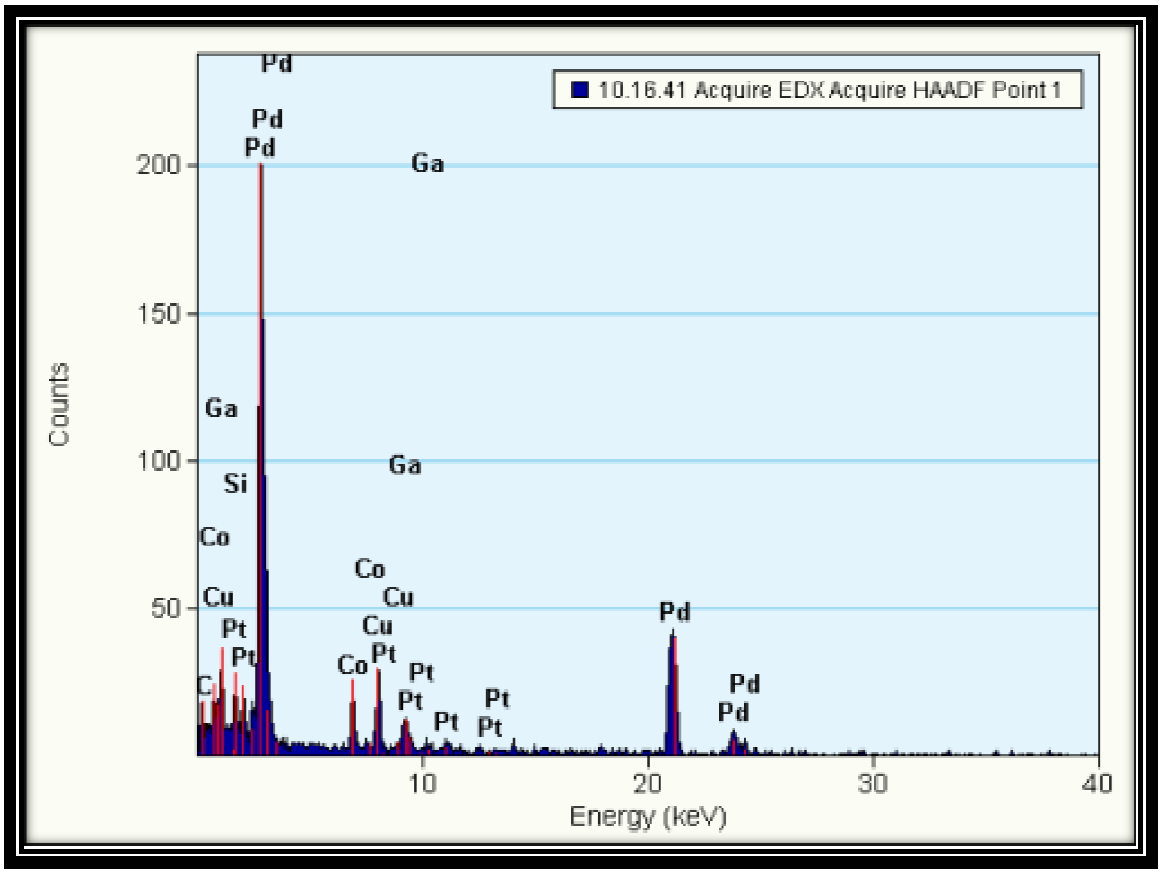

Figure 35: EDS analysis of the dual stack media showing the presence of both Co and Pd

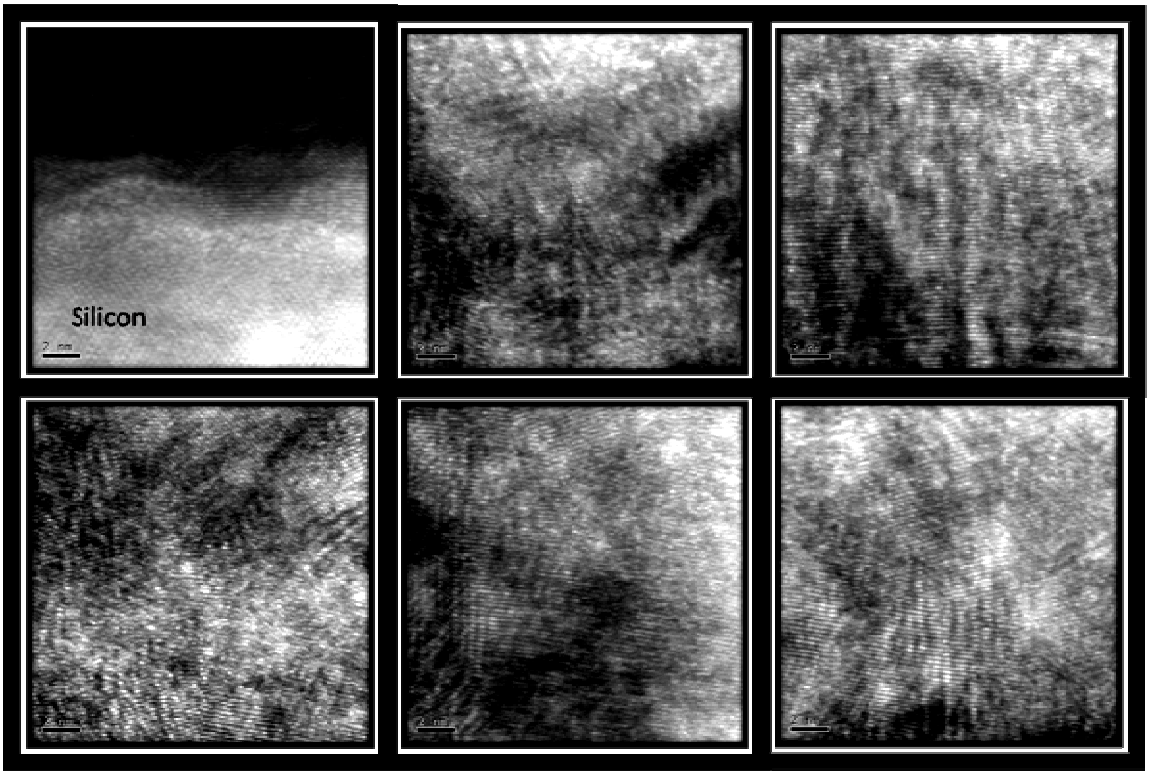

Figure 36: HRTEM images underlying the polycrystalline nature of the dual layer Co/Pd multilayers media.

Combinational (Co/Pd)/(Co/Pt) Multilayers ML 3D Media

In order to increase the number of decoupled layers to a maximum, other materials will need to be combined to form the 3D structure which exhibits a Curie temperature or coercivity gradient. In the example below, a combination of both Co/Pt and Co/Pd multilayers layers has been sputter deposited in order to develop a highly exchanged decoupled composition, suitable for 3D patterned media configurations. Two separate compositions of Pt(5nm)/{Co(0.45nm)/Pt(0.55nm)}x7/Pt(5.2nm) and Pd(5nm)/{Co(0.25nm)/Pd(0.55nm)}x7/Pd(5.3nm) were sputter-deposited on Si substrates. For both compositions, the base and processing pressures were ~ 2 $x10^{-7}$ torrs and 5 mtorrs, respectively. Figure 37 shows the magnetic properties of both thin films,

where the Co/Pt compositions exhibited relatively low coercivity, the Co/Pd composition showed higher.

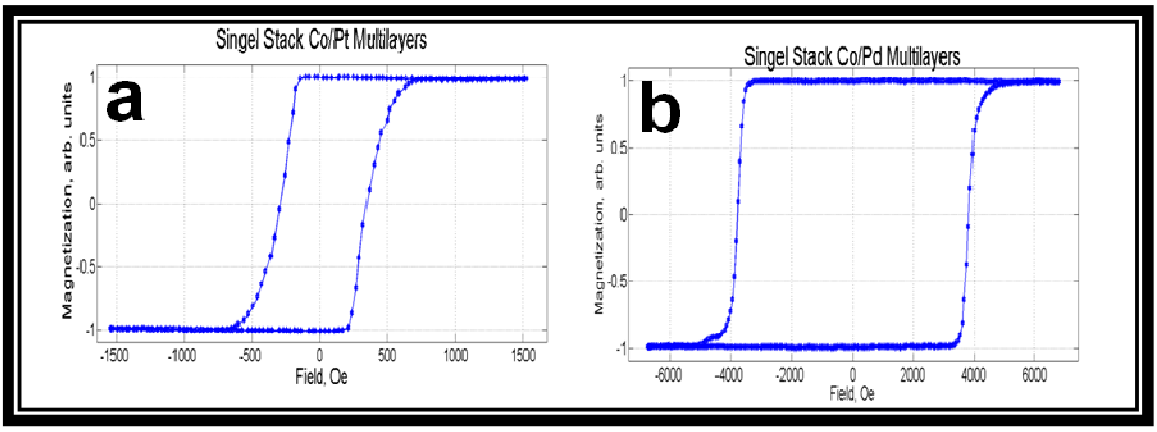

Figure 37: Kerr measurements of (a) low coercivity Co/Pt multilayers media and (b) high coercivity Co/Pd multilayers media.

The two layers where then stacked on top of each other in the following manner: Pt(5nm)/{Co(0.45nm)/Pt(0.55nm)}x7/Pt(2.5nm)/Pd(2.5nm)/{Co(0.25nm)/Pd(0.55nm)}x 7/Pd(5.3nm). In other word, the higher coercivity layer was deposited last. The following figure shows a dual layer ML 3D media with perfectly decoupled magnetic layers, each exhibiting a unique coercivity value and composition.

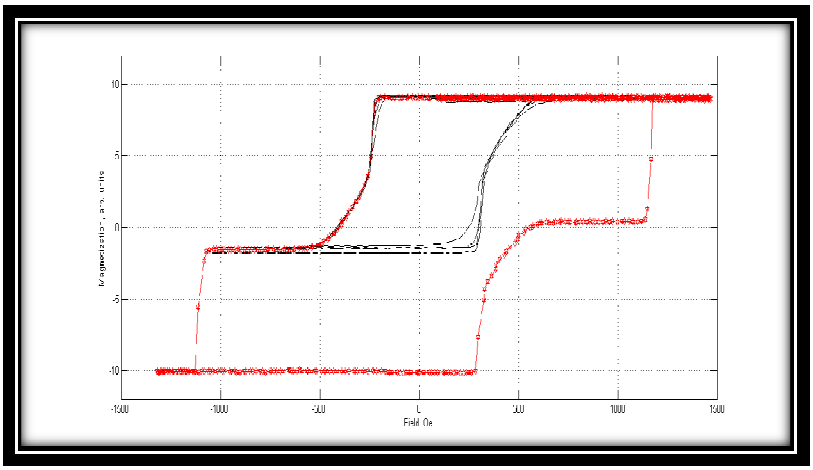

Figure 38: Kerr measurements of combinatorial Co/Pt and Co/Pd multilayers dual stack media.

It is believed that at least over six layers (or over 2^6 = 64 signal levels) could be independently fabricated and accessed in the above described manner. As earlier mentioned, using a different type of media and such signal enhancing mechanisms as the integration with a patterned soft underlayer and even soft interlayers might further increase signal to noise ratio (SNR) in ML 3D recording systems. The following section will address the encoding of a ML 3D system.

Multilevel Data Encoding

To further perfect the concept of generating a multilevel signal, various mechanisms have been developed and explored. The general task is to maximize the number of signal levels while maintaining SNR between the signal values in each pair of adjacent levels above approximately 5 dB. The 5 dB value is dictated by the requirements of the novel data coding methods, as described below. Before going into details of the new multilevel coding method, it may be helpful to recall how conventional coding works.

Summary of Conventional Encoding Methods

FM encoding has a simple one-to-one correspondence between the bit to be encoded and the flux reversal pattern. One only needs to know the value of the current bit. So called modified frequency modulation (MFM) improves encoding efficiency over FM by more intelligently controlling where clock transitions are added into the data stream; this is enabled by considering not just the current bit but also the one before it. This "looking backwards" allows improved efficiency by letting the controller consider more data in deciding when to add clock reversals. Run limited length (RLL) encoding takes this technique one step further. It considers groups of several bits instead of encoding one bit at a time. The idea is to mix clock and data flux reversals to allow for even denser packing of encoded data, to improve efficiency. The two parameters that define RLL are the *run length* and the *run limit* (and hence the name). The word "run" here refers to a sequence of spaces in the output data stream without flux reversals. The run length is the *minimum* spacing between flux reversals, and the run limit is the *maximum* spacing

between them. As mentioned before, the amount of time between reversals cannot be too large or the read head can get out of sync and lose track of which bit is where. Finally, so called partial-response maximum likelihood (PRML) sequence detection is even more advanced and today most common method. Partial-response means controlled inter-symbol interference (ISI). That is, the data represented by the received waveform are packed so closely together that they overlap (interfere). The "controlled" part means that there is some identifiable structure to the overlapping. This structure is "taught" to a sophisticated sequence detector that looks only for the possible controlled patterns of ISI in the received waveform. This provides a much more robust detection method in the presence of noise. This type of detection is often used with trellis coding to further improve detection. Trellis coding encodes the data such that the possible received sequences that are most similar are not used. This provides extra capability to distinguish between received waveforms in the presence of noise and distortion.

New Error-correcting Techniques for Multilevel Magnetic Recording

In the previous sections, it is shown that multilevel recording can substantially increase the capacity of storage systems versus its conventional two-level counterpart. On the other hand, multilevel recording reduces the separation between different amplitude levels (given the same power constraints), which can make the entire system more error-prone as more data becomes incorrectly recorded or retrieved in the "read-write" channel. To address this problem in our proposal, we intend to employ powerful error-correcting codes. In general, efficient error correction can reduce the overall error rates by a few orders of magnitude, which can also lead to higher recording densities in the entire

storage system. Thus, error correction becomes an efficient tool that can greatly reduce the errors caused by multilevel recording and higher densities.

The main overhead caused by many error-correcting algorithms is their excessive complexity or - equivalently - prohibitively slow data processing. Therefore, our main goal in this part of our proposal is to design the error-correcting techniques that combine powerful error-correcting performance with fast feasible processing. Namely, we intend to design the algorithms that approach optimum, maximum likelihood (ML) decoding without significant degradation of the data transmission rate in the overall system.

The existing methods of code design can be divided into three different categories. In the first group of graph-based techniques, a linear code is associated with some bipartite graph, with code symbols on the one side, and their parity checks on the other. Iterative decoding is then used similar to belief propagation in neural networks. This method combines relatively simple processing and powerful performance; however, it becomes efficient only on the relatively long blocks of thousand bits. The lack of analytical tools required to estimate low output error rates (of 10^{-12} and less) is another drawback of iterative techniques.

The second group employs algebraic methods. Here a code consists of a set of polynomials of some limited degree taken over a Galois field; a string of all values of a specific polynomial is called a codeword. This technique is especially efficient for large (non-binary) alphabets and leads to the optimum Reed-Solomon (RS) codes, which are currently designed into most storage systems. However, RS codes have relatively high complexity in correcting multiple errors. This excessive complexity combined with long

operations in Galois fields can slow down the overall performance, especially in multilevel signaling, which requires multiple error correction.

Finally, the third group consists of various concatenated techniques, which combine good short codes into the longer ones. Invented by Forney over 40 years ago, this technique still manifests itself as one of the most efficient, thanks to simple decoding procedures of multiple error correction. To further reduce decoding complexity, we intend to design new concatenated techniques using simple constituent codes.

Reed-Muller codes and Their Recursive Decoding

The technique to be used in the project has some similarities with general concatenated design. The main new tool is to employ constituent codes that can be considered as "self-contained" recursive constructions. Such constructions - already known in coding theory - preserve all the properties of the shorter, building, codes. These recursive techniques result in a simple low-complexity decoding, which repeatedly employs the same code properties multiple times on increasing lengths.

Reed-Muller (RM) codes represent the most notable example of recursive constructions and have been explored for five decades. These codes also yield a simple recursive decoding, which has been recently designed and analyzed in papers [73,74,75,76]. Namely, any RM code (m, r) of length $n = 2^m$ and distance $d = 2^{m-r}$ can be obtained from the two RM codes (m-1, r-1) and (m-1, r) 1 of length n/2. The decoding process can be relegated further using four RM codes of length n/4. After a few steps, the decoder finally arrives at the trivial end codes RM(m – r, 0) or RM(r, r), which are either fully redundant (repetition codes) or non-redundant (full codes). For both types, it is easy to use powerful

ML decoding. On the other hand, the received channel symbols are only recalculated in all intermediate recursive steps without any decoding. Due to this, decoding complexity has a low order of n log n or even a linear order n if incomplete hard decision decoding is concerned.

This combination of powerful end decoding and fast intermediate processing outperforms all other non exponential algorithms known for RM codes. In particular, it turns out that the algorithms of [43,44,45] substantially outperform the two conventional techniques of bounded distance decoding and majority decoding. Namely, new recursive techniques:

- Increase ln d times the number of errors d/2 corrected by bounded-distance decoding (for most error patterns);
- double the number of errors (d ln d)/4 corrected (with high probability) by conventional majority decoding; for the moderate lengths of 128 to 512, these techniques were enhanced in [4] with list decoding, which
- gives near-optimum performance (within 0.25 dB of ML decoding) with feasible complexity;
- outperforms all other decoding algorithms currently known for all existing codes.

Some results are given above in Figure 39 (a) and (b) for different RM codes of lengths 256 and 512, respectively. An important conclusion is that RM codes yield near-optimum performance and fast processing with complexity of order n log n. Then in Figure 40 (a) and (b), also the results for longer blocks obtained by concatenating different RM codes are plotted. In summary, these data illustrate that concatenated RM codes combine fast feasible processing and very low SNR of 2 to 3 dB on the Gaussian channels for various

block lengths of 256 to 4000 bits. These algorithms could be further enhanced in the future to correct specific (non Gaussian) error models that pertain to magnetic recording channels.

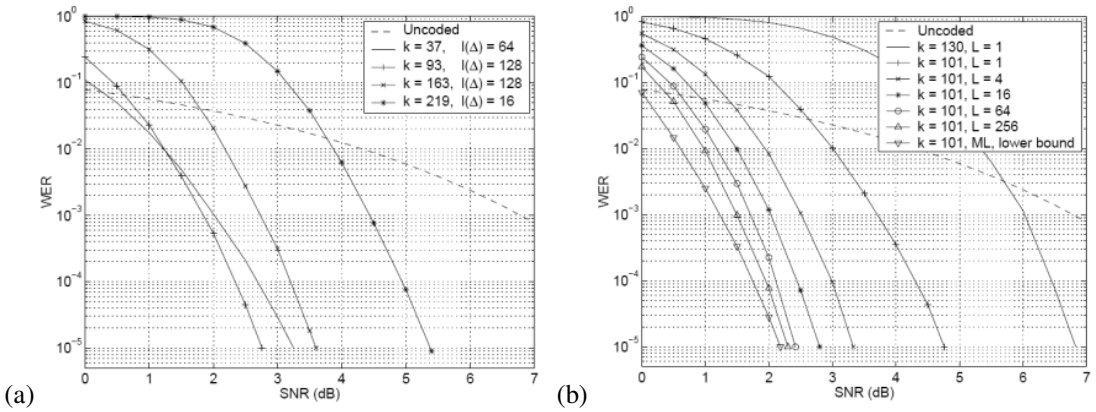

Figure 39: **(a)** exact bounds on Word Error Rates (WER) for ML decoding of RM codes of orders 2 to 5 on the length 256. The legend includes the list sizes l(Δ), for which recursive permutation algorithm performs within Δ = 0.25 dB from ML decoding. **(b)** Word Error Rates (WER) for the (512, 101)-subcode of the (512, 130) RM code of order 3. Different curves represent WER for recursive list decoding for varying lists L.

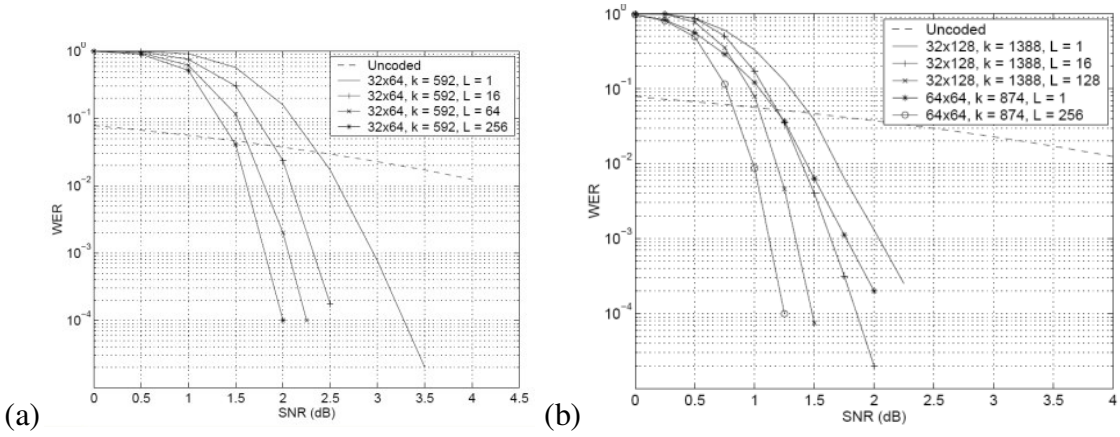

Figure 40: **(a)** Concatenated (n, k) code of length n = n1 × n2 = 2048, with variable lists of size L. **(b)** Concatenated (n, k) codes of length n = n1 × n2 = 4096, with variable lists of size L.

Conclusion

This chapter presents a review of the research to develop a multilevel mode of nanomagnetic 3D recording, a promising and challenging solution to increase the capacity of electronic and computer devices. The study is conducted from the system perspective. It is anticipated that through marrying the expertise in magnetic recording and state-of-the-art data encoding, some of the features of multilevel magnetic recording (multilevel signal and data coding) could be extended to any alternative magnetic data storage technology to further increase its data capacity by several factors. The key to the analyzed multilevel system is exploitation of the recently proposed concept of 3D media optionally with patterned soft magnetic underlayer and interlayers. Among the unique properties are the substantially increased (compared with conventional technologies) recording and sensitivity fields used for writing and reading information, respectively. This field increase results in adequate signal to noise ratio (SNR) to accommodate over 40 signal levels with 5 dB difference between any two adjacent levels. The proposed data coding methods are aimed at providing sufficient bit error rates for a system with a SNR of the order of 5 dB.

Ion Implantation for ML 3D Magnetic Recording Media

In the previous section, a detailed analysis was presented on how to vary the coercivity of different magnetic layers in ML 3D media by changing the processing pressure of sputter-deposited Co/Pd multilayers thin films or by combing Co/Pt (lower coercivity) with Co/Pd multilayers (high coercivity) thin films. In this section another method of altering the magnetic properties in magnetic thin films is presented. Ion implantation/irradiation can alter the coercivity, squareness, magnetization and other magnetic properties of magnetic thin films and may be used in the future to fabricate ML 3D media with coercivity and/or Curie temperature gradient across the vertical dimension of the media.

Introduction

The Focused Ion Beam milling technique has become a de-facto standard for hi-resolution nanofabrication. Since the FIB-milling process does not rely on specific chemical composition of the media used, features as small as 10 nm can be milled for a wide range of materials. Moreover, directional nature of the beam patterning helps to form three-dimensional structures virtually impossible to manufacture using other lithography techniques, such as e-beam or photolithography [77,78]. Another fundamental advantage of the FIB is that the surface of the material used does not need to be exposed to any kind of resist and/or undergo thermal treatment (such as baking of photoresist), which can alter the properties of some magnetic thin films. Furthermore, the entire procedure is performed in a vacuum chamber and multiple layers of structure patterning is also possible. These advantages make FIB especially attractive for rapid fabrication of prototype magnetic media and nanodevices [79,80,81,82].

However, the FIB and related ion milling nanofabrication methods possess their own inherent shortcomings. First, ion irradiation in vacuum chamber may cause significant local heating and subsequent annealing of the material used. Second, ion implantation/doping may change the material properties. Finally, the secondary deposition of the milled material may also change the properties of the final product. These problems are well understood, and numerous publications report the effect of heating and implantation of specific materials into different structures/substrates. Typical examples of such studies include implantation of 10 keV N^+ ions into crystalline Ni and amorphous FeB ribbons [83], Ar^+ treatment of of Fe/Cr multilayers [84] and Co/Pd

multilayers with energy around 200 keV [85,86], as well as the effect of high-energy 400 and 800 keV Ar^+ ions on Au/Fe multilayers [87]. Thermal annealing effect on the magnetic properties of multilayers based thin films has also been extensively studied [88,89]. It was suggested, that the implantation itself may become beneficial for fine tuning of the magnetic properties of magnetic recording medium [90].

As an illustration of the ion implantation effect on the magnetic properties of magnetic thin films, an array of nanostructures was FIB-milled from a CoCrPt-based longitudinal magnetic media. The ion beam dose was increased from a minimum for the top pattern (barely milling the protective layer = ion radiating) to a maximum for the bottom pattern (milling of the magnetic layer), Figure 41. Magnetic Force Microscopy (MFM) imaging reveals that decoupling of the nanostructures can occur much before the complete milling of the magnetic layer and hence indicating that implantation of gallium ions is sufficient to decouple the magnetic nanostructures, Figure 42.

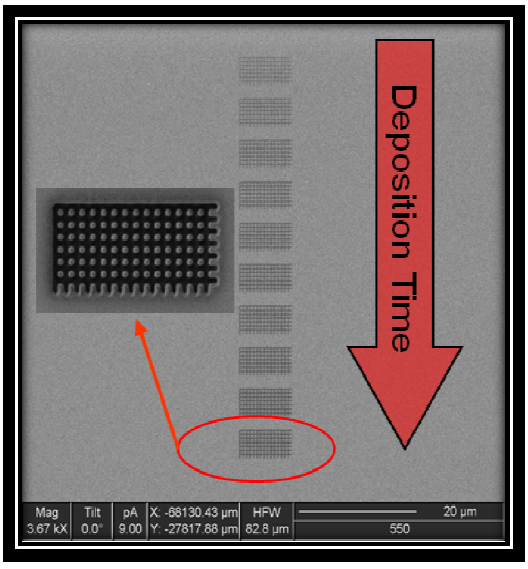

Figure 41: SEM image of FIB-milled patterns of nanostructures from a relatively low (minor milling of the protective layer) to a relatively high Ga^+ ions does (milling of the magnetic layer).

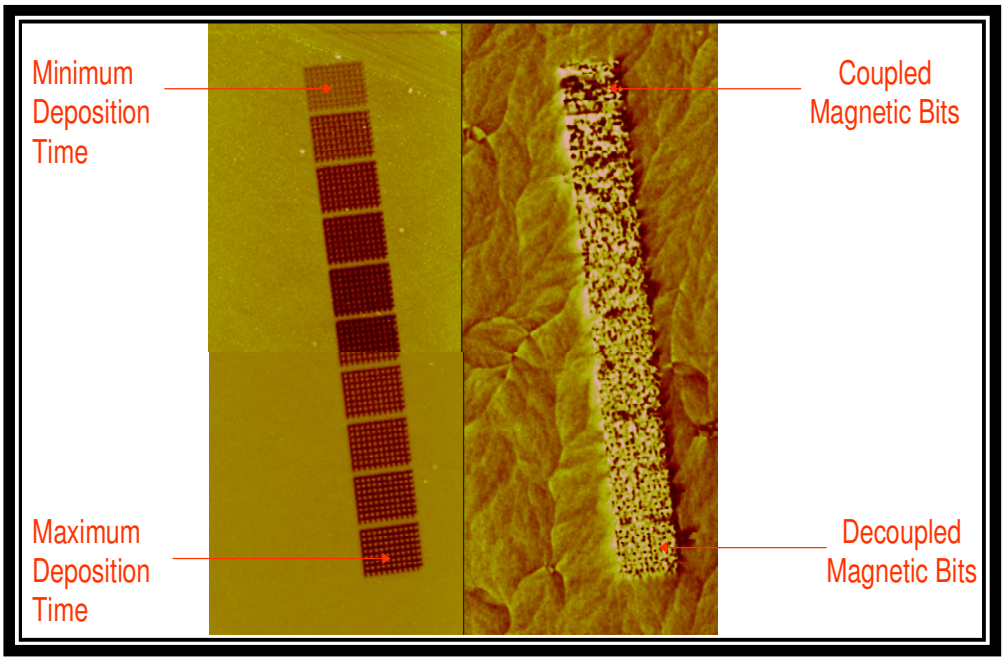

Figure 42: AFM/MFM images illustrating the effect of Ga^+ ions implantation on CoCrPt-based longitudinal magnetic recording media in which a Ga^+ ion dose much less than the one required to completely remove the magnetic thin film can exchange-decouple the magnetic nanostructures.

The experimental focus presented in this section will be on thorough characterization of Co/Pd multilayers medium treated with different gallium ion irradiation doses of extremely low energy ranging from 5 to 25 keV. Special attention is paid to the uniformity of the results: the very same film rather than a number of samples is used for all measurements and the probed sites are set at most 1 mm apart from one another.

Experimental Setup

Pre-deposition Sample Preparation

In order to adequately measure the effect Ga^+ ions implantation with different doses, it was of particular importance that the ion implanted regions of the magnetic material lie within few hundreds of microns from each other to effectively ensure the uniformity of the thin film composition within the region of interest.

A photolithography-template was thus transferred to a Si substrate to produce numerous vacant squares, each numbered, ranging from about 5 x 5 μm^2 to 30 x 30 μm^2. Figure 43 shows an optical image of the square patterns from a bright field mask. The substrates were prepared by first spin-coating AZ 5214E photoresist at 4000 RPM for 40 seconds (~ 1.5 µm thick), followed by baking at 115 °C for 2 minutes. A second type of photoresist layer of LOR 3B was spin-coated at 4000 RPM for 30 sec (~ 0.5 µm thick), followed by baking at 180 °C for about 5 minutes. The mask shown in Figure 43 was then used to expose the squares pattern onto the double photoresist layers. A Karl Suss MA-6 mask aligner was used to expose the patterns with UV light with power of 275 watts for 2.5 sec. In order to obtain the square pattern resist-free, the pattern was inversed by first baking the sample at 115 °C for 3 minutes and then flood exposing it for 60 seconds. The pattern was then developed with MF319 developer for 20 seconds. Figure 44 shows post developed optical image of one of the 20 x 20 μm^2 grid. Following the thin-film sputter-deposition, a two-step liftoff procedure was performed. The sample was firstly dipped in a Remover PG solution for about 1 min in order to remove the LOR 3B resist layer, followed by Acetone dipping to remove the AZ 5214E resist layer.

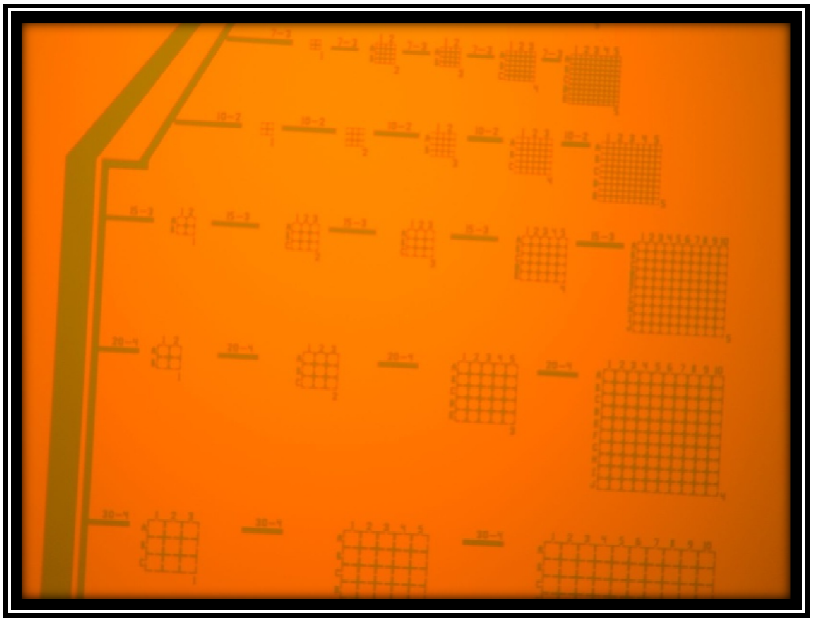

Figure 43: Optical image of squares pattern taken directly from a bright field mask

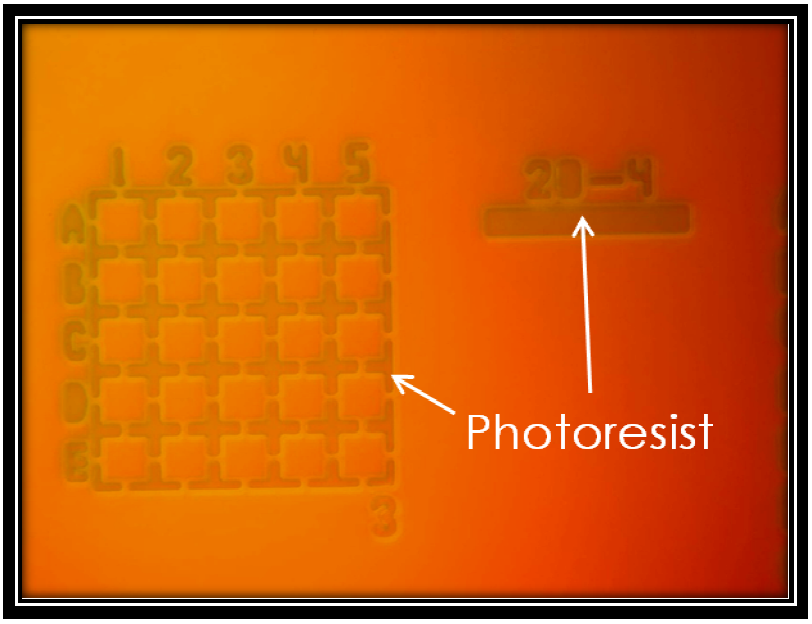

Figure 44: Optical image of post-developed double-layer photoresist showing a pattern grid with 20 x 20 μm^2 squares. The area of the squares is resist free.

Thin Film Deposition

An AJA international ATC ORION 5 HV sputtering system was used to sputter-deposit the thin film on the squares pattern grids, Figure 43 and Figure 44. The system features a con-focal sputter source flange oriented at specific angles. The specially designed chimney/ground shield/shutter system allows a high degree of deposition uniformity over substrates over twice the target diameter. The sample holder can also rotate with a rotational speed up to 54 RPM. The samples are inserted to the chamber through a load-lock mini-chamber, Figure 47. The system supports up to five targets and 4 power sources, 2 DC and 2 RF, Figure 48. One of the RF sourced is used for sample cleaning. The system is fully automated, enabling synchronous multilayers thin film deposition.

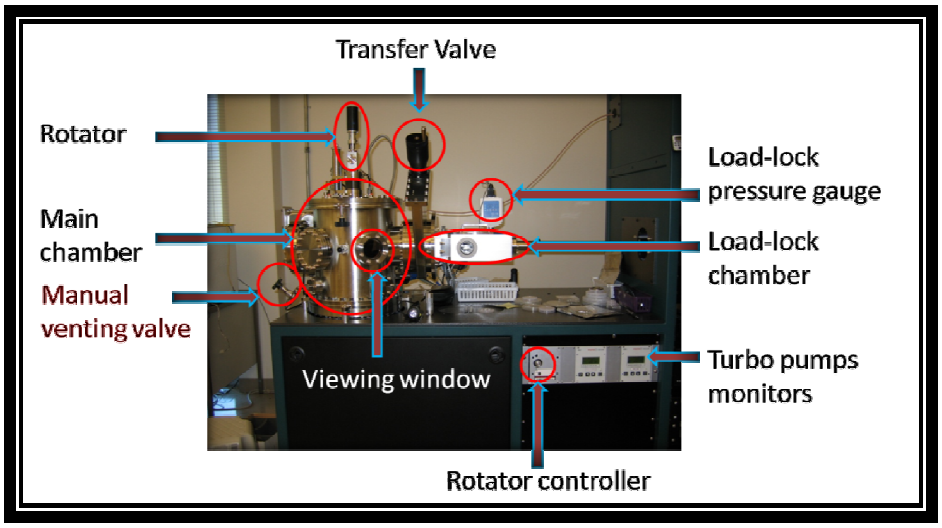

Figure 45: A photo showing the main components of sputtering system

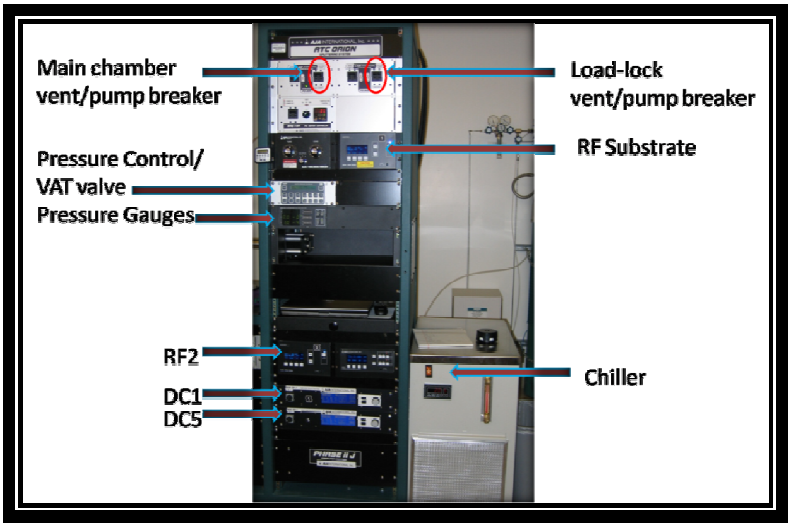

Figure 46: A photo showing the controlling instrumentations of the sputtering system.

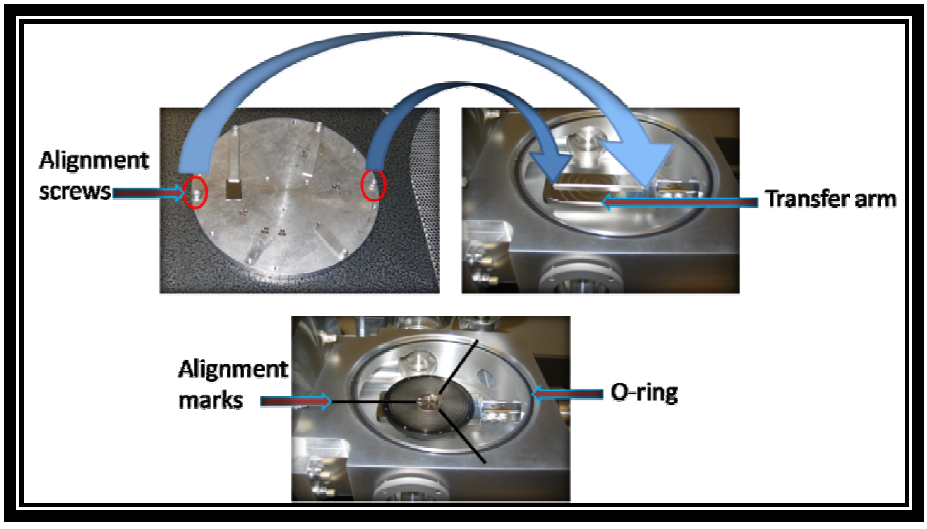

Figure 47: A photo showing the load-lock chamber together with the sample holder platform.

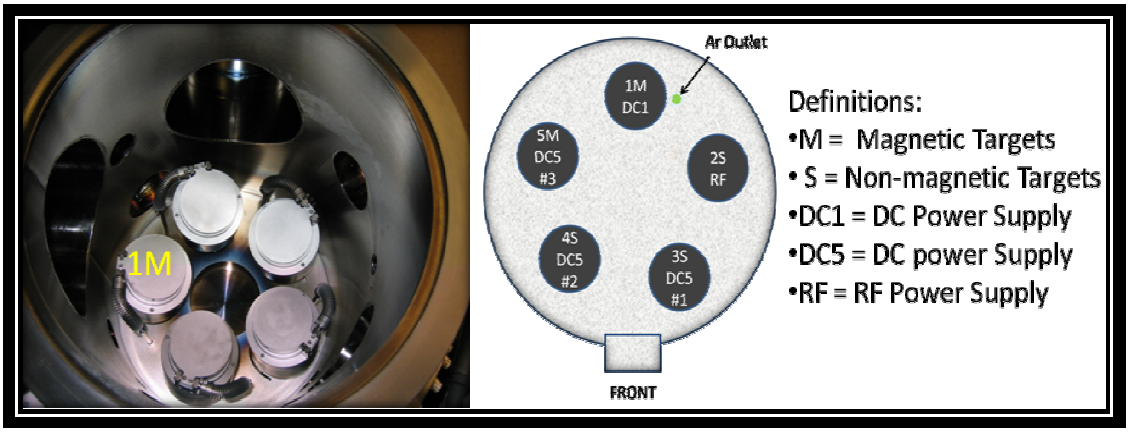

Figure 48: A photo of the main chamber showing the orientation of 5 2" sputtering sources (left) and a schematic of the sources' fictionalization.

A Co/Pd multilayers composition was sputter-deposited on a Si [100] substrate having the square patterns. The base pressure and processing pressure were $1.6*10^{-7}$ Torr and 5 mtorr, respectively. The sample holder was rotated at 54 RPM in order to minimize thickness gradients across the thin film. The substrate was cleaned via Ar^{+} ion milling with 17 Watts RF power for 2 minutes. The native SiO_2 was thus removed prior to the thin-film disposition. Both Co (DC1) and Pd (DC5 #1) were DC sputtered at room temperature with sputtering rates of 0.36Å/s and 0.37Å/s, respectively. The rates were determined via AFM scanning on photolithography-based thin-film features. A customized deposition control program was used to automatically manage simultaneous shutter movement: opening one shutter while closing the other thus eliminating the lag between depositions of the successive layers to ensure adequate interface and minimization of nucleation sites. An adhesion layer of Pd (5 nm) was initially deposited in order to create the exchange coupling between the Co/Pd bi-layers. Thirty pairs of alternating Co (5 Å) and Pd (5.5 Å) bi-layers were then deposited as the magnetic layer,

followed by a Pd (5 nm) capping layer. A liftoff process was then preformed in order to remove the remaining photoresist,

Gallium Ion Implantation

The FEI Nova Nanolab Dual beam SEM/FIB system was used for the ion implantation. Patterns with 100 point-to-point distance and different dwell time were calculated to feed the photolithography-prepatterned grid. An intentionally unfocused ion beam with round shaped spot size of about 1 μm in diameter is used for uniform Ga^+ ion implantation. 100 pA aperture was chosen to optimize the deposition time and eliminate non-linear effects. Ion implantation doses were separately calibrated and recalculated for different ion energies. Figure 49 shows a SEM image following a set of Ga^+ ion implantations with different doses on the 15 x 15 μm^2 square patterns. It is possible to see from this figure that for the higher Ga^+ ions does, the frame surrounding the square patterns (Si surface) was partially milled.

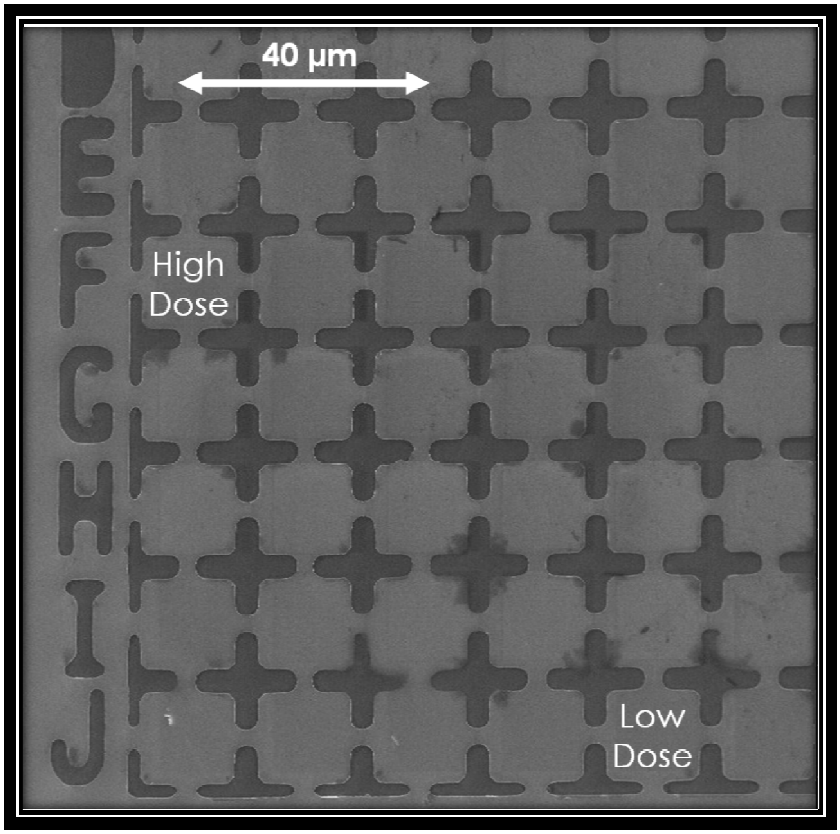

Figure 49: SEM image of a 15 x 15 μm^2 squares grid (after the lift off process) on which 25 different Ga^+ ions doses were implanted.

Magnetic Properties Measurements

The sample was mounted on an XYZ micrometer controlled translation stage in order to probe different features on the sample and achieve proper focusing spot. The probe beam is focused well within each of the 15-µm squares eliminating cross-talk between parts treated with different implantation dosage.

The magnetization history (hysteresis loops) are plotted using the photoelastic modulator (PEM)-based [91] focused magneto-optical Kerr effect microscopy (F-MOKE), which enabled diffraction-limited spatial resolution of 1.1 µm using an infinity-corrected objective of 0.35 numerical aperture. The objective hidden inside the pole of an

electromagnet is screened from magnetic field by the soft magnetic material of the pole itself, reducing the adverse effect of the parasitic Faraday rotation caused by the glass of the objective's lenses. The beam focused at the sample probes the out-of-plane (polar) magnetization component of the material. The schematic of the experimental setup is shown in Figure 50.

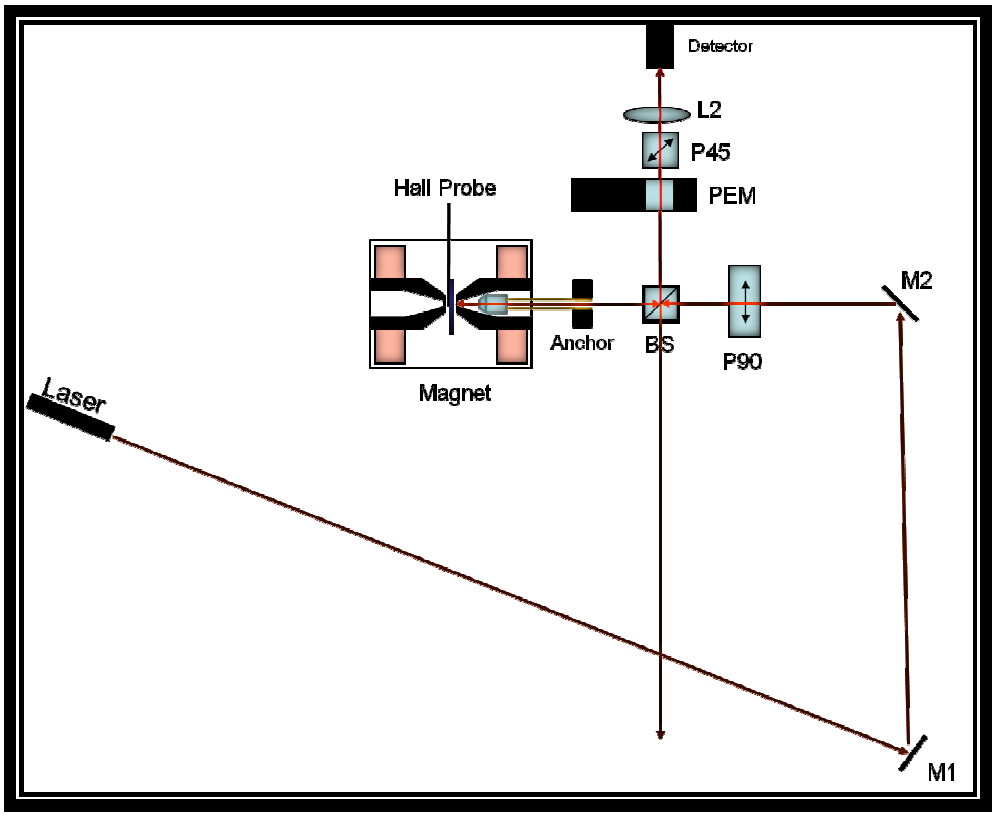

Figure 50: Schematic showing the experimental F-MOKE setup.

The LASER beam is being directed to the sample located between the poles of a powerful (up to 3 Tesla) electromagnet by two adjustable mirrors **M1** and **M2**. Standard two-mirror setup allows adjustment of both beam position and angle of incidence (in both vertical and horizontal directions). Thus, the beam can be sent along the axial holes bored in the electromagnet poles. The beam passes through a beam-splitter (**BS**) losing half its

intensity and then it is being focused on the sample surface by an infinity-corrected objective. Relatively long optical path from the laser to the objective allows the beam to diverge to about 4-mm spot, overfilling the objective inlet orifice and allowing for good (diffraction-limited) focusing to a spot 1- 2 microns in diameter. The reflected light passes through the objective again, forming a collimated beam and then exits through the same hole towards the beam splitter. The beam splitter directs half of the reflected beam to the detector's side, enabling the Kerr/Elipticity measurement and sample features imaging.

A few more remarks should be made on the F-MOKE configuration. Many transparent materials (including glass) impose polarization and/or ellipticty shift to the passing light when subjected to magnetic field (usually proportional to the field strength). This is known as Faraday Effect. While this shift is small on a course of say a few microns, it is very significant over millimeters, adding a parasitic signal to the real one. This is the reason why objectives with huge glass mass are seldom used for MOKE measurements.

Figure 51 schematically shows a typical distribution of field lines inside an H-frame electromagnet, where the central part of the poles is virtually field-free. Figure 52 demonstrates an enlarged view of an objective within the pole.

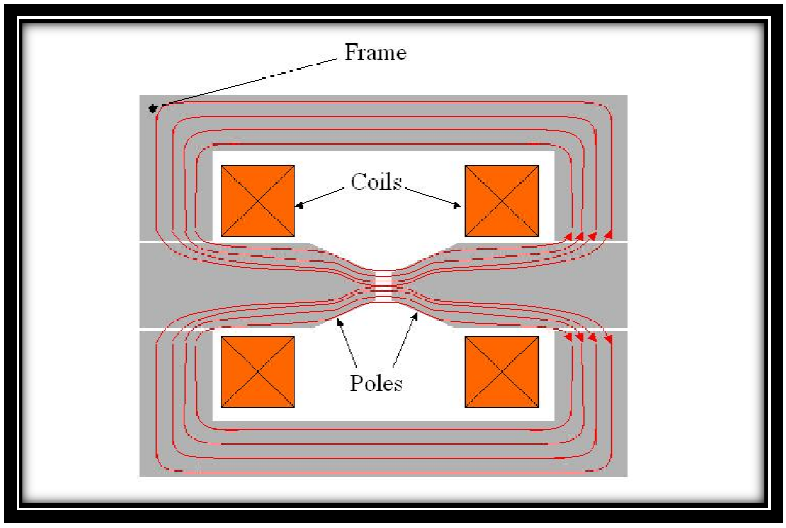

Figure 51: Schematic showing magnetic flux distribution in a typical H-frame electromagnet

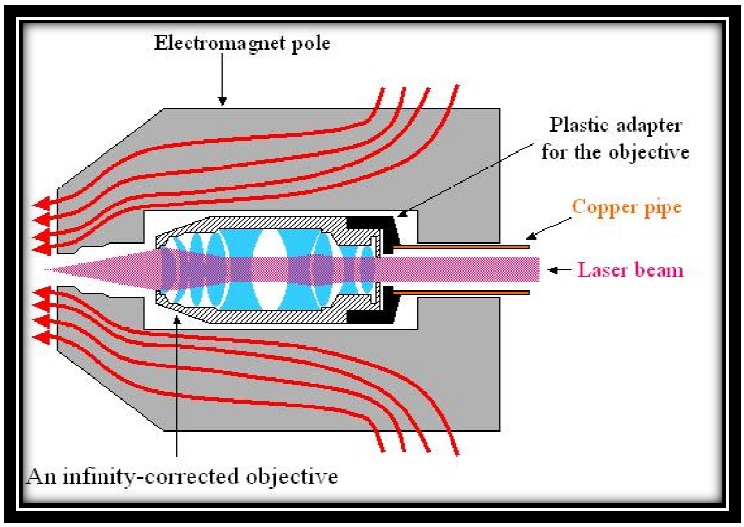

Figure 52: Schematic showing the objective position inside one of the electromagnet's poles.

The poles of the electromagnet are made of the soft magnetic material, and this is exactly what is needed to screen the objective from magnetic field, Figure 52. The field is practically zero where the objective is placed. Not only does this solves the Faraday Effect problem, but also adds stability to highly spatially resolved measurements. The field gradient and consequently the pulling force on the objective are negligible, which is

very significant for F-MOKE measurements as the depth of field is just around 3 microns. However, the magnetic field screening ceases as soon as the poles saturate, yielding huge parasitic signal at about 1.8 Tesla field.

In order to see what spot is being probed and where exactly the sample features are located, the beam is deflected from the detector to a CCD camera (Figure 53). The outgoing beam is deliberately defocused by shifting the stage back or forth. The intensity of the reflected beam is attenuated by proper combination of a neutral density optical filters in order not to saturate the CCD camera detector. The objective would then image the substrate on the CCD camera, Figure 54.

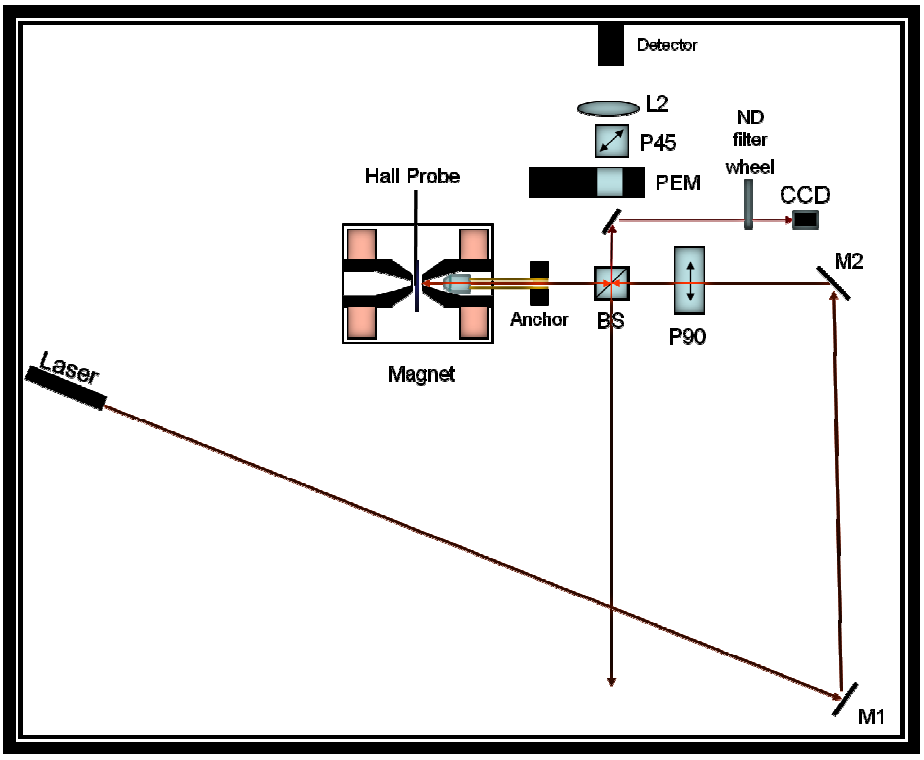

Figure 53: Schematic diagram showing how the F-MOKE setup was used to image the features under Kerr investigation with a CCD camera.

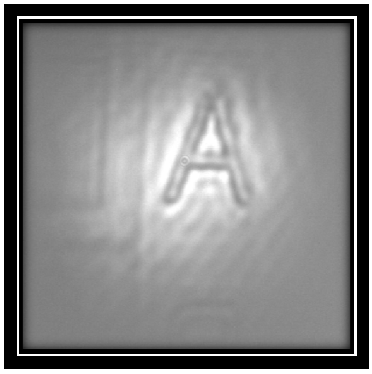

Figure 54: A captured image with the CCD camera of a position mark (letter A).

The point of interest is then brought to the center of the image (using a nano-manipulator) and the beam is then focused on the feature. The mirror used to defect the beam to the CCD camera is then lowered, directing the beam through the PEM, polarizer, focusing lens, and the photodetector. A computer program was then used to acquire the Kerr measurement from the feature under focus.

Results and Discussion

Figure 55 shows a set of hysteresis loops obtained within an unimplanted reference film as well as within the islands implanted with the same dosage of $1*10^{14}$ ions/cm^2 gallium ions of different energies. It is obvious that even this minimal dose (~10 times lower than previously reported result [92]) is sufficient to significantly alter the properties of the material, especially at higher acceleration voltages of 20 - 25 kV. On the other end of the spectrum, the minimal dose of $1*10^{14}$ ions/cm^2 is insufficient for affecting the magnetic properties at lower ion energies of 10 or 5 keV (the latter is not shown for lack of any appreciable difference with the bare film).

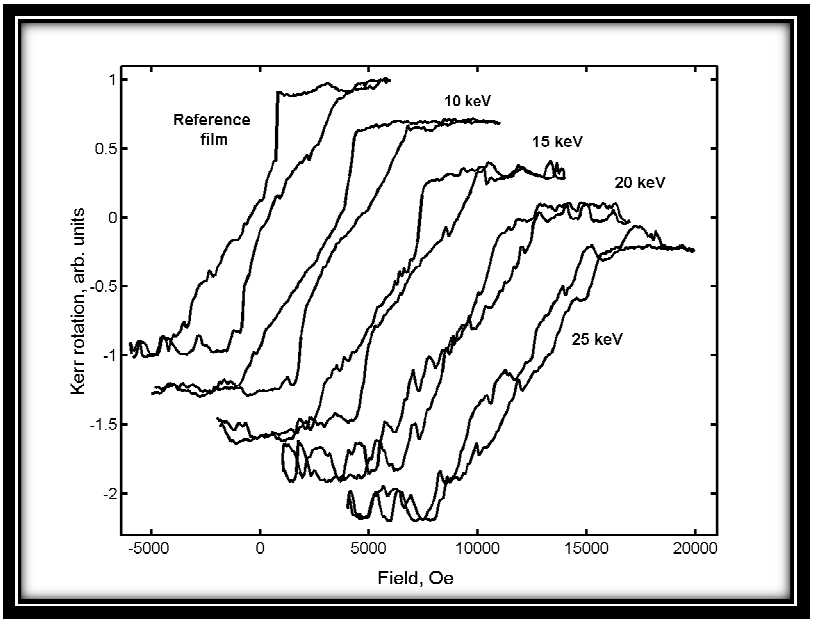

Figure 55: Evolution of the loop shape treated with the same dose of Ga^+ ion irradiation of $1*10^{14}$ ions/cm^2 with the ion beam energy. The leftmost loop corresponding to the untreated film is properly centered, while each subsequent loop is shifted 3000 Oe to the right and 0.3 arb. units down.

The particular material used does not exhibit sufficient coercivity or squareness of the hysteresis loop, therefore the loop area has been chosen in order to characterize the effect of the ion implantation on the loop shape and the strength of the perpendicular anisotropy.

Figure 56 demonstrates the effect of the ion dosage on the loop area for the ion energies of 5, 10 and 15 keV. It is clear that the minimal ion energy of 5 keV has minimal effect on the magnetic properties of the material regardless of the ion bombardment dose. One can argue that the 5-nm protection palladium layer holds its integrity and effectively prevents the penetration of the Gallium ions inside the bulk of the magnetic material. It is indeed the borderline energy where competing processes of ion milling and sputter-deposition of gallium nearly balance each other.

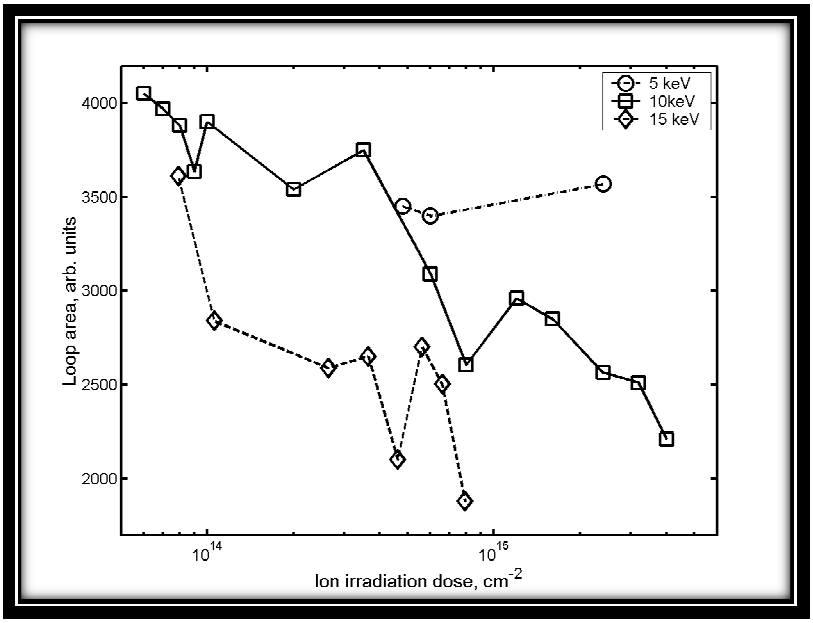

Figure 56: The dependence of the loop area on the ion irradiation dose for three selected values of the acceleration voltage.

Higher-energy ions with a dose of $6*10^{14}$ ions/cm^2 for 10 kV beam and $3.5*10^{14}$ ions/cm^2 for 15 keV ions penetrate into the multilayer material causing shrinkage of the hysteresis loops area. The total saturation magnetic moment, on the other hand, stays nearly unchanged (at least within the accuracy of the measurement and run to run variations).

Conclusion

The effect of gallium ion implantation on in Co/Pd multilayers thin film is presented. It is found that even the minimal dose of $1*10^{14}$ ions/cm^2 significantly affects the out-of-plane anisotropy of the film at ion energies above 20 keV. At lower beam energies of 10 or 15 keV, the ions still destroy the interface-induced perpendicular anisotropy albeit at much higher dosages of $6*10^{14}$ ions/cm^2 and $3.5*10^{14}$ ions/cm^2, respectively.

To put these number in perspective, the FIB-patterned prototype medium structure of 20 x 20 nm, would accept just no more than just 400 ions at $1*10^{14}$ ions/cm^2 dose, without

sufficiently altering the material properties at high energies of the beam acceleration voltage. On the other hand, it is exactly high acceleration voltage that plays the dominant role in improving the spatial resolution of the FIB patterning.

Magnetic Force Microscopy Enhanced Resolution

Introduction

High-precision microscopy is vital in order to further develop next generation nanoscale-based technologies, especially ultra-high density and ML 3D magnetic recording devices. Scanning probe microscopy (SPM) is generally recognized to be one of the most critical and unique techniques utilized for surface measurements with nanoscale accuracy [93,94]. In 1987, the magnetic force microscopy (MFM) mode of SPM emerged and has been used since then to directly visualize nanomagnetic domains and features [95]. Today, the span of MFM applications is truly diverse, from accurate analysis of secret information by the Federal Bureau of Investigation (FBI) to fundamental studies of magnetostatic bacteria [96]. Finally, the data storage industry currently utilizes MFM extensively to measure the magnetization distribution in magnetic recording media and heads in an effort to pack more data into a recording system [97,98], Figure 57.

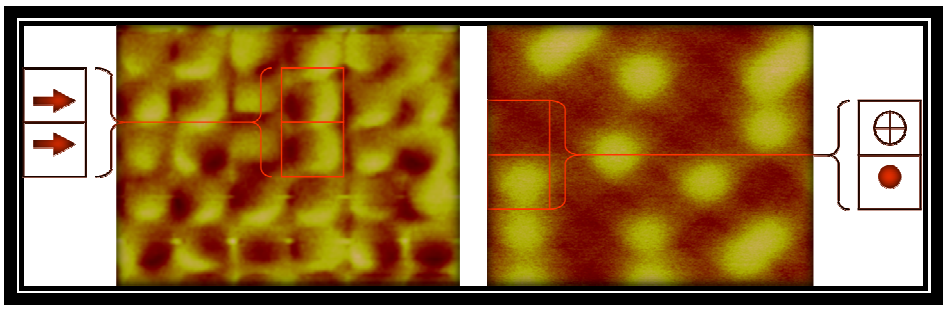

Figure 57: MFM images of sub 100 nm magnetic bits from both longitudinal (left) and perpendicular (right) patterned media.

The best commercially available MFM probes secure an optimal spatial (or lateral) resolution of ~ 25 nm when scanning in ambient conditions and ~ 10 nm when scanning in high-vacuum environment. Currently manufactured magnetic recording media are

composed of isolated nanomagnetic grains, approximately a few nanometers in diameter. Since each recorded bit encompasses about 50 to 100 grains, MFM is still an effective analysis tool to image recorded information. However, with the ever increasing demand for high areal density data storage devices, these nanomagnets/grains will eventually scale down to a couple of nanometers, at which time MFM systems with their current scanning capabilities will be ineffective in distinguishing smaller bit dimensions. Enhancement in MFM resolution is therefore crucial to preserve its significant role in the analysis of nanoscale magnetic features and to shed light on many open questions, understanding of which is essential for the progress of magnetic data storage technologies [99,100]. Moreover, quantitative investigation of ML 3D media will require both high lateral resolution and high sensitively, a quality that conventional MFM probe cannot provide. Hence, a significant contribution to the development of ML 3D and ultra-high densities magnetic recording can be made by enhancing the capabilities of MFM.

A comparison between the imaging methods for both Atomic Force Microscopy and MFM can help one better understand the lateral resolution limiting factor of conventional MFM probes.

The following highlights the main deference between AFM and MFM imaging:

1) AFM is scanned with tip-sample spacing of a few angstroms where Van der Walls forces dominate the interaction, whereas MFM is scanned at about 5 - 20 nm separation where long-range magnetostatic forces generate the MFM image.

2) The radius of curvature (ROC) for AFM tips is typically a few nanometers, while the ROC for MFM tips is about 20 nm for the better probes. This is because the finest MFM tips are fabricated by depositing magnetic materials over the sharpest AFM tips.
3) The AFM image is a result of the shape convolution between the tip dimensions and the specimen features. Thus, geometrical deconvolution of the tip-sample interaction can be applied to enhance the resolution effectively. On the other hand, the MFM signal is proportional to the convolution between the stray fields generated by the magnetic tip and the magnetization of the sample. Since the exact geometrical shape of the magnetic tip, its total magnetic moment, and thus its stray field distribution are primarily unknown, deconvolution is ineffective in obtaining better resolution.

Other disadvantages due to the current fabrication method of MFM probes:

1) The magnetic properties of MFM tips are rough estimates obtained from measurements performed on flat magnetic thin film and not from the magnetic tips.
2) Investigation of the specimen by applying external magnetic field while MFM scanning is unproductive since the magnetic field required to rotate the magnetization of most high coercivity MFM tips is only about 600 Oe. Thus, even in the analysis of relatively soft magnetic materials, the MFM signal generated while applying external magnetic fields can be the result of magnetization change in both the tip and sample.

Plateau Probes for MFM enhanced Resolution

The key to this innovation is in the creation of surface conditions that will enable the effective growth of granular, continuous, and 3D multilevel (ML) magnetic media on plateau probes. The type of media to be deposited on a plateau probe will be determined depending on the MFM application needed.

Granular magnetic media is composed of nanomagnetic grains (about a few nanometers in diameter), which are surrounded by a matrix of nonmagnetic material. On the other hand, continuous magnetic media is composed of uniformly distributed magnetic material. When the FIB resolution (~ 10 - 20 nm) cannot support the desired magnetic feature size, granular magnetic media is preferred over continuous media since the dimensions of the MFM tip will be determined by the grain size (less than a few nanometers) and not by the FIB-milling resolution. In addition, the percentage of the nonmagnetic material and thus the spacing between the grains control the coercivity values of the magnetic media by varying the magnetostatic and exchange interaction between the grains. Different magnetic compositions will exhibit different ranges of coercivity values. To illustrate, coercivity fields greater than 1 Tesla can theoretically be achieved with high anisotropy $L1_0$ materials such as FePt. Furthermore, both granular and continuous thin films can have a preferred orientation of magnetization based on the material and crystal structure of a seed layer deposited prior to the magnetic layer. Controlling the magnetization orientation of the MFM probe, will enable the imaging of different field components emanating from a specimen. Hence, proper surface conditions on the plateau are critical to enable crystal growth of various materials. It is also

important to note that the seed layer is not constrained only to one layer but can be composed from various layers, where each layer can exhibit a unique composition and function (adhesion, buffer, crystalline, etc.).

In the case of ML 3D media, various magnetic layers are stacked together while being separated from each other with a nonmagnetic/decoupling layer. Each layer exhibits a different coercivity value which enables the switching of magnetization in individual layers across the thickness of the media. As described in the previous chapter, Co/Pd and Co/Pt multilayers media are proper candidates for this application, which require optimal surface conditions prior to deposition. With such media it is possible to control the emanating magnetic field just above the surface of 3D structure by switching the magnetization of the decoupled layers across the media in a particular orientation. To illustrate, assuming that a MFM probe is fabricated from three decoupled magnetic layers, for which every magnetic layer has half the moment than the one beneath it (e.g. starting from the bottom layer: 8 m, 4 m, 2 m, where m is a base value of magnetic moment). In order to increase the sensitivity of this probe (to investigate high anisotropy materials, for example), all the layers should be magnetized in one direction. To reduce the sensitivity of the probe (to image domain wall of soft magnetic structure, for example), the bottom layer (8 m) should be magnetized in one direction while the others (4 m and 2 m) in the opposite direction. The final product will be a multipurpose 3D multi-sensitivity MFM probe. Nevertheless, in order to fabricate the above mentioned types of magnetic media on a probe, the surface conditions of a plateau probe must be similar to the ones required to fabricate them on large substrates.

Among other, the key advantages of MFM tips which area fabricated from plateau probes:

- MFM enhances resolution below 20 nm in ambient conditions
- Variable sensitivity field (using ML 3D media)
- Coercivity values ranging from about 0.005 - 5 Tesla
- Fine control of tip magnetic moment (potentially, one magnetic grain less than a few nanometers in diameter)
- Defined geometrical shapes of the tip (optimizes resolution via deconvolution of the obtain MFM image)
- Selective orientation of the tip magnetization (depending on the crystalline structure of the seed layer or shape anisotropy).
- Precise measurement of the tip's magnetic properties via F-MOKE measurements (Figure 58)

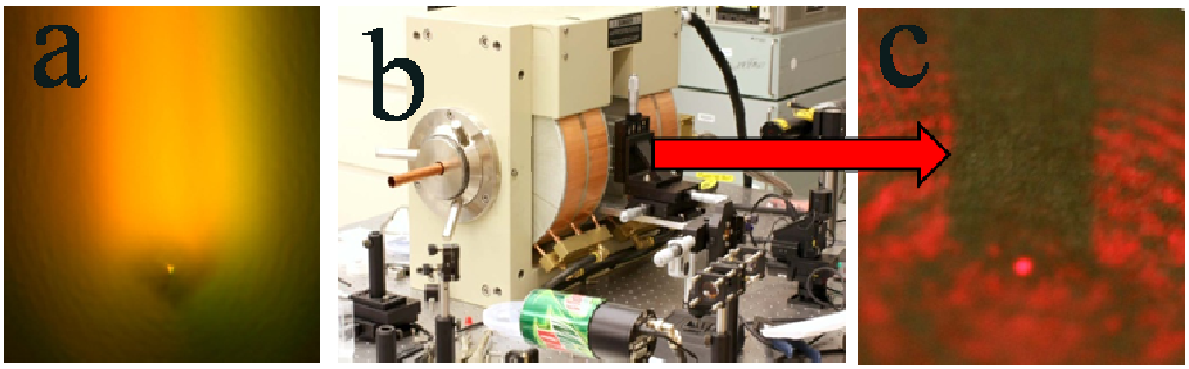

Figure 58: (a) an optical microscope top-view image where the brightest spot is the plateau (b) F-MOKE system as described in the previous chapter (c) an image taken with the F-MOKE, where the red "spot" is the reflection of linearly polarized light from a plateau probe which was coated with magnetic material. This red "spot" carries the magnetic properties of the material deposited on top of the plateau probe.

Plateau Probes Fabrication

One of the most productive and efficient methods to fabricate plateau probes with optimal surface conditions is by fabricating cantilevers (via wet chemical etching) with plateaus instead of sharp tips. This process is theoretically much simpler than the fabrication of ultra-sharp atomic force microscopy (AFM) probes. Another way of fabricating a plateau probe is by focused ion beam (FIB)-milling of a standard AFM probe. FIB systems have the capability to dry etch nanoscale features with resolution below 10 nm. The milling process takes place by focusing an accelerated beam of gallium ions to the substrate and then controlling the beam motion with electric lenses. The reset of this section will be dedicated to the fabrication of plateau probes and MFM tips from plateau probes via FIB-milling.

Figure 59 (a) through (e) illustrate the process flow used to fabricate a plateau probe via FIB-milling. Attempting to get a smooth surface/plateau by directly milling the tip, results in a relatively rough surface due to the different milling rates between the flat regions and the edges of the pyramid structure of a typical AFM probe. The edges of the pyramid are highlighted with white lines in Figure 59 (a). It was thus required to first mill a cylindrical structure out of the AFM tip and then mill the plateau. Figure 59 (b) shows a top-view of an AFM tip on which a milling template is superimposed. The template was composed of three doughnut-like milling patterns where the ion beam dose reduces with the diameter of the each pattern. Figure 59 (c) and (d) are top-view and side-view images taken after the cylindrical milling process. Since the cantilever holder, for a Dimension 3000 SPM system, had a tilt of ~ 10 degrees (with respect to the specimen's plane), the

cylinder was also milled at a compensation angle of ~ 10 degrees. A plateau was then FIB-milled on top of the cylinder at an angle ~ 90 degrees with respect to the cylinder's long axis, Figure 59 (e) and (f). Depending on the surface smoothness requirements, an ion beam current from about 10 pA – 50 pA could be used to mill the plateau. In general, the cylinder served two purposes: uniform milling rates for both the plateau and for the MFM tip following the magnetic thin film deposition.

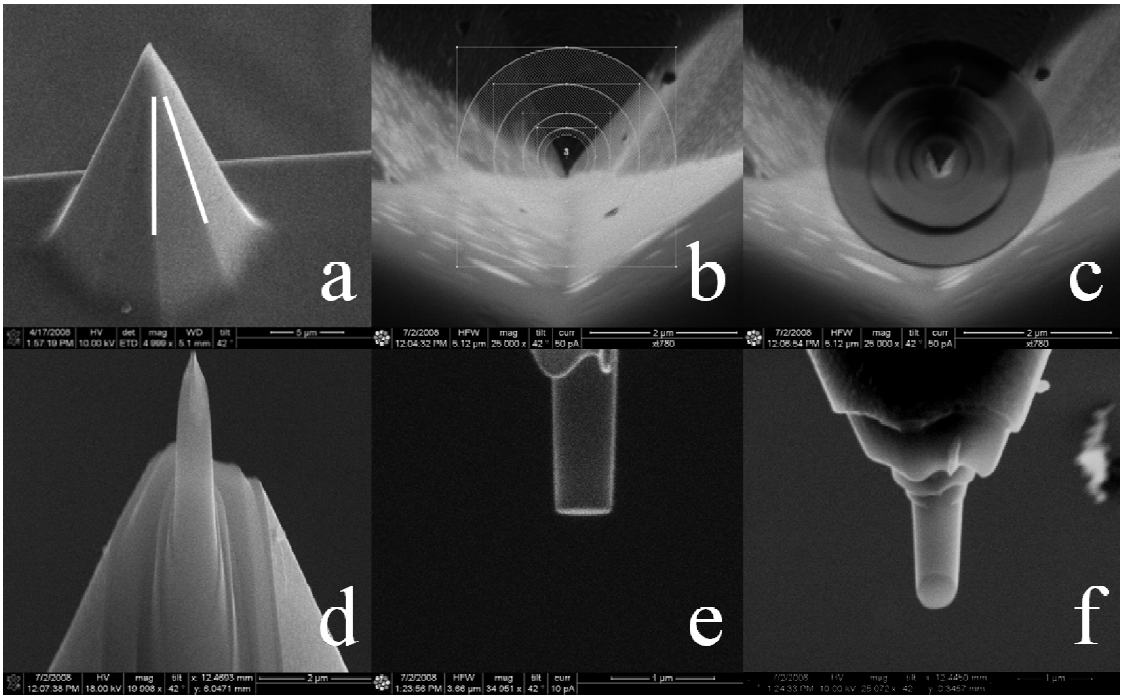

Figure 59: SEM Imaging of the FIB milling sequence for ~ 0.6 µm plateau probe (a) AFM probe (b) top-view of the AFM probe with a series of three doughnut shaped milling pattern (c) top-view of the AFM probe following the FIB-milling (d) side-view of the probe showing the milled cylinder (e) side-view of the probe after milling the plateau (f) tilted view of the plateau probe showing the surface area of the plateau

Once the plateau probe is fabricated, the type of seed, magnetic, and protective layers were chosen in order to meet a particular MFM imaging application and then deposited on the probe, Figure 60. A dual beam SEM/FIB was used to target a particular "spot" or region on the plateau via SEM imaging and then to remove the material around that

region via FIB-milling. For the tip milling process, a MATLAB program was utilized in order to produce three hexagonal milling patterns, which directed the ion beam in spiral motion on pixel-by-pixel bases. The largest milling pattern was designated to remove most of the material around the designated area (from which the MFM tip will be produced) and hence had the highest ion dose; following this pattern were two smaller hexagonal patterns with lower does, Figure 61 (b). To put thing into prospective, the milling time for the largest pattern lasted about a few minutes while the last pattern, which defined the dimensions of the MFM tip, took about a few seconds. Figure 61 (a) shows a sectional view of the milling procedure, while Figure 61 (b) shows the construction of the milling patterns together with their relative milling doses (darkest color being the highest).

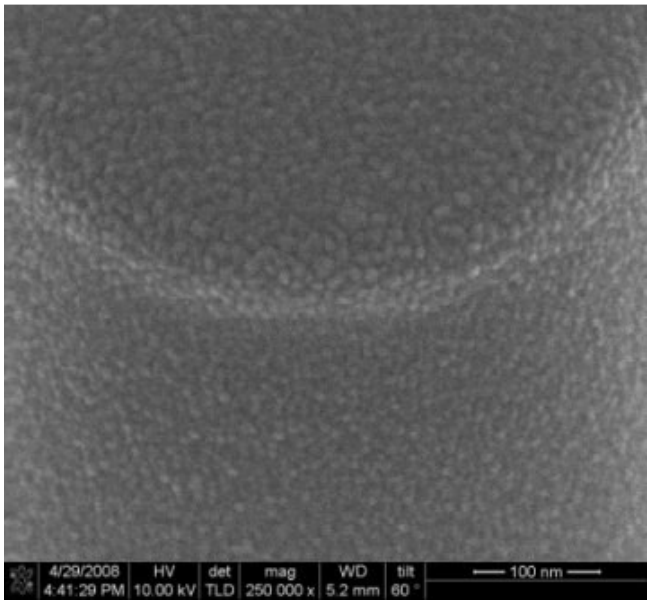

Figure 60: A tilted side-view SEM image of the plateau probe following sputter deposition of a magnetic thin film. The plateau is on the top of the image.

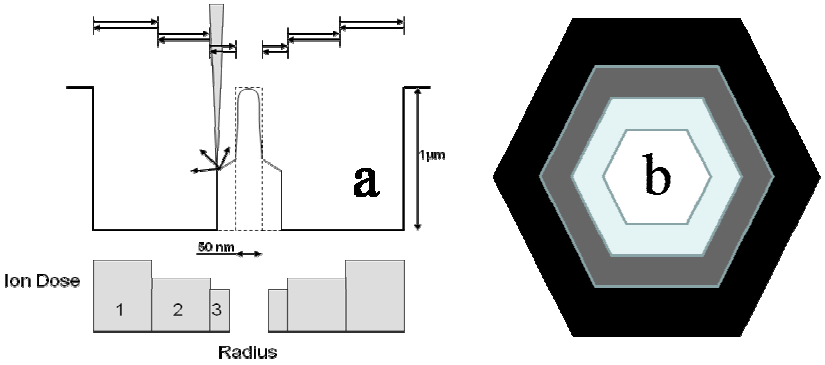

Figure 61: (a) a diagram showing the cross-sectional view of the tip milling process (b) a top view schematics of the tip milling process where the darker colors indicate higher ion doses.

Before attempting to mill an MFM tip from a plateau probe, a quick analysis was performed on a silicon substrate on which the same thin film composition had been deposited in order to determine the proper ion doses required to mill the desired dimensions of the MFM tip. Figure 62 shows a series of SEM images which reveal the milling process of a MFM tip from a plateau like structure.

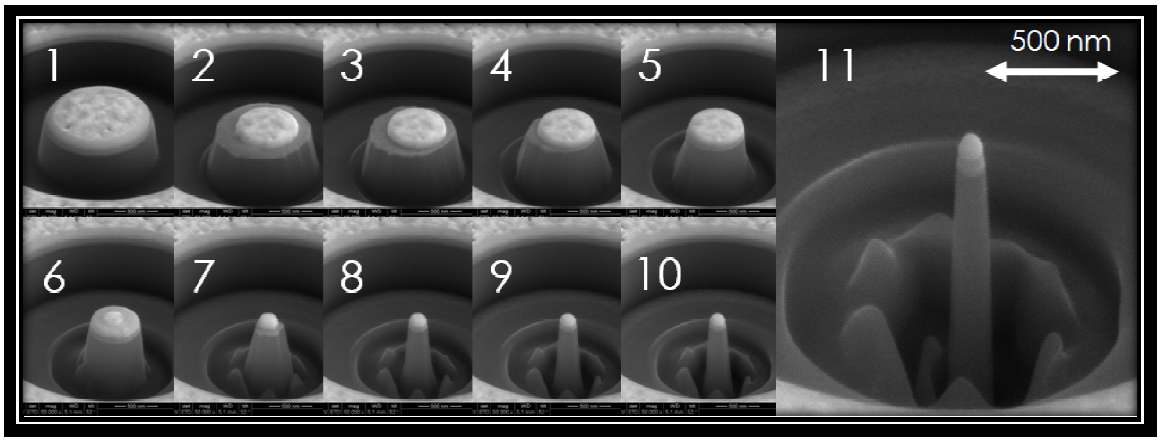

Figure 62: SEM images showing the FIB-milling sequence a plateau probe undergoes in order to fabricate a sharp MFM tip (looking carefully at the high resolution SEM image of the final product (image 11), one can distinguish the seed, magnetic, and protective layers of the MFM tip).

In the following chapter a detailed experiment conducted in order to fabricate high resolution and high coercivity FePt $L1_0$ MFM tip from a plateau probe is presented.

Plateau-Based FePt $L1_0$ MFM Probe

In the following study, a specially designed and fabricated plateau probe (~ 500 nm in diameter) with almost perfectly flat plateau-like surface is FIB-milled out of a standard AFM probe in order to create the required surface conditions for thin film deposition with finely controlled deposition/growth parameters. The uniqueness of this probe lies in the generated surface conditions of the plateau which enables the fabrication of complex magnetic thin-film structures similar to the ones found in various types of magnetic recording media such as CoCrPt-based, FePt $L1_0$, and even the most sensitive to surface conditions, Co/Pt and Co/Pd multilayers media.

For the purpose of this paper, the FePt $L1_0$ media which exhibits both relatively high-coercivity and high magnetic moment has been chosen [101]. In the next section a trivial experiment has been conducted to approximately verify the coercivity of a FePt L10 based MFM probe.

Experiment

The probe fabrication process entails FIB milling of a plateau cylinder, a series of non-magnetic and magnetic thin films sputter deposition, FIB milling of the plateau cylinder to a sharp tip, and annealing of the tip. To start with, a standard AFM probe [Figure 63(a)] was FIB milled to produce a cylinder with ~ 500 nm in diameter and ~ 6 µm in length [Figure 63(b)]. Ion beam current of 50 pA was initially used to mill the cylinder. The probe was then tilted 90 degrees in reference to the cylinder long axis and FIB-milled with 10 pA beam current to produce a smooth plateau surface [Figure 63(c)]. Since the cantilever holder is tilted by ~ 10 degrees in reference to the specimen plane,

the cylinder was therefore milled at a compensation angle of about 10 degrees in order to insure normal incidence between the apex of the probe and the surface of the specimen [Figure 64(a)]. The FIB milling and SEM Imaging were performed using a NOVA 600 Dual-Beam FIB system by FEI.

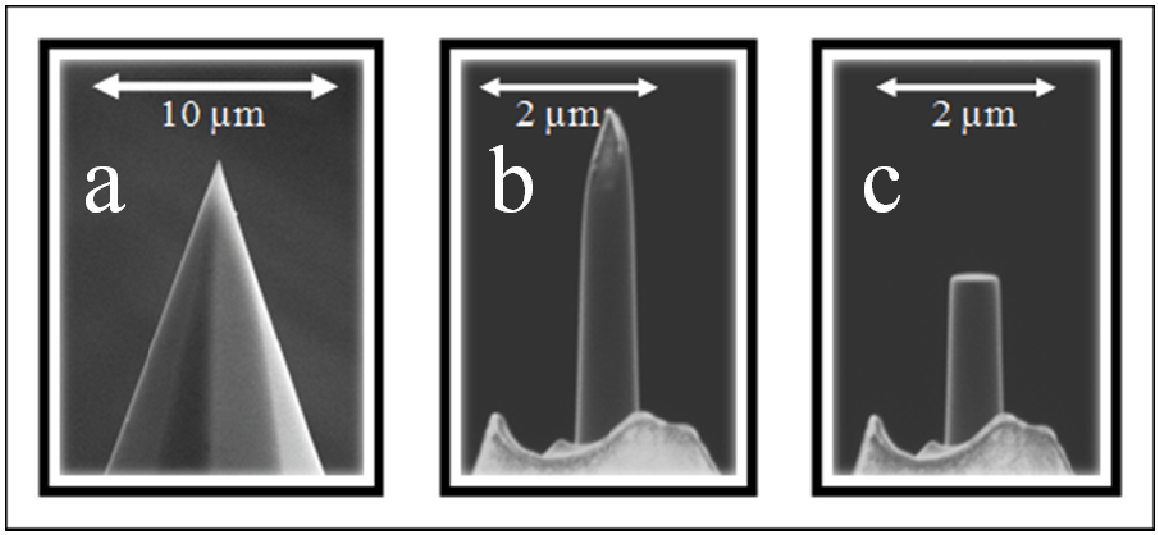

Figure 63: A sequence of side view SEM images highlighting the milling process required to transform a standard AFM probe to a plateau probe.

A composition of Pd(5nm)/MgO(8nm)/FePt(10nm)/MgO(8nm) was then sputter deposited on the plateau probe, followed by a deposition of Pd (5 nm) protective layer. The sputtering process was performed using an AJA Orion 5 system, where both Pd and FePt were sputtered deposited using DC power with rates of ~ 0.35 Å/s and ~ 0.50 Å/s, respectively. MgO was sputter deposited using RF power with a sputtering rate of about ~ 0.07 Å/s. The base and processing pressures were ~ 2 x 10^{7} Torr and 5 mTorr, respectively. The probe was heated to 100°C throughout the whole sputtering process.

A MATLAB program was written in order to generate a text file that controlled the ion beam path on pixel-by-pixel bases, forming hexagonal milling path which traveled in a

spiral motion with an outwards-inwards direction. A series of three hexagonal beam paths, each having distinct dimensions and ion dose, were executed to fabricate a tip with ~ 25 nm curvature radius. Figure 64(b) shows the pixel representation of one milling sequence (top), while the figure in the bottom shows the relative ion doses used for each sequence. Hence, the plateau probe was milled from its outer radius with the highest ion dose to its inner radius with the minimum ion dose. The whole milling process took about 3 minutes, while the last hexagonal sequence tool less than 3 seconds. Figure 64(c) shows a side view of the final product taken at a 30 degrees angle. The probe was then annealed at 650°C for ~ 15 min in a high-vacuum environment in order to drive the material to its $L1_0$ phase.

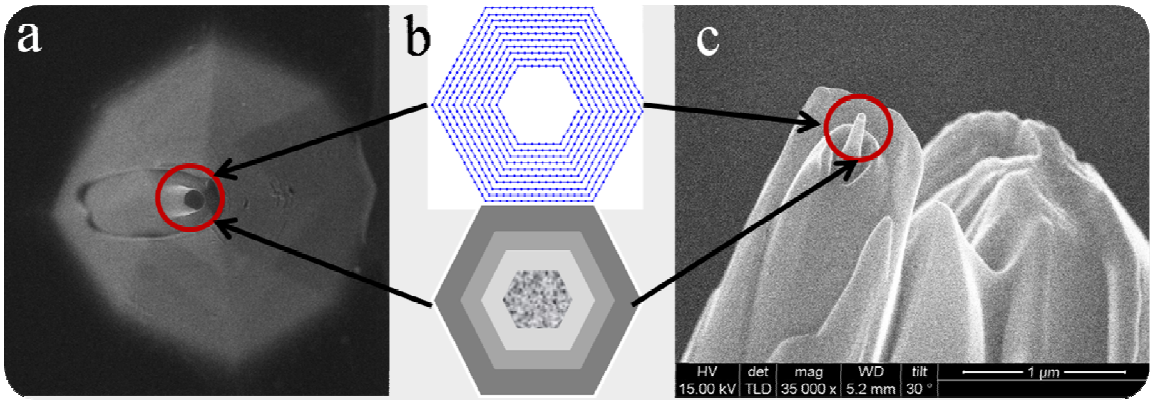

Figure 64: (a) Top view SEM image of the plateau probe after sputter deposition (b) Ion beam milling path (top) and ion dose representation (c) final state of the probe after the tip milling.

MFM analysis, with both the FIB-milled FePt probe and a commercial MFMR probe from NanoWorld, was performed on CoCrPt-based perpendicular magnetic media on which a series of tracks with linear densities ranging from 200 KFCI to 1200 KFCI was repeatedly recorded. The imaging was performed under ambient conditions in the

tapping/lift mode under phase detection. A Dimension 3000 scanning probe microscopy system (by Veeco) was used for the MFM scanning.

Results and Discussion

Figure 65 (a) and (c) show SEM images of both a commercial MFMR probe from NanoWorld and the FIB-fabricated FePt probe. While the commercial probe is complex in shape and is fully covered with magnetic material, the FePt probe has magnetic material just on its apex for which both the thickness and lateral dimensions of the magnetic material can well be approximated. Deconvolution can thus be applied to further enhance the lateral resolution of the acquired MFM image102. Figure 65 (b) and (d) are 2 x 2 μm^2 MFM images of regions taken from a specially recorded reference magnetic disk with the conventional MFMR probe and with the FIB-fabricated FePt probe, respectively. A set of tracks with varying linear densities from 200 to 1200 KFCI were continuously recorded onto the reference ultra-high-density perpendicular magnetic disk for a radial distance of about 30 µm. Hence, if MFM imaging would show "blank" regions on the recorded area, this would be only because the resolution of the probe is not adequate to detect the ultra-high density information recorded in these regions. It can be seen from Figure 65(b) that the conventional probe is not capable of reading all the tracks with relatively high linear densities, i.e. with bit features of smaller than approximately 30 nm. This explains the presence of relatively large fainted regions (with no distinguishable features) where otherwise ultra-high density information could have been detected. On the contrary, the above described FIB-milled FePt probe can distinguish all

the tracks recorded into the disk. That is why in the latter case, the entire 2 x 2 μm^2 region shown in Figure 65(d) is covered by tracks.

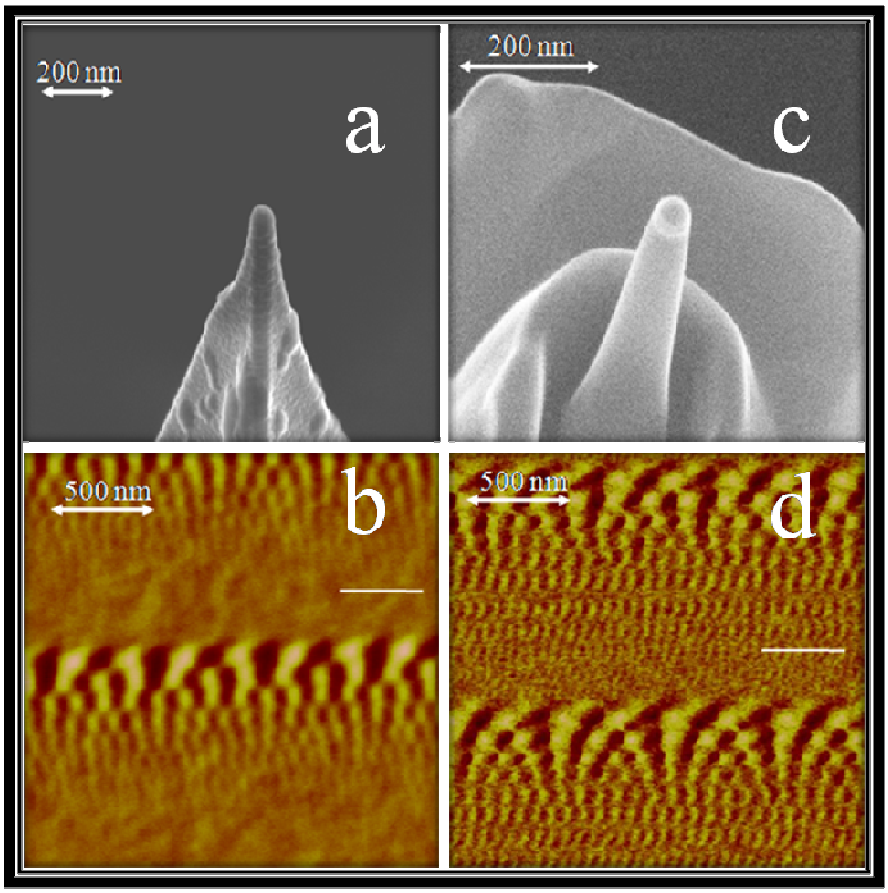

Figure 65: (a, c) SEM images of the MFMR and FIB-milled FePt probes (b, d) 2x2 μm^2 MFM images obtained with each probe.

In order to quantify the lateral MFM resolution it is possible to measure the full-width-half-maximum (FWHM) response of a nanomagnetic feature [103]. Figure 66 (a) and (b) represent cross-section profiles corresponding to the solid white lines in Figure 65 (b) and (d), respectively. The section profiles are taken from tracks with similar linear densities (1000 KFCI) for adequate resolution comparison. Approximately 17 nm FWHM is recorded for the FIB-fabricated FePt probe, while the commercial MFMR generated a

relatively poor image quality with no distinguishable magnetic features. The relative poor resolution of the commercial probe can be attributed to the fact the while the FIB-fabricated probe has magnetic material only on its apex, the commercial probe is fully covered with magnetic material and thus a larger and more complex magnetic field distribution interacts with the magnetization of the media.

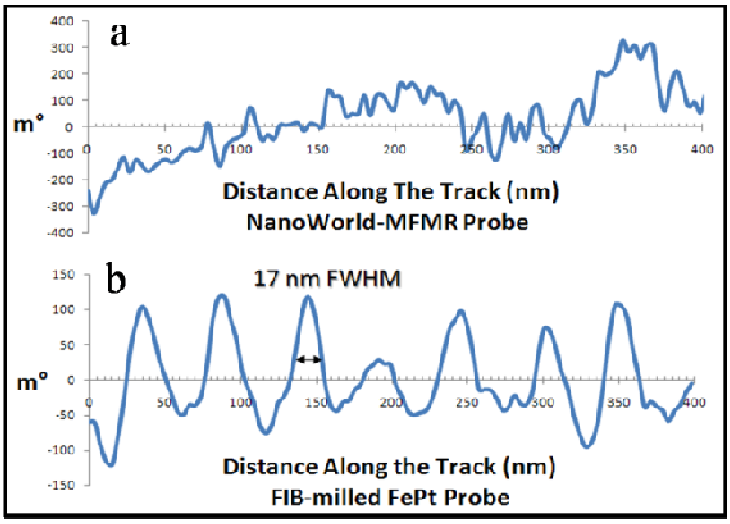

Figure 66: (a, b) Section analysis corresponding to the solid white lines in FIG. 3 (b, d), respectively.

Conclusion

To conclude, the feasibility of effectively growing FePt $L1_0$ media on an FIB-milled plateau probe from which a relatively high resolution and high coercivity MFM probe was FIB-fabricated. Sub-20 nm lateral resolution was demonstrated in ambient conditions. Further optimizations of these types of probes and incorporation of deconvolution could enhance the lateral resolution and thus facilitate the development of next generation ultra-high areal density and ML 3D magnetic recording devices.

*Some of the material presented in this section was "accepted for publication by the Journal of Applied Physics."

High Coercivity/Moment FePt $L1_0$ MFM Probes

To fabricate a high-coercivity MFM probe, a 20-nm thick layer of Fe-Pt (45-55) was sputter-deposited on a regular silicon AFM probe. Protective layers and seed layers where also employed in the deposition process. To create the ultra-high-anisotropy $L1_0$, the magnetic mixture was annealed at temperature of 650 C° for approximately 15 minutes. The image taken by the $L1_0$ MFM probe of information tracks recorded into ultra-high anisotropy and high-moment perpendicular media is shown in Figure 67 (b).

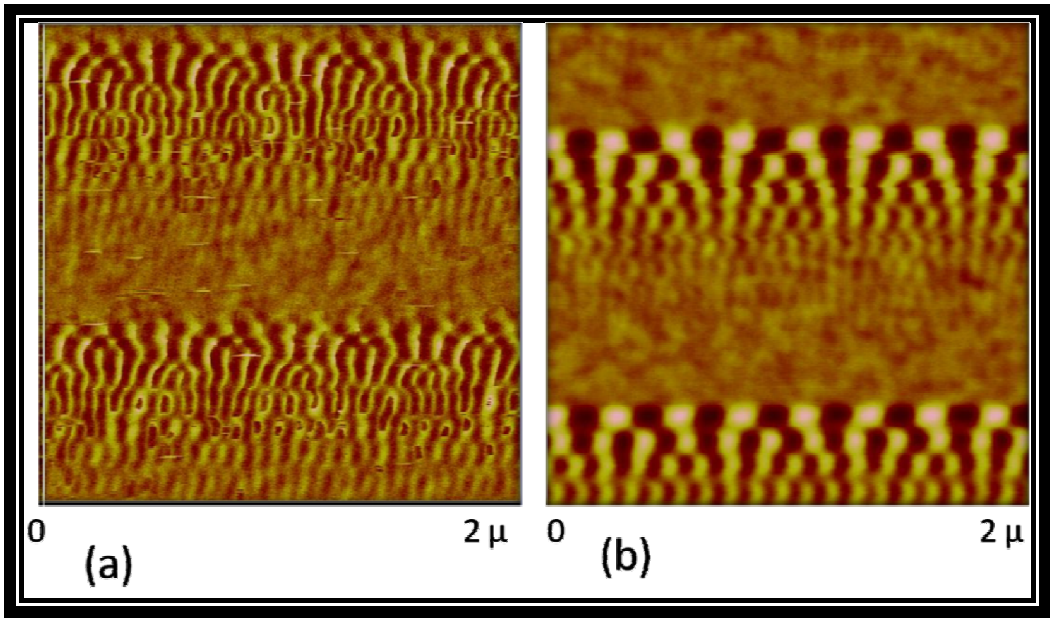

Figure 67: MFM images of magnetic tracks recorded into a high-anisotropy and high-moment perpendicular magnetic recording media continuously and imaged back by (a) a low coercivity MFM probe and (b) a hard L10 probe.

A comparison of the two images in Figure 67 (a) and (b), respectively, illustrates the main different in imaging by a relatively "soft" conventional probe and an adequately "hard" $L1_0$ probe. In the latter case, the information bits represented by oppositely polarized magnetic regions can be clearly distinguished.

To give a more quantitative evaluation of the "hardness" of $L1_0$ probes, the following experiment was performed. Assuming that the coercivity even of the highest coercivity probe is still less than 2 T, a field of 2 T was applied to saturate the probe in the direction of the field. Then, the probe was used to image a magnetic pattern in a specially prepared reference sample. To track the position of the probe during imaging, a special mark was "scratched" into the sample (using a Candela system) just across the magnetically recorded tracks, as shown in Figure 68. Then, the experiment was repeated with applying the external field in the opposite direction and gradually increasing the strength of the field. One can observe that the polarity of the measured signal at the point of observation, as shown in Figure 68, could be reversed only when the applied field was larger than approximately 0.8 T. Consequently, the conclusion could be drawn that the coercivity field of the $L1_0$ probe is larger than 0.8 T.

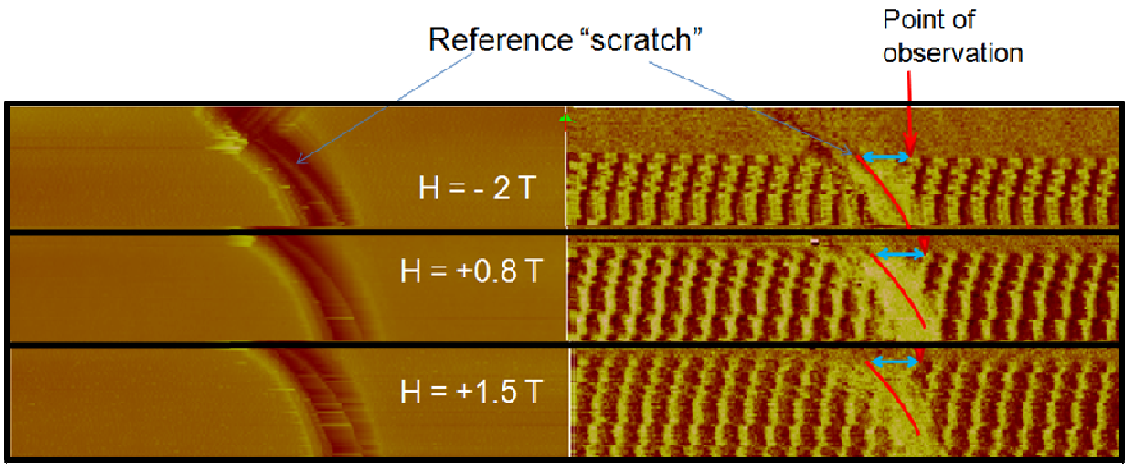

Figure 68: A set of three pairs of images, AFM (left) and MFM, taken by a $L1_0$ probe after applying an external field of – 2 , +0.8, and +1.5 T, respectively.

Multi-domain MFM Probes

This chapter entails experimental data which demonstrate magnetic force microscopy with sub-10-nm resolution under ambient conditions. To achieve this record high resolution, multi-domain states in a nanomagnetic probe were controlled. Two demagnetized (multi-domain) FePt (45/55) films sputtered on a silicon probe and separated by a 8-nm thick MgO layer were further annealed at temperature of 650 C to trigger the high-anisotropy $L1_0$ phase. A field of above 2 T was applied to drive the probes into a saturated "single-domain" state. The multi-domain probes were equivalently compared with conventional MFM probes via comparative imaging of benchmark magnetic recording disks.

Experiment

First, two presumably magnetostically and consequently anti-ferromagnetically coupled 10-nm thick layers of FePt (45/55) alloy were deposited via sputter deposition on a regular silicon AFM probe. To break the short-range quantum-mechanical exchange coupling while maintaining an anti-ferromagnetic magnetostatic coupling, the two layers were separated by a 8-nm thick layer of magnesium oxide (MgO). For imaging magnetic recording media, it is often preferred to use ultra-high anisotropy probes. It is known that $L1_0$ phase of FePt (~ 45/55) mixture can indeed provide anisotropy higher than 1 T. To create $L1_0$ phase, the magnetic mixture was being annealed at temperature of 650 C for approximately 15 minutes. In this case, heating the tip region pursued two goals. First, heating was necessary to create the ultra-high anisotropy magnetic phase. Second, as a result of annealing, the magnetization had a chance to relax into a global equilibrium

demagnetized or, in other words, multi-domain state. To illustrate the concept, Figure 69 shows an exaggerated view of the most trivial possible magnetization configuration in the sharp tip. In the multi-domain or anti-ferromagnetic state, the flux in each layer is balanced off by the oppositely directed flux in the other layer everywhere in the probe, with the exception of a relatively small region in the tip of the probe where perfect balance is difficult to achieve because of the drastic difference in the physical dimensions between the two layers. In other words, in this unbalanced region, the amount of the material with one direction of the magnetization exceeds the amount of the material with the opposite direction of the magnetization. Consequently, this unbalanced region defines the effective region of the magnetic probe. Depending on the curvature of the original silicon probe and the thicknesses of the magnetic layers, the unbalanced magnetic region can be varied in a relatively wide range. Throughout the further description, this probe type is referred to as Nanomond probe.

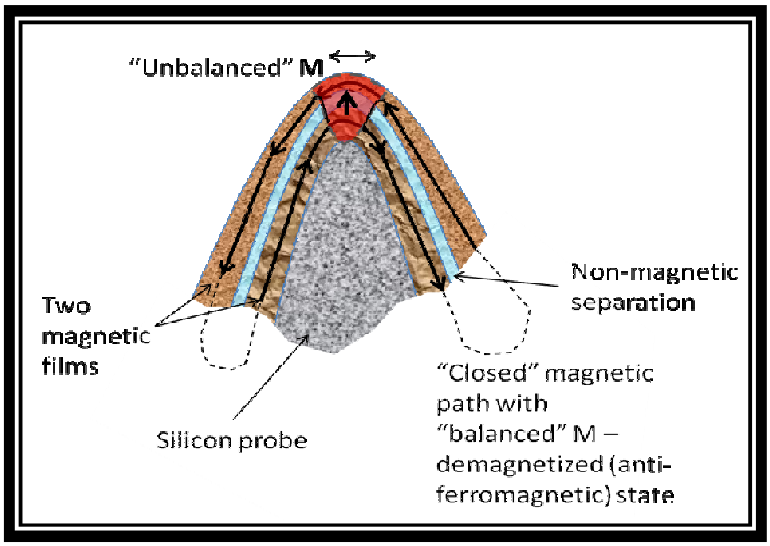

Figure 69: Schematic to illustrate the magnetization configuration in an anti-ferromagnetic MFM probe. The red region shows the tip region where the magnetization in the two layers does not cancel out. This "unbalanced" region defines the resolution of the probe.

Results and Discussion

Figure 70 shows two sets of MFM images of 2 x 2 μm^2 and 5 x 5 μm^2 regions taken from a specially recorded reference magnetic disk by a commercial MFM probe (left image) and the above described Nanomond probe, respectively. A set of tracks with varying linear densities were continuously recorded into the reference ultra-high-density perpendicular magnetic disk with a state-of-the-art Guzik spinstand. In other words, the entire disk was covered with sub-100-nm tracks of bits with the length in each track gradually changing from one track to the next. Therefore, if MFM imaging would show "blank" regions on the disk, this would be only because the resolution of the probe is not adequate to detect the ultra-high density information recorded in these regions. It can be seen that the conventional probe is not capable of reading all the tracks with relatively high linear densities, i.e. with bit features of smaller than approximately 25 nm. This explains the presence of relatively large monochromatic ("blank") regions (with no distinguishable features) where otherwise ultra-high density information could have been "seen". On the contrary, the above described anti-ferromagnetic/multi-domain probe can "see" all the tracks recorded into the disk. That is why in the latter case, the entire 2 x 2 μm^2 region can be "seen" to be covered by tracks. In fact, this probe can be used to detect information with areal densities much above 1 Tbit/in^2. A more quantitative sectional line graph measured along the high-density track is shown in Figure 71 and Figure 72.

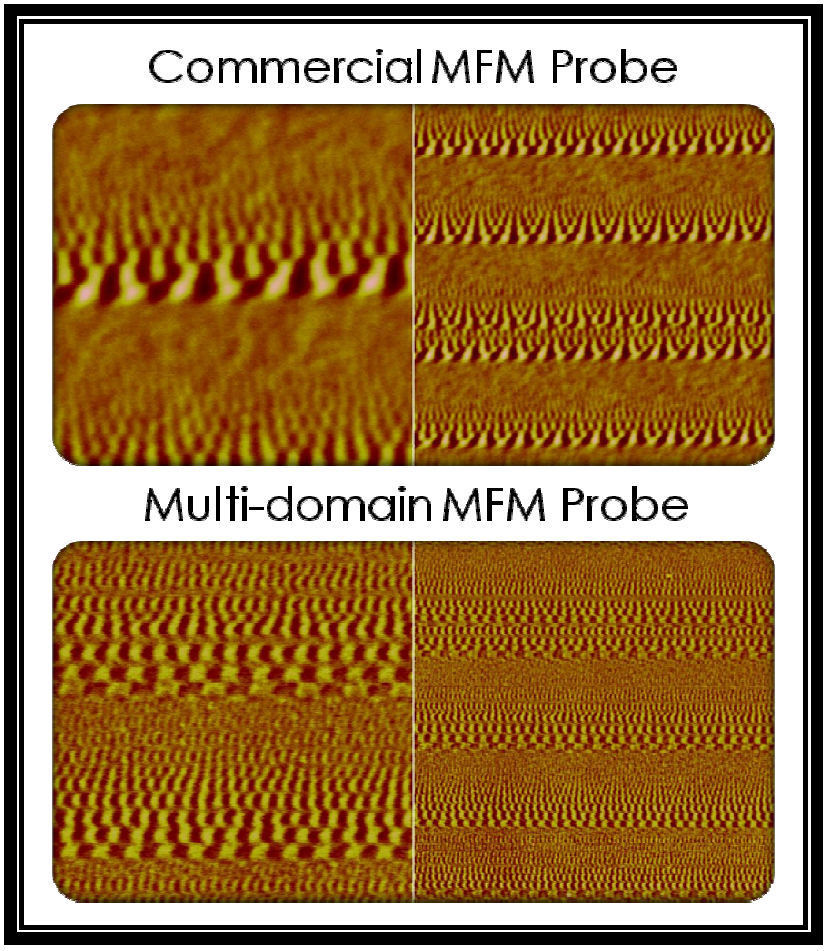

Figure 70: MFM images of 2 µm (left) and 5 µm (right) square regions in reference magnetic disks with continuously recorded sub-100-nm wide tracks of varying linear densities read back by conventional commercial MFM probes ("MFMR" by Nanoworld) (left image) and a sub-10-nm-resolution multi-domain (anti-ferromagnetic) MFM probe.

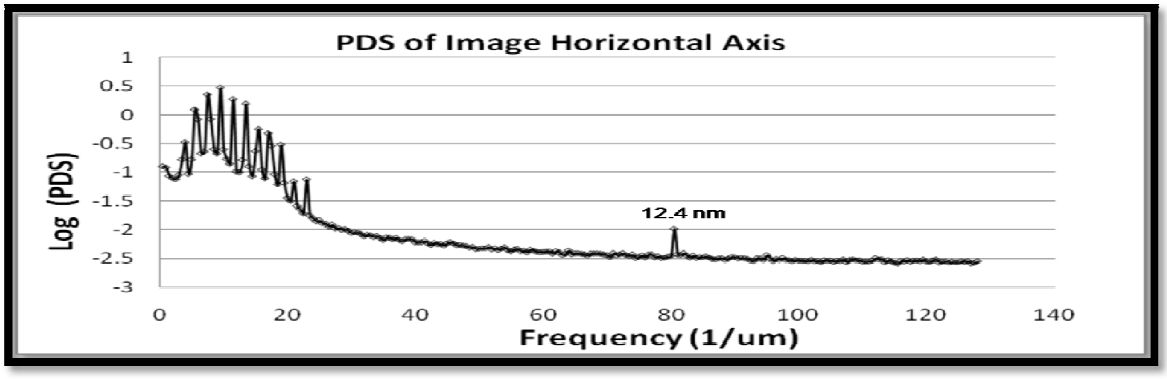

Figure 71: A power spectral density analysis of the 2 µm MFM image taken with the multi-domain MFM probe indicating a period of 12.4 nm.

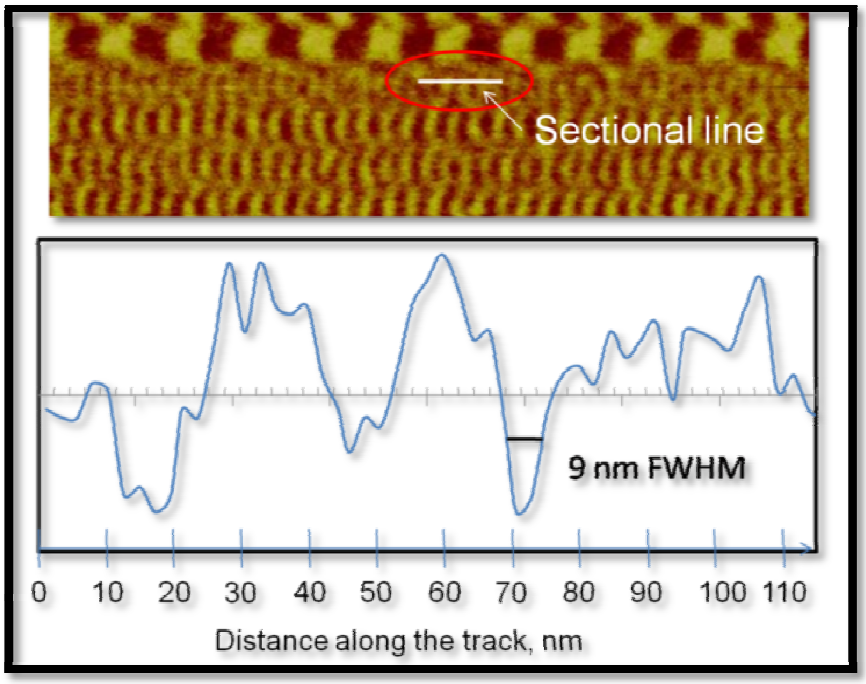

Figure 72: A quantitative section line measurement of MFM signal measured along a high-density track.

To confirm that such high resolution is indeed inherent to the multi-domain configuration of the probe, the following experiment was conducted. The same probe was exposed to the field of over 2 Tesla along the probe axis. Because the coercivity of each layer in the above described probe is of the order of 1 Tesla, as was mentioned via a specially designed MFM experiment in the previous chapter, the field of 2 Tesla is sufficient to drive the probe in a saturated (almost single-domain) state, i.e. with the magnetization in both layers in the same direction. In this regard, the ferromagnetic probe is equivalent to a conventional MFM probe with one magnetic layer. The saturated probe was also used to scan the same reference disk. For comparison, MFM images taken by the multi-domain and "single-domain" probes are shown in Figure 74 left and right, respectively. One can note that the single-domain probe is in all aspects similar to a conventional

MFM probe, with the only difference that two magnetic layers are used instead of one layer as in the conventional case. As expected, the resolution of the single-domain probe is not as good though the strength of the signal is greater compared to the multi-domain probe. In other words, though the larger amount of the magnetic material contributes to the increase of the signal, the greater size of the effective probe tip also results in the inferior resolution compared to that for the anti-ferromagnetic probe.

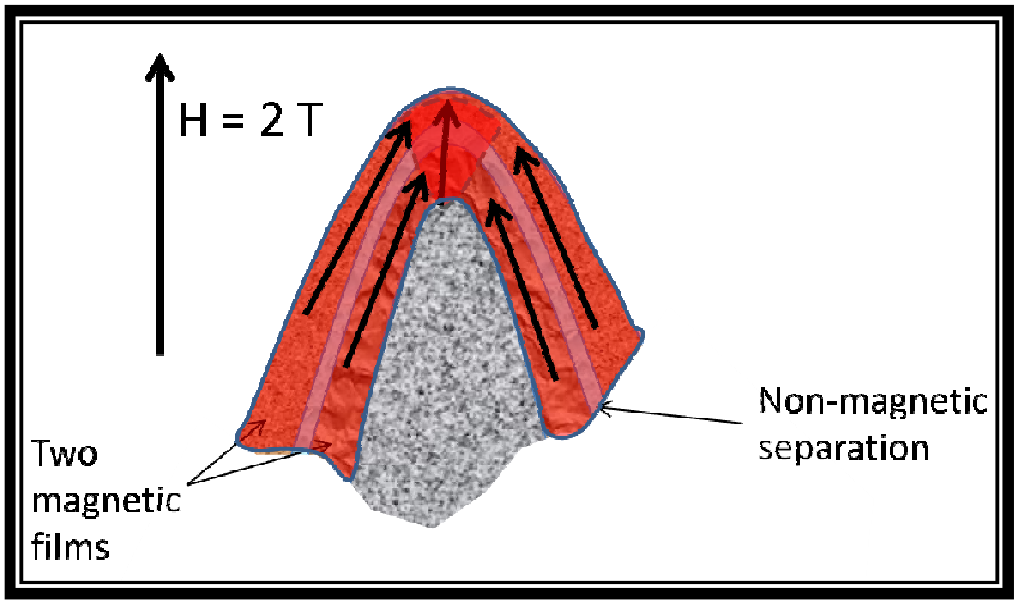

Figure 73: Schematic illustrating a saturated (ferromagnetic) state of the bi-layer MFM probe.

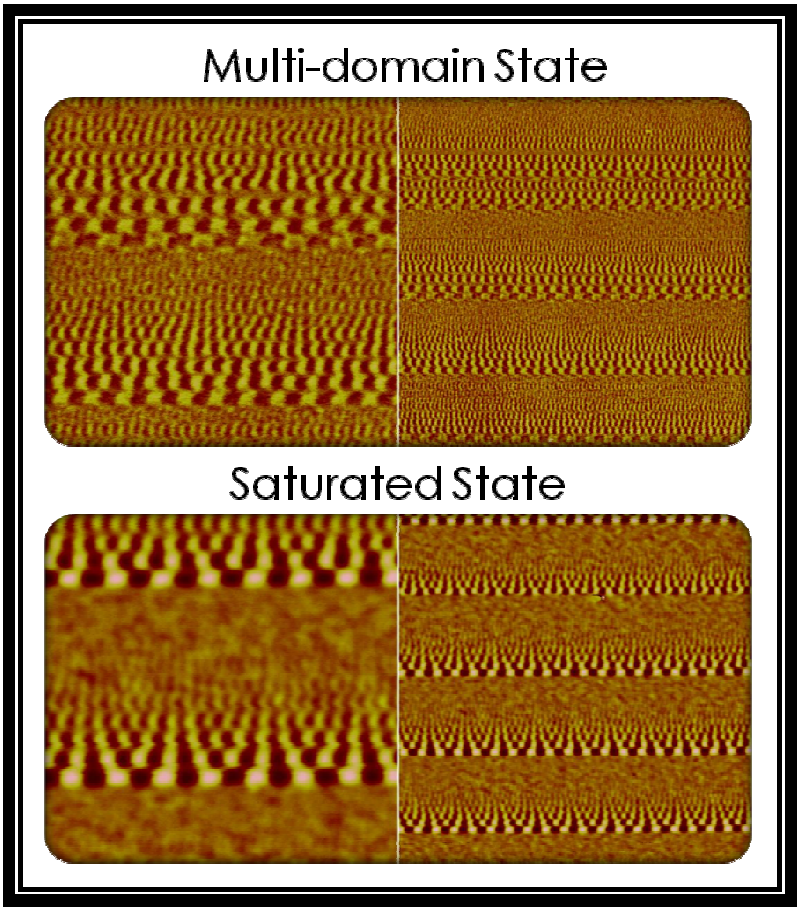

Figure 74: MFM images of 2-micron square regions in reference magnetic disks with continuously recorded sub-100-nm wide tracks of varying linear densities read back by a sub-10-nm-resolution multi-domain (anti-ferromagnetic) MFM probe after annealing (left image) and after magnetizing at a field of greater than 2 Tesla.

Conclusion

This chapter presents an experimental evidence of magnetic force microscopy with sub-10-nm resolution under ambient conditions. To achieve such unprecedented spatial resolution, the tip region was driven in a multi-domain state by sputter-depositing two magnetically decoupled FePt magnetic layers, followed by an annealing treatment.

*Some of the material presented in this chapter was reprinted with permission from Nissim Amos, et al., Applied Physics Letters, 93, 203116, 2008. Copyright 2008, American Institute of Physics.

Conclusion

This study addressed design configuration, media fabrication, and characterization techniques for a particular ML 3D magnetic recording device. The newly developed ML 3D magnetic recording media enables selective reading and writing of up to 4 distinct signal levels, in comparison to only two signals in conventional 2D-based magnetic recording media. It is believed that at least over six layers (or over $2^6 = 64$ signal levels) could be independently accessed in a ML 3D magnetic recording device. In addition, a study on the effect of Ga^+ ions implantation revealed a potential fabrication process for varying the magnetic properties across the vertical dimension of 3D-based magnetic media. Furthermore, newly developed fabrication techniques for MFM probes were presented. Specifically, plateau probes to enhance the overall capabilities of MFM and high lateral resolution (below 10 nm in ambient conditions) multi-domain MFM probe.

References

[1] R. L. White, "The physical boundaries to high-density magnetic recording," *J. Magn. Magn. Mater.* **209**, 1-5 (2000).

[2] G. A. Bertero, S. Malhotra, B. Bian, J. Tsoi, M.l Avenell, D. Wachenschwanz, and T.amashita, "Longitudinal Magnetic Media Designs for 60–200-Gb/in^2 Recording," *IEEE Trans. Magn.*, **39** (2), 651-6 (2003).

[3] S. H. Charap, P.-L. Lu, Y. He "Thermal Stability of Recorded Information at High Densities," *IEEE Trans. Magn.*, **33** (1), 978-83 (1997).

[4] S. Iwasaki, Y. Nakamura & K. Ouchi, "Perpendicular magnetic recording with a composite anisotropy film," *IEEE Trans. Magn.*, **15** (6), 1456 (1979).

[5] M. Mallary, A. Torabi, M. Benakli, "One terabit per square inch perpendicular recording conceptual design," *IEEE Trans. Magn.* **38** (40), 1719-24 (2002).

[6] D. A. Thompson, "The role of perpendicular recording in the future of hard disk storage," *J. Magn. Soc. Jap.*, **21** (S2), 9 (1997).

[7] F. Liu, K. Stoev, P. Luo, Y. Liu, Y. Chen, J. Chen, J. Wang, F.G. Shan, K.T. Kung, M. Lederman, M. Krounbi, M. Re, A. Otsuki, S. Hong, "Perpendicular recording heads for extremely high-density recording," *IEEE Trans. Magn.*, **39** (4), 1942-8 (2003).

[8] Khizroev, Sakhrat and Dmitri Litvinov. Perpendicular Magnetic Recording. Kluwer Academic Publishers, 2004.

[9] S. Iwasaki and Y. Nakamura, "An analysis for the magnetization mode for high density magnetic recording, " *IEEE Trans. Magn.*, **13**, 1272 (1977).

[10] M. Mallary, A. Torabi, and M. Benakli, "One terabit per square inch perpendicular recording conceptual design," *IEEE Trans. Magn.*, **38**, 1719-24 (2002).

[11] N. H. Bertram and M. Williams, "SNR and density limit estimates: a comparison of longitudinal and perpendicular recording," *IEEE Trans. Magn.*, **36** (1), 4-9 (2000).

[12] K.-Z. Gao and H.N. Bertram, "Magnetic recording configuration for densities beyond 1 Tb/in^2 and rates beyond 1 Gb/s," *IEEE Trans. Magn.*, **38**, 3675-83 (2002).

[13] M. Albrecht, C. T. Rettner, A. Moser, M. E. Best, and B. D. Terris, "Recording performance of high-density patterned perpendicular media," *Appl. Phys. Lett.,* **81** (15), 2875-7 (2002).

[14] M. Albrecht, S. Anders, T. Thomson, C. T. Rettner, M. E. Best, A. Moser, and B. D. Terris, "Thermal stability and recording properties of sub-100 nm patterned CoCrPt perpendicular media," *J. Appl. Phys.,* **91**, 6845 (2002).

[15] M. Albrecht, S. Ganesan, C. T. Rettner, A. Moser, M. E. Best, R. L. White, and B. D. Terris, "Patterned Perpendicular and Longitudinal Media: A Magnetic Recording Study," *IEEE Trans. Magn.*, **39** (5), 2323-5 (2003).

[16] C. E., D. Smith, J. Wolfe, D. Weller, S. Khizroev, and D. Litvinov, "Physics of patterned magnetic medium recording: Design considerations," *J. Appl. Phys.,* **98** 024505 (2005).

[17] E. A. Dobisz, Z. Z. Bandic´, T. Wu, and T. Albrecht, "PatternedMedia: Nanofabrication Challenges of Future Disk Drives," *Proceedings of the IEEE*, **96** (11), 1836-46 (2008).

[18] Y. Hijazi, R. Ikkawi, N. Amos, A. Lavrenov, N. Joshi, D. Doria, R. Chomko, D. Litvinov, and S. Khizroev, "Patterned Soft Underlayers for Perpendicular Media," *IEEE Trans. Magn.,* **42** (10), 2375 (2006).

[19] J. Moritz, S. Landis, J. C. Toussaint, P. Bayle-Guillemaud, B. Rodmacq, G. Casali, A. Lebib, Y. Chen, J. P. Nozières, and B. Diény, "Patterned Media Made From Pre-Etched Wafers: A Promising Route Toward Ultrahigh-Density Magnetic Recording," *IEEE Trans. Magn.*, **38** (4), 1731-36 (2002).

[20] L. J. Qiu, J. Ding, A. O. Adeyeye, J.H.Yin, J. S. Chen, S. Goolaup, and N. Singh, "FePt Patterned Media Fabricated by Deep UV Lithography Followed by Sputtering or PLD," *IEEE Trans. Magn.*, **43** (6), 2157-59 (2007).

[21] K. Naito, H. Hieda, M. Sakurai, Y. Kamata, K. Asakawa, "2.5-inch disk patterned media prepared by an artificially assisted self-assembling method," *IEEE Trans. Magn.*, **38** (5), 1949-51 (2002).

[22] A. A. Zhukov, A. V. Goncharov, P. A. J. de Groot, P. N. Bartlett, and M. A. Ghanem, "Magnetic antidot arrays from self-assembly template methods ," *J. Appl. Phys.,* **93**, 7322 (2003).

[23] Y. Kitade, H. Komoriya, and T. Maruyama,"Patterned Media Fabricated by Lithography and Argon-Ion Milling," *IEEE Trans. Magn.*, **40** (4), 2516-18 (2004).

[24] M. Albrecht, S. Anders, T. Thomson, C. T. Rettner, M. E. Best, A. Moser, and B. D. Terris, "Thermal stability and recording properties of sub-100 nm patterned CoCrPt perpendicular media," *J. Appl. Phys.,* **91**, 6845 (2002).

[25] S. Hosaka, Z. Mohamad, M. Shirai, H. Sano, Y. Yin, A. Miyachi, and H. Sone, "Nano-dot and -pit arrays with a pitch of 25 nm × 25 nm fabricated by EB drawing, RIE and nano-imprinting for 1 Tb/in^2 storage," *Microelectronic Engineering,* **85** (5-6), 774-7 (2008).

[26] S. Khizroev, Y. Hijazi, N. Amos, E. Felissaint, N. Joshi, R. Ikkawi, R. Chomko, and D. Litvinov, "Physics of Perpendicular Recording with a Patterned Soft Underlayer," special information technologies issue, *J. Nanoscience and Nanotechnology,* **7**, 243-54 (2007).

[27] S. Khizroev, Y. Hijazi, N. Amos, R. Chomko, and D. Litvinov, "Considerations in the design of three-dimensional and multi-level magnetic recording," *J. Appl. Phys.,* **100**, 63907 (2006).

[28] H. F. Hamann, Y. C. Martin, and H. K. Wickramasighe, "Thermally assisted recording beyond traditional limits," *Appl. Phys. Lett.,* **84** (5), 810 (2004).

[29] T. McDaniel, W. Challener, "Issues in heat-assisted perpendicular recording," *IEEE Trans. Magn.* **39** (4), 1972-9 (2003).

[30] M. A. Seigler, W. A. Challener, E. Gage, N. Gokemeijer, G. Ju, B. Lu, K. Pelhos, C. Peng, R. E. Rottmayer, X. Yang, H. Zhou, and T. Rausch, "Integrated Heat Assisted Magnetic Recording Head: Design and Recording Demonstration," *IEEE Trans. Mag*., **44** (1),119-24 (2008).

[31] B. X. Xu, H. X. Yuan, J. Zhang, J. P. Yang, R. Ji, and T. C. Chong, "Thermal effect on slider flight height in heat assisted magnetic recording," *J. Appl. Phys.,* **103** 07F525 (2008).

[32] R. Ikkawi, N. Amos, Y. Hijazi, D. Litvinov, and S. Khizroev, "Design, Fabrication, and Characterization of Near-field Apertures for 1 Tbit/in^2 Areal Density," *IEEE Trans. Mag*., **44** (11), 1-4 (2008).

[33] R. Ikkawi, N. Amos, A. Lavrenov, R. Chomko, D. Litvinov, and S. Khizroev, "Near-field Optical Transducer for Heat Assisted Magnetic Recording for Beyond 10 Tbit/in^2 Densities," *J. Nanoelectronics and Optoelectronic.* **3**, 44-54 (2008).

[34] R. Ikkawi, N. Amos, A. Krichevsky, R. Chomko, D. Litvinov, and S. Khizroev, "Nanolasers to Enable Data Storage Beyond 10 Tbit/in^2," *Appl. Phys. Lett*., **91**, 153115 (2007).

[35] S. Khizroev, Y. Hijazi, N. Amos, R. Chomko, and D. Litvinov, "Considerations in the design of three-dimensional and multi-level magnetic recording," *J. Appl. Phys.,* **100**, 63907 (2006).

[36] S. Khizroev, "Three-dimensional magnetic memory and/or recording device," US patent application 20060028766, filed February 9, 2006; 11/197,377, filed Aug 4, 2005, with provisional patent, 60/598,645, filed Aug 4, 2004, disclosure filed Feb 21, 2003.

[37] M. Albrecht, G. Hu, A. Moser, O. Hellwig, and B.D. Terris: "Magnetic dot arrays with multiple storage layers", *J. Appl. Phys.*, **97**, 103910 (2005).

[38] Chikazumi, Soshin and C. D. Graham, Physics of Ferromagnetism (International Series of Monographs on Physics. Oxford University Press, 1997.

[39] Cullity, B. D. and C. D. Graham. Introduction to Magnetic Materials. 2nd ed.: Wiley/John & Sons, 2008.

[40] Khizroev, Sakhrat, and Dmitri Litvinov. Perpendicular Magnetic Recording. Kluwer Academic Publishers, 2004.

[41] Taratorin, Alexander. Magnetic Recording Systems and Measurements. California, Guzik Technical Enterprises, 2004.

[42] Maissel, Leon I., and Glang Reinhard. Handbook of Thin Film Technology. New York: McGraw-Hill, 1970.

[43] Madou, Mark J. Fundamentals of Microfabrication: The Science of Miniaturization. 2nd ed.: Taylor & Francis, 2002.

[44] Sarid, Dror. Scanning Force Microscopy: With Applications to Electric, Magnetic, and Atomic Forces. 2nd ed.: Oxford University Press, 1994.

[45] Bhushan, Bharat, Harld Fuchs, and Masahiko Tomitori. Applied Scanning Probe Methods VIII : Scanning Probe Microscopy Techniques. New York: Springer-Verlag, 2008.

[46] D. A. Thompson and J. S. Best, "The Extendibility of Magnetic Recording for Data Storage," IBM executive briefing, January 1998.

[47] M. H. Kryder, "Data storage technologies for advanced computing," *Scientific American,* **117**, 72 (1987).

[48] S. H. Charap, P.-L. Lu, Y. He "Thermal Stability of Recorded Information at High Densities," *IEEE Trans. Magn.*, **33** (1), 978-83 (1997).

[49] N. H. Bertram and M. Williams, "SNR and density limit estimates: a comparison of longitudinal and perpendicular recording," *IEEE Trans. Magn.*, **36** (1), 4 (1999).

[50] G. A. Bertero, S. Malhotra, B. Bian, J. Tsoi, M.l Avenell, D. Wachenschwanz, and T.amashita, "Longitudinal Magnetic Media Designs for 60–200-Gb/in^2 Recording," *IEEE Trans. Magn.*, **39** (2), 651-6 (2003).

[51] S. Iwasaki and Y. Nakamura, "An analysis for the magnetization mode for high density magnetic recording," *IEEE Trans. Magn.*, **13**, 1272 (1977).

[52] S. Khizroev, M. H. Kryder, Y. Ikeda, K. Rubin, P. Arnett, M. Best, D. A. Thompson, "Recording heads with trackwidths suitable for 100 Gbit/in2 density," *IEEE Trans. Magn.*, **35** (5), 2544-6 (1999).

[53] S. J. Greavesa, H. Muraoka, and Y. Kanai, "Discrete track media for 600 Gbits/in^2 recording," *J. Appl. Phys.,* **99**, 08F903 (2006).

[54] K. Hattori, K.Ito, Y. Soeno, M. Takai, and M. Matsuzaki, "Fabrication of Discrete Track Perpendicular Media for High Recording Density," *IEEE Trans. Magn.,* **40** (4), 2510-15 (2004).

[55] M. Albrecht, C. T. Rettner, A. Moser, M. E. Best, and B. D. Terris, "Recording performance of high-density patterned perpendicular media," *Appl. Phys. Lett.*, **81** (15), 2875-7 (2002).

[56] C. Chappert, H. Bernas, J. Ferré, V. Kottler, J.-P. Jamet, Y. Chen, E. Cambril, T. Devolder, F. Rousseaux, V. Mathet, and H. Launois,"Planar Patterned Magnetic Media Obtained by Ion Irradiation," *Science*, **280** (5371), 1919-22 (1998).

[57] D. Weller and A. Moser, ""Thermal Effect Limits in Ultrahigh-Density Magnetic Recording," *IEEE Trans. Magn.,* **35**, 4423 (1999).

[58] H. F. Hamann, Y. C. Martin, and H. K. Wickramasighe, "Thermally assisted recording beyond traditional limits," *Appl. Phys. Lett.,* **84** (5), 810 (2004).

[59] T. McDaniel, W. Challener, "Issues in heat-assisted perpendicular recording," *IEEE Trans. Magn.* **39** (4), 1972-9, (2003).

[60] M. H. Kryder, E. C. Gage, T. W. McDaniel, W. A. Challener, R. E. Rottmayer, G. Ju, Y.-T. Hsia, M.F. Erden, "Heat Assisted Magnetic Recording," *IEEE Trans. Mag*., **96** (11),1810-35 (2008).

[61] M. A. Seigler, W. A. Challener, E. Gage, N. Gokemeijer, G. Ju, B. Lu, K. Pelhos, C. Peng, R. E. Rottmayer, X. Yang, H. Zhou, and T. Rausch, "Integrated Heat Assisted Magnetic Recording Head:Design and Recording Demonstration," *IEEE Trans. Mag*., **44** (1), 119-24 (2008).

[62] S. Khizroev, Y. Hijazi, N. Amos, D. Doria, A. Lavrenov, R. Chomko, T.-M. Lu, D. Litvinov, "Three-dimensional magnetic recording – an emerging nanoelectronic technology," *J. Nanoelectronics and Optoelectronics,* **1**, 1-18 (2006).

[63] S. Khizroev, R. Chomko, Y. Hijazi, N. Amos, "Three-dimensional magnetic recording devices," Pentagon report, Report # A752434, 2005

[64] Khizroev, Sakhrat, and Dmitri Litvinov. Perpendicular Magnetic Recording. Kluwer Academic Publishers, 2004.

[65] D. Litvinov, M. Kryder, and S. Khizroev, "Recording physics of perpendicular media: soft underlayers," *JMMM*, **232** (1-2), 84-90 (2001).

[66] S. Khizroev, M. H. Kryder, Y. Ikeda, K. Rubin, P. Arnett, M. Best, D. A. Thompson, "Recording heads with trackwidths suitable for 100 Gbit/in2 density," *IEEE Trans. Magn.*, **35** (5), 2544-6 (1999).

[67] D. Litvinov and S. Khizroev, "Orientation-sensitive magnetic force microscopy in future probe storage applications," *Appl. Phys. Lett.,* **81** (10), 1878 (2002).

[68] F. Candocia, E. Svedberg, D. Litvinov, S. Khizroev, "Deconvolution processing for increasing the resolution of magnetic force microscopy measurements," *Nanotechnology*, **15**, S575-84 (2004).

[69] S. Khizroev, Y. Hijazi, N. Amos, E. Felissaint, N. Joshi, R. Ikkawi, R. Chomko, and D. Litvinov, "Physics of Perpendicular Recording with a Patterned Soft Underlayer," *J. Nanoscience and Nanotechnology,* **7**, 243-54 (2007).

[70] S. Khizroev, Y. Hijazi, N. Amos, R. Chomko, and D. Litvinov, "Considerations in the design of three-dimensional and multi-level magnetic recording," *J. Appl. Phys.,* **100**, 63907 (2006).

[71] M. H. Kryder, E. C. Gage, T. W. McDaniel, W. A. Challener, R. E. Rottmayer, G. Ju, Y.-T. Hsia, M.F. Erden, "Heat Assisted Magnetic Recording," *IEEE Trans. Mag.*, **96** (11),1810-35 (2008).

[72] Chunsheng E, J. Rantschler, S. Zhang, D. Smith, V. Parekh, S. Khizroev, D. Litvinov, "Integranular interactions of low temperature atmosphere annealed Co/Pd magnetic multilayers," *J. Appl. Phys.,* **101**, 09D108 (2007).

[73] I. Dumer, "Recursive decoding and its performance for low-rate Reed-Muller codes," *IEEE Trans. Info. Theory*, **50**, 811-23 (2004).

[74] I. Dumer and K. Shabunov, "Recursive error correction for general Reed-Muller codes," *Discrete Applied Mathematics,* **154**, 253-69 (2006).

[75] I. Dumer, "Soft decision decoding of Reed-Muller codes: a simplified algorithm," *IEEE Trans. Info. Theory,* **52** (3), (2006).

[76] I. Dumer and K. Shabunov, "Soft decision decoding of Reed-Muller codes: recursive lists," *IEEE Trans. Info. Theory,* **52** (3), (2006).

[77] S. Khizroev, A. Lavrenov, N. Amos, R. Chomko, D. Litvinov, "Focused Ion Beam as a Nanofabrication Tool for Rapid Prototyping of Nanomagnetic Devices," *Microscopy and Microanalysis*, **12**, 128 (2006).

[78] S. Khizroev, Y. Hijazi, N. Amos, E. Felissaint, N. Joshi, R. Ikkawi, R. Chomko, and D. Litvinov, "Physics of Perpendicular Recording with a Patterned Soft Underlayer," *J. Nanoscience and Nanotechnology*, **7**, 1-12 (2007).

[79] Y. Hijazi, R. Ikkawi, N. Amos, A. Lavrenov, N. Joshi, D. Doria, R. Chomko, D. Litvinov, and S. Khizroev, "Patterned Soft Underlayers for Perpendicular Media," *IEEE Trans. Magn.,* **42** (10), 2375 (2006).

[80] Y. J. Chen, K. W. Ng, S. H. Leong, Z. B. Guo, J. Z. Shi, and B. Liu, "Recording Performance of Discrete Track Patterned Media Fabricated by Focused Ion Beam," *IEEE Trans. Mag.*, **41**, 6, (2005).

[81] B. S. H. Pang, Y. J. Chen, and S. H. Leong, "Smooth Discrete Track Media Fabricated by Focused Ion Beam," *Applied Physics Letters,* **88**, 094103 (2006).

[82] Joshua Symonds, "Nanoscale Magnetic Characterization of FIB Patterned Bits on Perpendicular Magnetic Recording Media," *2005 NNIN REU Research Accomplishments,* 142-143 (2005).

[83] Eugeniusz Klugmann, Csaba S. Daroczi, Peter Kollfir, "Influence of Ion Implantation on Magnetic Properties of Crystalline Nickel and Amorphous Fe-B Ribbons," *IEEE Trans. Mag.,* **30** (2), 521-523, (1994).

[84] Nowak (A), J. Dubowik, F. Stobiecki, B. Szymański, M. Schmidt, M. Kopcewicz, and J. Jagielski, "Effect of annealing and ion implantation on interlayer exchange coupling in Fe/Cr multilayers," *Physica Status Solidi (A), Applied Research*, **196** (1), 45-48 (2003).

[85] J.A. Romano, E.C. da Silva, L.F. Schelp, J.E. Schmidt, R. Meckenstock, J. Pelzl, "Effects of Ar-ion implantation and thermal treatment on magnetic properties of Co/Pd multilayers: a ferromagnetic resonance study," *JMMM*, **205**, 161-169 (1999).

[86] L.F. Shelp, M. Carara, A.D.C. Viegas, M.A.Z. Vasconcellos, "Structural and magnetic behavior of Ar-implanted Co/Pd multilayers: Interfacial mixing," *J. Appl. Phys.,* **75**, 5262 (1994).

[87] I. Sakamoto , S. Honda , H. Tanoue , N. Hayashi , M. Nawate and Y. Ikeda, "Ion Beam Mixing of Au/Fe Multilayers by Ar Ion Implantation," *IEEE Trans. Mag.,*939-942 (1999).

[88] Rachid Sbiaa and Seidikkurippu N. Piramanayagam, "Patterned Media Towards Nano-bit Magnetic Recording: Fabrication and Challenges," *Recent Patents on Nanotechnology*, **1**, 29-40 (2007).

[89] Nowak (A), J. Dubowik, F. Stobiecki, B. Szymański, M. Schmidt, M. Kopcewicz, and J. Jagielski, "Effect of annealing and ion implantation on interlayer exchange coupling in Fe/Cr multilayers," *Physica Status Solidi (A), Applied Research*, **196** (1), 45-48 (2003).

[90] Y. B. Zhang and J. A. Woollam, "Annealing effects of CoNi multilayers," *IEEE Trans. Mag.,* **31** (6), 3262-4 (1995).

[91] R. Atkinson, G. Didrichsen, W.R. Hendren, I.W. Salter and R.J. Pollard, "High-resolution optical imaging of magnetic-domain structures," *Phys. Rev. B*, **62**, 12294-302 (2000).

[92] C.C. Faulkner, Del. Atkinson, D.A. Allwood, R.P. Cowburn, "Rapid tuning of $Ni_{81}Fe_{19}$ bilayer magnetic properties by focusing ion beam intermixing," *JMMM,* **319**, 9-12 (2007).

[93] G. Binnig, H. Rohrer, Ch. Gerber, and E. Weibel, "Surface Studies by Scanning Tunneling Microscopy," *Phys. Rev. Lett.*, **49**, 57-61 (1982).

[94] D. M. Eigler and E. K. Schweizer, “Positioning Single Atoms with a Scanning Tunneling Microscope,” *Nature*, **344**, 524 (1990).

[95] Y. Martin and H. K. Wickramasinghe, "Magnetic imaging by 'force microscopy' with 1000 Å resolution," *Appl. Phys. Lett*., **50**, 1455–1457 (1987).

[96] R. B. Proksch, T. E. Schaffer, B. M. Moskowitz, E. D. Dahlberg, D. A. Bazylinski, and R. B. Frankel, "Magnetic force microscopy of the submicron magnetic assembly in a magnetostatic bacterium," *Appl. Phys. Lett*., **66** (19), 2582 (1994).

[97] P. Rice, J. Moreland, A. Wadas, "DC magnetic force microscopy imaging of thin-film recording head," *J. Appl. Phys*, **75** (10), 6578 (1994).

[98] E. B. Svedberg, S. Khizroev, and D. Litvinov, “Magnetic force microscopy study of perpendicular media,” *J. Appl. Phys.,* **91** (8), 5365-5370 (2002).

[99] S. Khizroev, W. Jayasekara, J. A. Bain, R. E. Jones, Jr., M. H. Kryder, “MFM quantification of magnetic fields generated by ultra-small single pole perpendicular heads,” *IEEE Trans. Magn.*, **34** (4), pt.1, 2030-2 (1998).

[100] Khizroev, Sakhrat, and Dmitri Litvinov. Perpendicular Magnetic Recording. Kluwer Academic Publishers, 2004.

[101] Z. L. Zhao, J. S. Chen, J. Ding, J. B. Yi, B. H. Liu, and J. P. Wang, “High Coercivity FePt Thin Films With Ag Intermediate Layers Deposited at 400 C,” *IEEE Trans. Magn.*, **41** (10), 3337-9 (2005).

[102] F. Candocia, E. Svedberg, D. Litvinov, S. Khizroev, “Deconvolution processing for increasing the resolution of magnetic force microscopy measurements,” *Nanotechnology* **15**, S575-84 (2004).

[103] D. Rugar, H. J. Mamin, P. Guethner, S. E. Lambert, J. E. Stern, I. Mc- Fadyen, and T. Yogi, “Magnetic force microscopy: General principles and application to longitudinal recording media,” *J. Appl. Phys.*, **68**, 1169–1183 (1990).